Department of Precision and Microsystems Engineering

Ferrofluid linear long stroke stage
A passive alternative to air bearings

S.W.M van den Toorn

Report no   : 2020.005
Coach   : S.G.E. Lampaert
Professor   : J.W. Spronck and R.A.J. van Ostayen
Specialisation   : Mechatronic System Design
Type of report   : Master of Science Thesis
Date   : 27 January 2020

Challenge the future

Ferrofluid linear long stroke stage

A passive alternative to air bearings

by

S.W.M. van den Toorn

to obtain the degree of Master of Science

at the Delft University of Technology,

to be defended publicly on Tuesday January 27, 2020 at 1:45 PM.

This thesis is confidential and cannot be made public until January 27, 2022.

An electronic version of this thesis is available at `http://repository.tudelft.nl/`.

TUDelft

Acknowledgements

This work would not have been possible without the endless supporting effort from my surroundings. Foremost to thank are my parents, they have been supporting me through better or worse for over 25 years. Without them I wouldn't have been able to be where I am today. Next to them I would like to thank my girlfriend, you are an integral part of my life and I thank you for supporting me throughout my academic and rowing career.

This thesis started in the office of Jo Spronck. Jo's direct, often a bit blunt but always caring approach have helped me overcome challenges and have guided me throughout this project. I would like to thank him for that.

I would like to thank Stefan Lampaert as well for being there whenever I needed help, for making things a little bit simpler when I got carried away in the details and for having confidence in me. You will be a wonderful father.

I would further like to thank Ron van Ostayen for the weekly meetings, the help with COMSOL and for the very thorough proofreading of the papers.

My academic career has been intertwined with rowing. I would like to thank all of the people that rowed with me, have coached me or have competed against me. You all have made me grow, believe in myself and helped me achieve epic results. I especially want to thank Jari de Vries, for all the kilometres we rowed together and the even larger amount of coffee.

Finally, I would like to thank everyone that has contributed to this thesis in any way shape of form, the technical staff of PME for the aid in the construction and verification of the stage, and Dick Plettenburg for making the time to be a member of my graduation committee.

Stefan van den Toorn
Delft, January 2020

Abstract

Stick-slip friction is the resulting effect of the transition between the dynamic and static friction coefficient. This effect determines the minimal sustained speed and minimal incremental motion of a movement system, limiting the performance in precise positioning systems. Available bearing types without stick-slip suffer from complexity, high cost, energy storage (for example in flexures) or need for active components (for example in magnetic bearings). The ferrofluid bearing has none of these issues. This makes it a potential alternative for current bearings in precise positioning systems.

Ferrofluid is a colloidal suspension of magnetic particles in a carrier liquid. This gives the unique property of a fluid that is drawn towards the highest magnetic field intensity. The ferrofluid can be used in two ways to construct a bearing; the pocket bearing and pressure bearing arrangements. This research focuses on the latter, as the pocket bearing has shown bad repeatability. The pressure bearing consists of a ferrofluid in a magnetic field in between bearing surfaces. As a load is applied, the space between bearing surfaces decreases. This results in the ferrofluid being displaced from the least energetic configuration in the magnetic field which induces a normal force on the bearing surfaces.

The objective of this study is to improve the performance of the ferrofluid pressure bearing by removing or improving the limitations in stroke length and repeatability. This is done by the creation of a long-stroke linear ferrofluid demonstrator stage. The challenges in the creation of this stage are primarily focused on limiting the effects of trail formation, addressing the evaporation of the ferrofluid, and achieving a sufficient load capacity and stiffness to be a feasible alternative to other bearing types.

The load capacity and stiffness of the ferrofluid pressure bearing are functions of the magnetic field intensity and the magnetic saturation of the ferrofluid. For the ferrofluid, the EFH3 fluid from Ferrotec is chosen for its high saturation magnetization and low viscosity. The magnetic field intensity in the pressure bearing is generated by an array of permanent magnets. The intensity and gradient in the magnetic field intensity can be varied by altering variables such as the orientation of the magnetization, remanent flux density, width, height and number of magnets. Configurations with iron and/or gaps between the magnets are also modelled. By using finite element modelling there is found that for bearing applications the most cost and weight effective method is to arrange long slender magnets in an up-down magnetization configuration with a thin iron bottom plate. The load and stiffness of this configuration is validated and implemented in the demonstrator stage.

The repeatability in existing ferrofluid stages is compromised by trail formation and evaporation of the ferrofluid. Trail formation is the loss of ferrofluid due to the shear force overcoming the magnetic body force on the ferrofluid. The demonstrator stage features ferrofluid reservoirs and a symmetric bearing design to prevent out-of-plane height loss due to this loss of fluid. Evaporation affects the viscosity and saturation magnetization of the ferrofluid. It is shown that for limited amounts of mass loss due to evaporation, the ferrofluid can be restored to the original specification by adding carrier liquid. Figure 1 shows an illustration of the designed demonstrator stage.
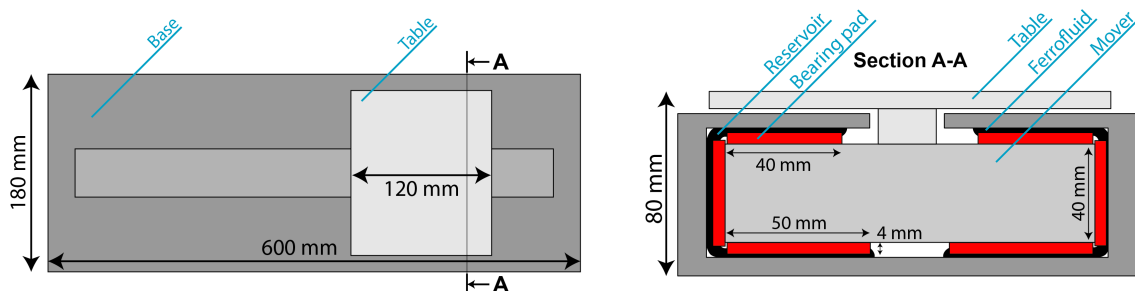
Figure 1: Schematic illustration of the demonstrator design (left: top view, right: cross section) with the corresponding dimensions.

Figure 2 shows a 3D render of the demonstrator stage assembly. This stage has a stroke of 460 mm with a load capacity of 120 N and a stiffness of 0.44 N/μm. The outer dimensions of the stage are 600x180x80 mm (LxWxH). The stage shows a highly repeatable behaviour, the difference between the height of the mover stationary and after a complete stroke with 1 kg payload at 0.25 m/s is $< \pm 3$ μm and $< \pm 7$ μm at 0.5 m/s. The damping of the stage is a function of the velocity and the amount of payload. It is measured to be ~2 N·s/m for a velocity of 0.2 m/s without payload to ~4 N·s/m for a velocity of 0.4 m/s with 1.75 kg payload. When compared to previous implementations of the ferrofluid bearing, this stage performs at least comparable in terms of stiffness and load capacity, but improves considerable on the range of motion and the out-of-plane repeatability.

From the research can be concluded that a ferrofluid bearing is a stick-slip free alternative to ball bearings when requiring a passive bearing without high requirements for load capacity or out-of-plane stiffness of repeatability. Compared to an aerostatic stage, the ferrofluid bearing can give the same stick-slip-free motion while being passive, at the cost of a reduction in out-of-plane repeatability and stiffness. Nevertheless, the ferrofluid bearing can approach the same out-of-plane stability for limited payload and velocity. Making the ferrofluid bearing a feasible alternative to aerostatic bearings, depending on the demands of the application.
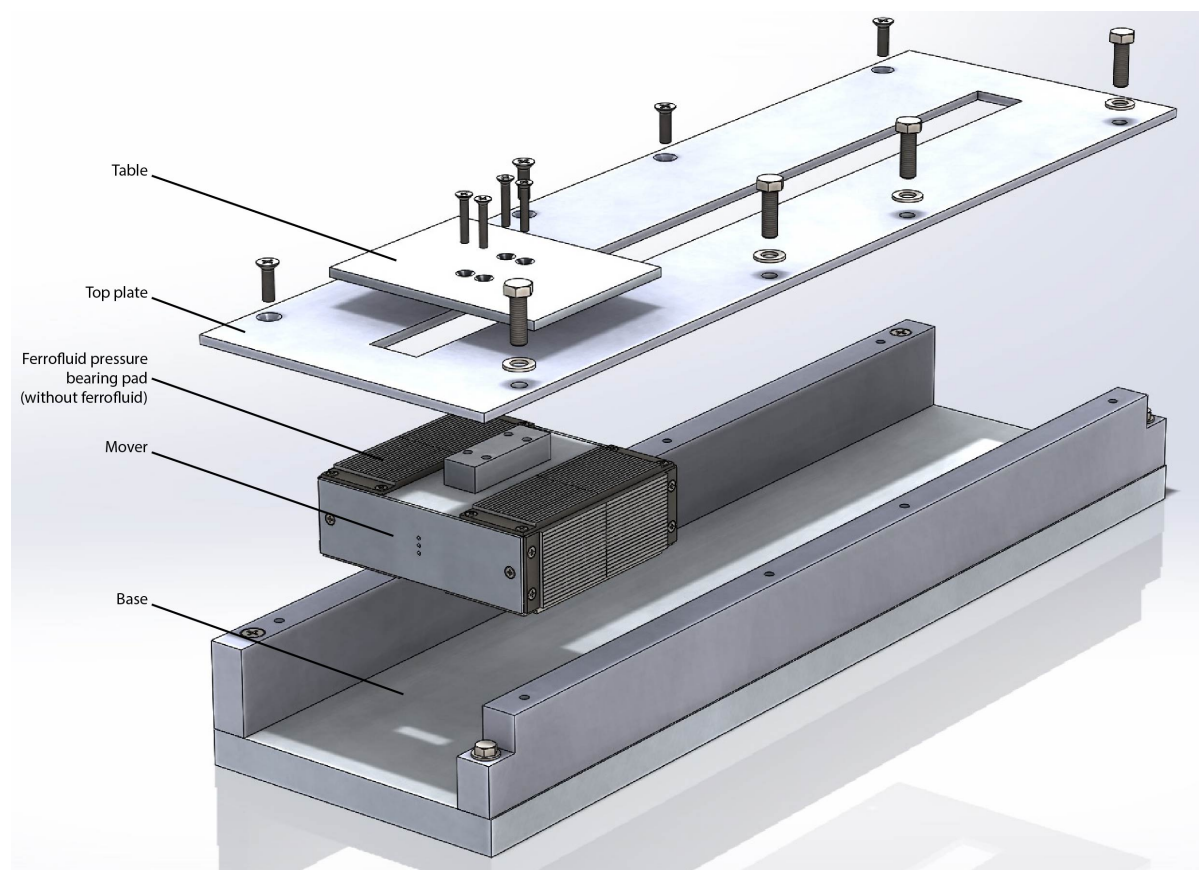

Figure 2: Render of the realized linear stage assembly.

Contents

$$1$$

Introduction

1.1. Background

The world around us is getting smaller, technology is bringing us closer to each other than ever before. Meanwhile the technology itself is shrinking as well, the transistors in a CPU are nowadays 18 times smaller than 20 years ago [48]. This shrinking is not limited to semiconductors, common every-day appliances like vacuum cleaners, refrigerators, washing machines and cell phones have all shrunk or increased in capacity while remaining the same size. All these devices have to be constructed and need to function properly. Thus, it is important that all parts are put together properly and all moving parts move in the right way. This asks for increasingly precise positioning in the assembly and operation, often with severe restrictions in terms of environment, dimensions or cost. This brings new and difficult challenges, one of which is the approach when dealing with the effects of stick-slip. The effect of stick-slip friction start playing an important role in the achievable accuracy and precision, when positioning to the sub-micrometre level.

1.2. Stick-slip

Stick-slip is the resulting effect of the transition between the dynamic and static friction coefficient. This phenomenon determines the lower performance bounds of a movement system: the minimum incremental motion and the lowest sustained movement velocity [3]. These motion characteristics have a direct influence on the controllability of a system and can lead to oscillations around the desired position. In order to ensure proper functioning of precise positioning systems at the sub-micrometre scale, this effect has to be eliminated. As it is a highly complex and non-linear phenomenon, the modelling of the stick-slip is difficult and limited [20]. This makes it hard to predict and compensate for stick-slip. Thus, the logical conclusion would be the elimination of the effect altogether by using stick-slip free bearing systems. The commercially available bearing systems that are free from stick-slip suffer from complexity, cost or energy storage as drawback [31]. However, there is a promising bearing: the ferrofluid bearing. The ferrofluid bearing can potentially be a passive bearing without previously mentioned drawbacks.

1.3. Ferrofluid bearing

The ferrofluid (FF) bearing, originally envisioned by Rosensweig [34, 35] consist out of three elements: a ferrofluid in between bearing surfaces in a magnetic field. The ferrofluid is a stable colloidal suspension of small magnetic particles in a carrier fluid. The magnetic particles are coated in a surfactant to prevent agglomeration [36]. Figure 1.1 shows an illustration of the particles in a ferrofluid. When subjected to a magnetic field, the magnetic particles are drawn towards the highest magnetic field intensity. Resulting in a pressure build up in the ferrofluid.
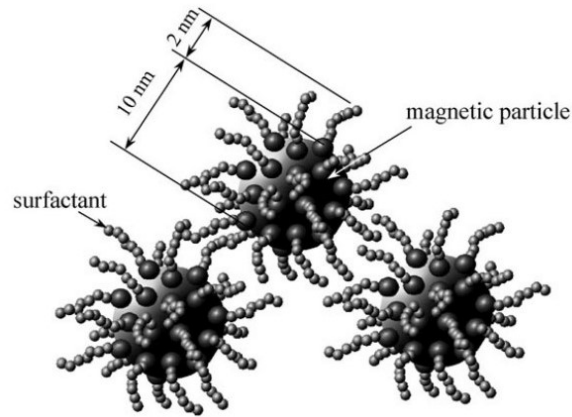
Figure 1.1: Illustration of coated magnetic particles in a ferrofluid. Illustration from [30].

Passive ferrofluid bearings can be divided in two categories: pressure and pocket bearings. The working principle of these bearings is illustrated in figure 1.2. Both bearing types create a load capacity by harnessing the pressure build up in the ferrofluid in a magnetic field. This pressure is pressed directly against the bearing surface in the pressure bearing [34]. In the pocket bearing, a volume is sealed in-between the bearing surfaces. This enclosed volume is usually a pocket of air. A displacement of the bearing surface increases the pressure inside the air pocket as it is sealed, creating the load bearing effect [23].
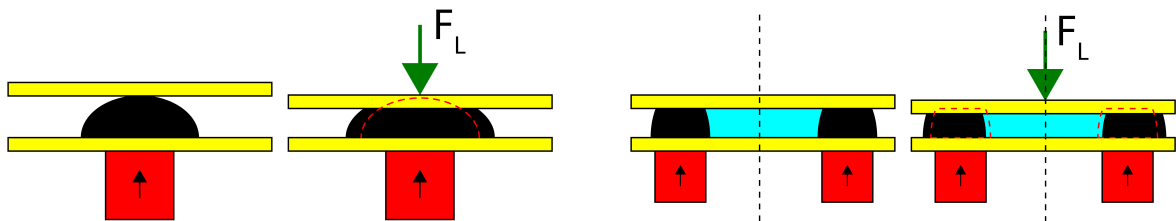

Figure 1.2: Working principle of the ferrofluid pressure (left) and pocket (right) bearing. Red indicates the magnet, the ferrofluid is indicated using black, the bearing surfaces are yellow and the enclosed air pocket is cyan.

1.4. Literature of ferrofluid bearing implementations

Passive ferrofluid bearings also have been implemented in several planar [8, 18, 29, 46] and linear positioning systems [5, 47]. Of these stages the best performing stage was made by Van Moorsel [46], it has a maximum stroke length of 30 mm, suffers from 60 μm displacement in the out-of-plane direction due to fluid loss under translation and has a out-of-plane stiffness of 0.8 N/μm. These are typical values for current state of the art of ferrofluid bearing stages. And are low in comparison to the air bearing stages of similar dimensions where the strokes of several decimetres are common. The out of plane displacement is in the order of several micrometre and an out-of-plane stiffness in the order of 10-100 N/μm [31, 33].

This illustrates the reason for the lack of commercial use of the ferrofluid bearing. While the ferrofluid bearing has many advantages over more conventional bearing types (low cost, compactness, only viscous friction and a lack of active components), they are currently outweighed by the major drawbacks of the ferrofluid bearing (a limited stroke and a low repeatability). If some of these drawbacks can be removed or improved, the ferrofluid bearing can be used to fill a gap in the market where a low-cost passive stick-slip-free motion is required without a demand for high out of plane stiffness.

1.5. Objective

The objective of this study is to improve the performance of the ferrofluid bearing by removing or improving the limitations in stroke length and repeatability. To accomplish this objective, a long stroke linear passive ferrofluid stage is developed, designed and tested. This stage is then compared to an aerostatic bearing stage of similar specification. The challenges in the creation of this stage are primarily focused on limiting the effects of trail formation, addressing the evaporation of the ferrofluid, and achieving a sufficient load capacity and stiffness to make the ferrofluid bearing a feasible alternative to other bearing types.

1.6. Thesis overview

Chapter 2 describes the set of challenges involved in the design of a long stroke linear stage based on ferrofluids. The body of this thesis is built around a set of papers. The first paper in chapter 3 discusses the design of ferrofluid pressure bearing pads. The outcomes of the paper in chapter 3 is used in the second paper in chapter 4, which discusses the design of a long stroke linear passive ferrofluid stage. Chapter 5 contains a discussion of the research in this thesis. The conclusions are presented in chapter 6 and recommendations for future research can be found in chapter 7.

<div align="right">

2

</div>

Background

To improve the performance of the ferrofluid bearing, the main drawbacks of a limited stroke and bad repeatability need to be improved or removed. The bad repeatability in the bearing is primarily caused by the loss of pocket volume and trail formation [24, 46, 47]. The limited stroke is primarily the caused by of trail formation [47]. These sources of the drawback will be discussed in this chapter, together with the ferrofluid itself. The ferrofluid is an important design variable as it influences the evaporation of the ferrofluid, the damping of the mover and the load capacity of the stage.

2.1. Ferrofluid bearing types

This section will start with explaining the working principle and characteristics of the two ferrofluid bearings types in detail. This will be followed by the benefits of both bearing types. Finally, the most suitable bearing type for the application in a precision positioning system will be evaluated.

2.1.1. Pressure bearing

Figure 2.1 shows the working principle of the pressure bearing. The bearing is loaded with force F_1 and F_2 with $F_1 < F_2$. The magnetic field intensity is shown at the fly heights h_1 and h_2. The fly height is defined as the distance between the bearing surfaces. The grey shaded area illustrates the integral of the magnetic field intensity over the ferrofluid surface area. Adding more load causes the top bearing surface to move down, which increases the value of the evaluated integral due to two distinct effects: a higher magnetic field intensity and a larger ferrofluid surface area. The field intensity is increased due to the top bearing surface moving closer to the magnet. Due to the constant volume of ferrofluid, a reduction in height causes an increase in ferrofluid surface area.

Using formula 2.1 [36] the evaluated integral can be related to the load capacity. In this formula F_L is the load capacity, μ_0 the permeability in vacuum, M_s the saturation magnetization of the ferrofluid and H the magnetic field intensity. The area is defined as the wetted surface area of the ferrofluid on the top bearing surface.

$$F_L = \mu_0 M_s \int_S H dA \qquad (2.1)$$

Formula 2.2 [36] shows the stiffness of the pressure bearing. The stiffness is a function of the increase of ferrofluid area and the change of magnetic field intensity in the direction of the fly height. In practice, the increase in the integral term due to the increase in ferrofluid area is negligible as the edge of the ferrofluid is located at a low magnetic field intensity. The stiffness is thus only a function of the gradient in the magnetic field in the direction of the fly height.

$$k = -\mu_0 M_s \frac{d}{dh} \int_S H dA \qquad (2.2)$$

Figure 2.1: Effect of increase in payload in ferrofluid pressure bearing with magnetic field intensity at the interface of the ferrofluid with the top bearing surface. Red indicates the magnet, the ferrofluid is indicated using black and the bearing surfaces are yellow.

2.1.2. Pocket bearing

In figure 2.2 the working principle of a ferrofluid pocket bearing is explained. There can be seen that for an increase in load ($F_1 < F_2 < F_3$), the location of the seal shifts and the fly height is reduced. The air in the pocket stays constant when the bearing is loaded by F_1 and F_2. When the load is further increased, the volume of the enclosed air pocket is reduced until a new equilibrium is found at h_3 with $h_3 < h_2$.

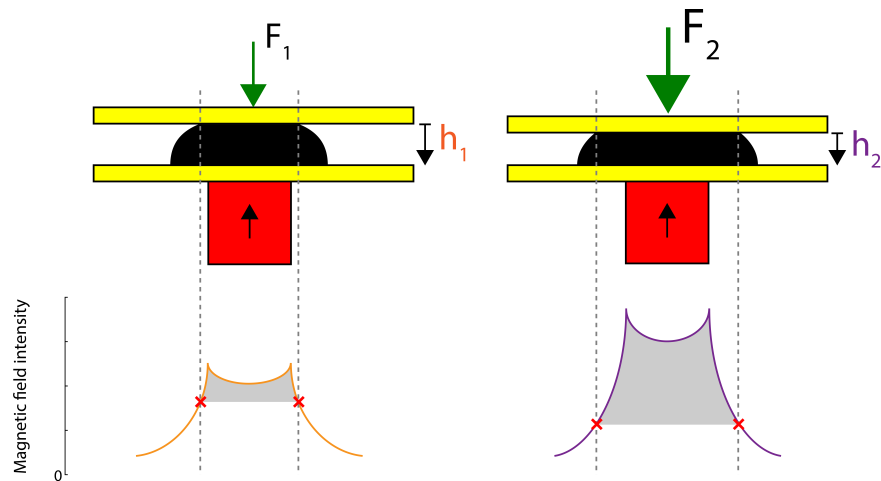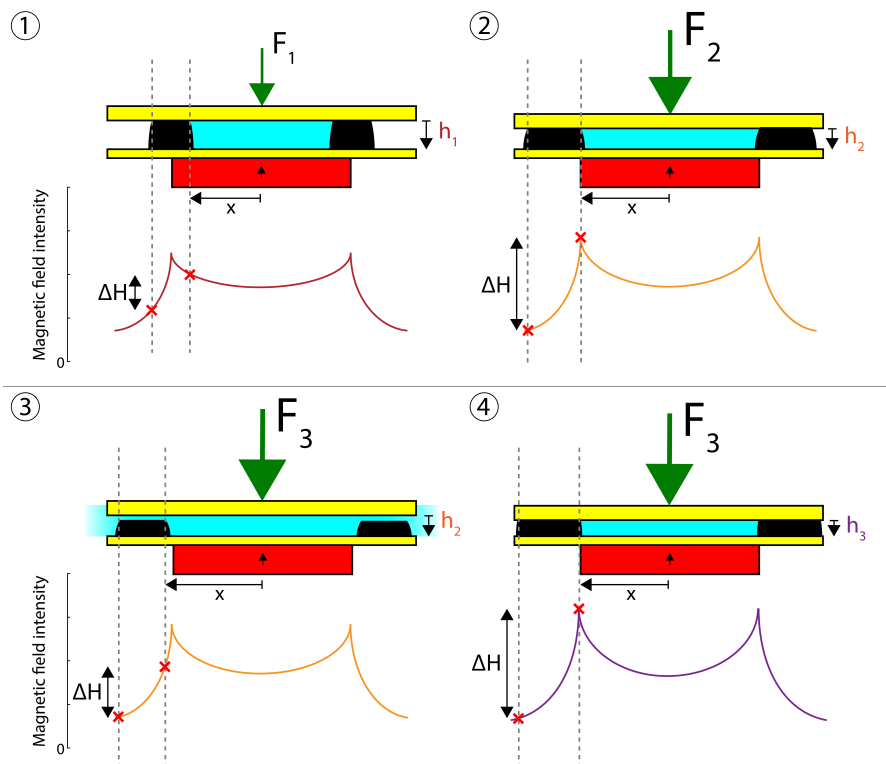Figure 2.2: Effect of increase in payload in ferrofluid pocket bearing with magnetic field intensity at the interface of the ferrofluid with the top bearing surface. Red indicates the magnet, the ferrofluid is indicated using black, the bearing surfaces are yellow and the enclosed air pocket is cyan.

The load capacity of the pocket bearing is defined in equation 2.3 [23] in which p_i and p_o are the

pressures in the pocket and outside respectively, ΔH is the difference in magnetic field intensity at the inner and outer seal interface and A_p is the area of the enclosed pocket. These terms can be seen in figure 2.2. In this formula the contribution to the load capacity of the ferrofluid itself is assumed negligible, this is valid for larger pockets with limited amount of ferrofluid.

$$F_L = (p_i - p_o)\, A_p = \mu_0 M_s \Delta H A_p \tag{2.3}$$

By looking at the magnetic field intensity in figure 2.2 and by using equation 2.3 [23], the behaviour of the pocket bearing can be explained. As the load is increased from 1 to 2, the height is reduced from h_1 to h_2. As the air in the pocket is relatively stiff in comparison to the seal, the seal is displaced outwards to maintain a constant air volume. Due to this displacement ΔH increases and as a result the normal force on the top bearing surface is increased. When the load is further increased to F_3 the seal is forced outwards even further, this time the ΔH is reduced. Thus, the seal will fail and some volume of air will be expelled from the pocket. When h_3 is reached, the top bearing surface has moved closer to the magnet, increasing the magnetic field intensity enough to seal the pressure needed to bear the load F_3. The process between 1 and 2 is reversible because the pocket volume remains constant. Between 2 and 4, some pocket volume is expelled and thus the fly height is permanently reduced.

The stiffness of the pocket bearing can be calculated using equation 2.4 in which x is the location of the seal. Due to the constant pocket volume the height of the pocket can be related to the width and thus the location of the seal, this relation can be seen in the equation by the term $\dfrac{dx}{dh}$. As a result, this equation is only valid for a compression without loss of air from the pocket.

$$k = -\mu_0 M_s \frac{dx}{dh}\frac{d\Delta H}{dx} A_p \tag{2.4}$$

2.1.3. Comparison of bearing type
Literature shows that in comparison to the pressure bearing, the pocket bearing has higher load capacity and stiffness due to the creation of a pocket. The damping of a pocket bearing is lower due to less fluid in contact with the bearing surfaces. However, due to the variable pocket volume, this performance comes at the cost of a bad repeatability in the fly height [24, 46, 47].

There can be dealt with the loss of air by preventing the air from escaping or restoring the air in the pocket. Prevention of air loss can be done using a mechanical stop that prevents a larger displacing than the pocket seal can handle. Restoring the air in the pocket can be done by taking the bearing surfaces apart, allowing air to flow back into the pocket and then reassemble the bearing. An alternative would be to supply pressurized air to the pockets through a system incorporated in the base or mover.

However, these solutions have very significant downsides. The mechanical stop would require very tight tolerances and doesn't guarantee the pocket volume is constant, as the load capacity is dependent on other factors such as translation velocity. Air can also slowly diffuse through the ferrofluid. Restoring the air requires a system sensing when air is lost, thus complicating the bearing system. Using pressurized air to restore the volume of air in the pocket would require an active system, neutralizing the benefit of a passive bearing.

Another downside of the pocket bearing is the need for a uniform magnetic field. The seal is only as strong as its weakest point. Thus, care must be taken not to place other magnets close to the seal and sharp corners in the seal must be avoided as they can form weaknesses. Usually a ring magnet is taken to provide a uniform magnetic field. Pressure bearing pads can be formed more freely as they don't require the integrity of a seal.

The pocket bearing has since been optimized by Boots [7]. No literature was found on the optimal configuration of pressure bearings, leaving a knowledge gap and room for improvement.

While the pocket bearing is better at load capacity, stiffness and has a lower damping, the pressure bearing has a higher repeatability, can be formed more freely, can be used in close proximity to other

magnetic fields and can potentially be optimized to increase performance. This makes the pressure bearing the preferred bearing type for this application.

2.2. Trail formation

Figure 2.3 shows the trail of a pocket bearing after translation. The trail is formed when the shear force overcomes the magnetic body force acting on the ferrofluid. The shear force is a function of viscosity and the flow profile in the ferrofluid between the bearing surfaces. The magnetic body force is determined by the saturation magnetization of the ferrofluid and the derivative magnetic field intensity in translation direction at the ferrofluid interface. Without compensation, the loss of FF results in a loss in fly height as there is less pressurized ferrofluid and thus less normal force, which in turn increases the damping in the system. Eventually the continued loss of FF will result in contact between the bearing surfaces, thus limiting the stroke of the bearing [24, 47].

Figure 2.3: Trail formation underneath a glass plate supported by a pocket bearing. Figure from [22].

As the flow between bearing surfaces, especially the begin and end of the bearing are not fully understood. The exact amount of flow towards the trail is hard to predict. Nevertheless, as the variables are known and their role in the trail formation itself, some remarks to reduce the trail formation can be given. To reduce trail formation either the shear force has to be reduced or the magnetic body force has to be increased. To reduce the shear force on the ferrofluid, the viscosity and velocity can be lowered. The magnetic body force can be increased by increasing the gradient of the magnetic field intensity in the movement direction. The gradient can be increased by placing iron next to the magnet or by using magnets with a higher remanent flux density. A different way to increase the magnetic body force is to increase the saturation magnetization of the ferrofluid.

To ensure performance of the stage it is important the ferrofluid that is lost due to trail formation is not essential for the load capacity. This can be ensured by creating a reservoir from which the bearing can draw to replace the ferrofluid that is lost. This reservoir can either be located on the base or on the mover. The ferrofluid level can be controlled passively by gravity, capillary forces or magnetic forces. The worst possible fluid loss can be found by integrating a Couette flow between the bearing surfaces. This is illustrated in figure 2.4. The volume of the fluid loss (V) then results from equation 2.5.
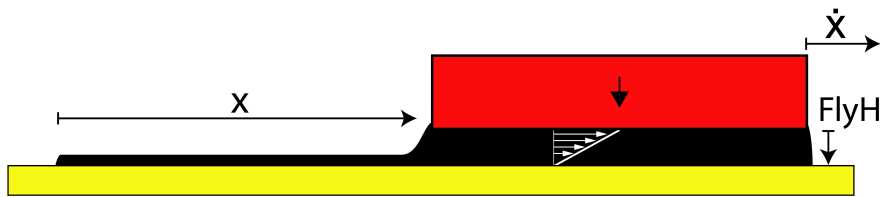
Figure 2.4: Trail formation in cross-section of a ferrofluid bearing with the in-plane width W, displacement x, velocity $\dot{x}$ and the distance between bearing surfaces $FlyH$. The Couette flow of the fluid is drawn inside the ferrofluid.

$$V = \frac{x}{\dot{x}} \int_0^{FlyH} \left(\frac{\dot{x}}{FlyH} * h \right) dh \cdot W \tag{2.5}$$

Equation 2.5 can be simplified to equation 2.6. Using realistic values for the parameters: $FlyH = 2.5 * 10^{-4}\,m$, $W = 0.1\,m$, $x = 0.3\,m$, the volume of the ferrofluid loss would be a maximum of 7.5 ml. As

the ferrofluid loss is relatively small, the magnet of the bearing itself can be used to control the ferrofluid reservoir.

$$V = \frac{1}{2}x \cdot FlyH \cdot W \tag{2.6}$$

For the sustained use of the stage it is important that the lost ferrofluid is collected by the mover. Ferrofluid close to the magnet will flow back to the magnet, driven by the gradient in the magnetic field. As the gradient in the magnetic field exponentially decays with the distance away from the magnet, to create a meaningful flow of ferrofluid at distances of several centimetres a powerful magnet would be required. For longer strokes this will be a problem, as the required magnets create significant stray flux and will interact with magnetic objects outside the stage. A solution would be to translate the mover back over the trail to absorb it. This system has as an issue that gravity also works on the ferrofluid. As a result, it requires a magnet at the lowest point in the bearing and the magnets to be configured such that the ferrofluid can move between them.

A different solution to the loss of ferrofluid would be a number of collection magnets incorporated into the base. This would be a magnet with a small cross section but spanning the whole stroke in length. These magnets collect the trail and redistribute it over the length of the bearing. Close proximity of the collection magnets and the magnets in the bearing would allow for the transfer of ferrofluid. This system can double as a ferrofluid reservoir. However, a severe downside of this system is the need for a uniform magnetic field over the full length of the stroke. Any imperfection in the magnetic field will cause unwanted stiffness or cogging to occur.

2.3. Ferrofluid

The properties of the ferrofluid are dominant in the performance of the stage, the damping of the mover is proportional to the viscosity of the ferrofluid [22], and the load capacity and stiffness are proportional to the saturation magnetization of the ferrofluid (equations 2.1 to equation 2.4). Thus, care has to be taken in choosing the ferrofluid. The most important properties are viscosity, saturation magnetization and vapour pressure of the carrier liquid. These properties are highly interlinked.

The vapour pressure and viscosity are interlinked through the intermolecular force (IMF). A decrease in the IMF increases the vapour pressure and decreases the viscosity, thus generally a decrease in vapour pressure results in an increase in viscosity [17]. Formulas 2.7 [21, 40] and 2.8 show the relation between the other properties. Here η is the viscosity of the FF, η_0 the viscosity of the carrier fluid, F_{SP} is the fraction of solid phase, R and ϕ_{max} are constants in the Krieger-Dougherty function. M_s is the saturation magnetization of the ferrofluid and Ms_{solid} the magnetization saturation of the solid material.

$$\eta = \eta_0 \left(1 + \frac{3}{2}F_{SP}\right)\left(1 - \frac{F_{SP}}{\phi_{max}}\right)^{(-R*\phi_{max})} \tag{2.7}$$

$$M_s = Ms_{solid} * F_{SP} \tag{2.8}$$

For the solid material in ferrofluids generally magnetite (Fe_3O_4) is chosen, which has a saturation magnetization of around 0.6 T for bulk material. Although other magnetic materials exist with a higher saturation magnetization such as FeCo (2.4 T), Fe (2.15 T) or Co (1.8 T) the particles are more expensive in manufacturing and prone to oxidation when exposed to the atmosphere [16, 39]. However, the latter doesn't have to be a problem in a vacuum or inert atmosphere.

2.3.1. Evaporation

The amount of evaporation is, aside from the vapour pressure of the carrier fluid, dependent on the surrounding pressure, temperature of the ferrofluid and surface area. As time progresses, the carrier fluid will slowly dissipate until eventually only the solid fraction remains. The influence of the evaporation on the viscosity and magnetization saturation can be deduced from equations 2.7 and 2.8. The

fraction of solid phase will increase due to the evaporation of the carrier fluid and thus the viscosity and magnetization saturation as well. Furthermore, the increased fraction of solid phase will increase chain formation and will eventually start to affect the colloidal stability [30]. As this affects the performance of the stage, measures have to be taken to prevent it.

In order to safeguard the performance of the stage overtime, either the evaporation rate must be low or the effects of evaporation must be countered. The most obvious way to reduce evaporation is to reduce the vapour pressure of the carrier fluid. This is necessary for use of the bearing in (near) vacuum conditions. However, this comes at the price of higher viscosity which is unwanted because of the damping and higher trail formation. If a more volatile carrier fluid can possibly be used with a system that replaces the evaporated carrier fluid, a constant composition of the FF can be assured. This would be the equivalent of lubrication in a regular bearing.

2.3.2. Damping
The primary damping source in the system is the energy dissipation in the ferrofluid under translation. A second source of damping is the Eddy current damping. Both damping sources are a proportional to the velocity, as a result no static friction is present in the system. The presence of this damping is beneficial to the control of the stage.

A limited amount of damping is beneficial for the system. The negligible damping air bearing systems causes severe problems with controlling the system, even leading to research into the addition of damping [43, 44]. The problems are caused by the relatively low stiffness in the actuation direction combined with the mass of the mover and the low damping. This creates an underdamped resonance peak at a relatively low frequency. In order to prevent this resonance frequency from being excited in a proportional controller, the input to the actuator has to be shaped. This makes for a relative slow system. An increase of the performance by adding a derivative term to the controller minimizes tracking error but aggravates tuning [38]. Care has to be taken to attenuate sensor noise in establishing the derivative as this can excite the underdamped resonance frequency as a result [10].

The fluid damping in the ferrofluid bearing has been researched by Lampaert [22]. Equation 2.9 shows the relation between the fluid damping C, the viscosity of the ferrofluid η and the fly height $FlyH$ according to Lampaert.

$$C = 4\eta \cdot \frac{A}{FlyH} \tag{2.9}$$

The used model is a Couette flow with pressure gradient. Among others, this equation results from the assumption of zero fluid loss. In real world application there will be trail formation, and thus fluid loss, resulting in lower damping. From the formula, different ways to reduce or increase the damping are observed. The damping can be reduced by reducing ferrofluid viscosity and the bearing surface area or by an increase in fly height. A change in the flow profile can also reduce the damping. Figure 2.5 shows how the flow profile can be manipulated by allowing for the ferrofluid to recirculate. The bearing configuration on the left can have up to four times lower damping than the configuration on the right though. In practice the reduction in damping will be less, as the recirculation will also cause a pressure drop, and therefore the flow profile will not be exact that of a Couette flow. A secondary beneficial effect of the recirculation is a reduction of the shear force on the ferrofluid, thus reducing the amount of trail formation.

2.3.3. Evaluation of ferrofluid
Thus, the choice of ferrofluid inherently is a trade-off between primarily viscosity, saturation magnetization and vapour pressure. For this research the kerosene based EFH3 and ester based APG 513A ferrofluids from Ferrotec are used. The EFH3 is chosen for its relatively high saturation magnetization of 66 mT and low viscosity of 12 mPa·s [11]. The APG 513A is chosen for its well described behaviour in literature and has a saturation magnetization of 44 mT with a viscosity of 150 mPa·s [13]. As the APG 513A is ester based it has a lower vapour pressure than the kerosene based EFH3, it will have a lower evaporation rate [45]. Still, the vapor pressure in both ferrofluids can't be considered negligible, thus the effects of evaporation need to be considered.
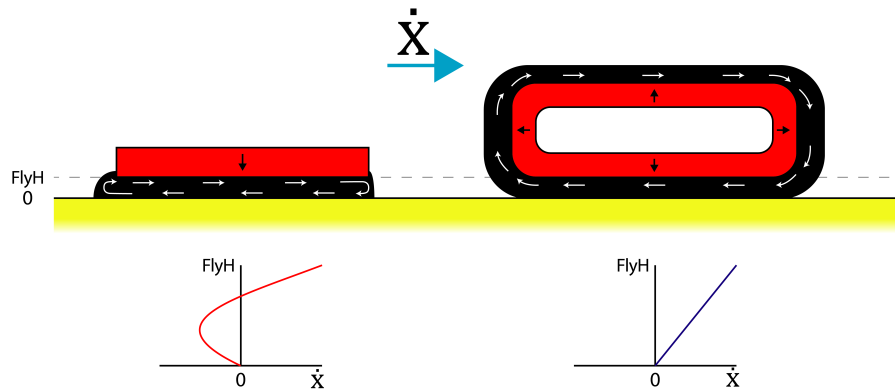
Figure 2.5: Flow profile comparison between the flow in a magnetic fluid bearing according to Lampaert and the flow in a bearing with recirculation.

2.4. Summary

This section summarizes the choices made in this chapter:

- The ferrofluid pressure bearing will be used in the long stroke stage, as it has a higher repeatability, can be used in close proximity to other magnetic fields and can potentially be optimized to increase performance.

- The trail formation problem will be addressed by the creation of a ferrofluid reservoir. As back-of-the-envelope calculations show the fluid loss is relatively small, the design will be based on a reservoir on the mover, potentially using the magnets of the bearing patch to contain the reservoir.

- To eliminate the effects of evaporation, research is done into the restoring of the ferrofluid performance after evaporation by addition of carrier fluid.

- The relatively high damping in the ferrofluid stage aids in the controllability of the stage, the possibility of a recirculation path in the ferrofluid bearing will be investigated.

- The EFH3 and the APG 513A ferrofluids from Ferrotec are chosen for use in this study. The EFH3 is chosen for its relatively high saturation magnetization and low viscosity and the APG 513A is chosen for its well described behaviour in literature.

3

Paper: Design considerations for ferrofluid pressure bearing pads

Design considerations for ferrofluid pressure bearing pads

Stefan W.M. van den Toorn[a], Jo W. Spronck[a], Ron A.J. van Ostayen[a] and Stefan G.E. Lampaert[a]

[a]Department of Precision and Microsystems Engineering, Delft University of Technology, Delft, The Netherlands

ARTICLE INFO

ABSTRACT

This research discusses different magnet configurations to improve the load and stiffness of a ferrofluid pressure bearing. It is shown that magnets with a small cross-section magnetized alternatively up and downwards combine a high load capacity and moderate stiffness while being low on material cost and complexity. Magnets magnetized alternatively left-right alternated with iron give the highest load capacity and stiffness, albeit at the cost of weight and complexity. It is shown that an increase in the number of magnets and is beneficial for the stiffness in both magnetization configurations, as is an increase in remanent flux density of the magnet. A metal bottom plate made of iron reduces the necessary height of the magnet in the up-down magnetization configuration. The model was validated using bearing pad arranged in the up-down configuration. The force-displacement curve of this pad was measured in a load frame, using the APG 513A ferrofluid from Ferrotec. A load capacity of 1.75 N/cm^2 was achieved, this exceeds previous pressure bearing implementations and performs comparable or better than implementations of single seal ferrofluid pocket bearings. Thus, making this the ferrofluid pressure bearing a passive alternative in motion systems where the designer otherwise would have had to use an active bearing.

1. Introduction

Bearings regularly used in precise positioning systems suffer from high cost, need for active components or the presence of stick-slip[1]. The stick-slip phenomenon prevents a smooth continuous motion of the bearing, especially at low speeds[2]. The ferrofluid bearing has none of these issues and thus could be an interesting alternative.

The ferrofluid bearing consists out of a magnet array and a magnetic fluid. This fluid is a colloidal suspension consisting of magnetic particles in a carrier fluid[3]. In a magnetic field these particles are drawn to the highest field intensity and as a result produce a pressure in the fluid. A bearing can be created by placing the fluid in a magnetic field in between two bearing surfaces[4]. As the bearing is loaded, the surfaces move closer together and the fluid is displaced from the equilibrium position, which in turn inducing a reaction force. This is called the ferrofluid pressure bearing. Alternatively, the pressure in the fluid can be used to seal a pocket of air and a displacement of the bearing surface will pressurize this air resulting in a normal force. This is called the pocket bearing[5].

Figure 1 shows the working principle of the ferrofluid pressure bearing. Using equation 1 and 2 the load and stiffness of the pressure bearing can be calculated[6]. In these formulas F_L is the load capacity, μ_0 the permeability in vacuum, M_s the saturation magnetization of the ferrofluid and H the magnetic field intensity. The area is defined as the surface area of the ferrofluid on the top bearing surface. It can be seen in figure 1 that an increase in payload causes the bearing surfaces to move closer together, thus increasing the area over which the integral is taken, as well as the increasing the overall magnetic field intensity. In practice only the latter will be significant as the outer fluid edge is at low
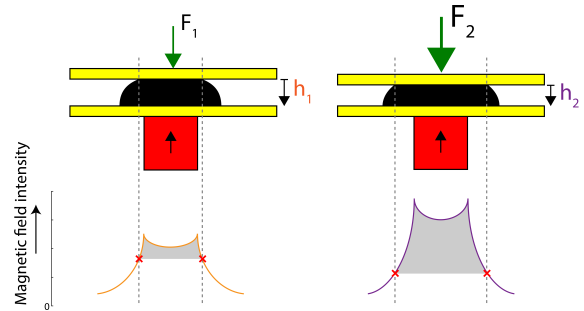
✉ s.w.m.vandentoorn@student.tudelft.nl (S.W.M.v.d. Toorn)
ORCID(s):

Figure 1: Effect of increase in payload in ferrofluid pressure bearing with magnetic field intensity at the location of the top bearing surface. With $F_1 < F_2$ and $h_1 > h_2$

magnetic field intensity.

$$F_L = \mu_0 M_s \int_S H \, dA \qquad (1)$$

$$k = -\mu_0 M_s \frac{d}{dh} \int_S H \, dA \qquad (2)$$

Although ferrofluid pressure bearings can be found in literature[4,7,8], the actual implementation of this bearing type is very limited in load capacity and stiffness[9–12]. When an application demands a certain load capacity and stiffness the ferrofluid pocket bearing is seen as the preferred bearing type[5], although in comparison with the pocket bearing, the out of plane repeatability of the pressure bearing is much higher as no air can escape. For a similar surface area, a pressure bearing will also have more tilt stiffness. While the optimal configuration of pocket bearings has been researched by Boots[13], this has yet to be done for the pressure bearing.
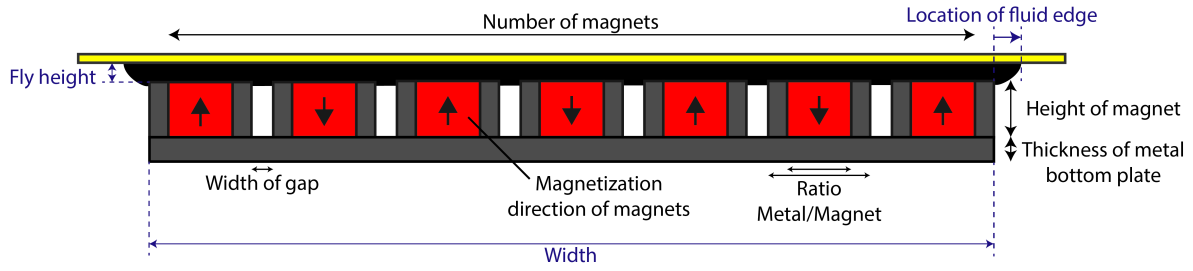
Figure 2: Design variables (black) and model constants (blue) in a cross-section of the bearing pad. The length of the pad is defined into the plane.

Table 1
Design variables and their respective ranges.

Variable	Symbol	Type	Range	Unit	Range based on
Number of magnets	N_{mag}	Discrete	1-50	-	Manufacturability
Magnetization direction of magnets	Mag_{dir}	Discrete	↑↓, ↑↑, ↑←, ←→	-	Assumed optimum
Width of gap	W_{gap}	Continuous	0-3	mm	Assumed optimum
Ratio metal/magnet	$R_{\frac{Met}{Mag}}$	Continuous	0-0.5	-	Assumed optimum
Thickness metal bottom plate (MBP)	H_{mbp}	Continuous	0-2	mm	Assumed optimum
Height of magnet	H_{mag}	Continuous	0.5-4	mm	Manufacturability
Remanent flux density of the magnet	Mag_{str}	Continuous	1.1-1.5	T	Manufacturability

Table 2
Model constants.

Constant	Value	Unit
Width	50	mm
Length	100	mm
Fly height	0.1	mm
Relative permeability ferrofluid	1	-
Saturation magnetization ferrofluid	52.5	kA/m
Relative permeability metal	4000	-
Saturation magnetization metal	1.4	T
Relative permeability magnets	1	-
Location fluid edge	5	mm

The optimal pressure bearing consists of an optimal fluid in an optimal magnetic field. Research has been done on the magnetic fluid. Although not specifically for bearing applications, there are some fluids that are well suited. Less is known about the optimal magnetic field. The purpose of this paper is to give an insight in the design of the magnetic field for application in a pressure bearing pad and to provide a direct comparison between the pressure and pocket bearing.

2. Modelling of pressure bearing pad

The magnetic field can be manipulated by arranging multiple magnets in relation to each other with the addition of metal with high permeability. In order to obtain an understanding of the influence of the different variables, a model has been made.

The pressure bearing model is based on a 2D simulation of a cross-section of the bearing pad using COMSOL Multiphysics[14]. This simulation assumes the bearing pad continues infinitely in and out of the plane as seen in figure 2. Using the LiveLink interface, a COMSOL model is parametrically coded in Matlab[15], then run in COMSOL and again post processed in Matlab. In this model several variables were varied, these are listed in figure 2 and table 1. The Halbach magnetization configuration was left out as it produces a constant field with little gradient, which would result in a low stiffness bearing[16]. The build volume was taken to be 50x100x4 mm (width x length x height), the length being defined as in and out of the plane as seen in figure 2. The used constants in modelling the pressure bearings can be seen in table 2 and figure 2. As the minimum fly height is dictated by manufacturing tolerances and damping, it is set at 0.1 mm for all parameter configurations. The error in simulation caused by the finite bearing length is evaluated in a 3D model and found to be negligible. For the metal between the magnets and for the bottom plate iron has been chosen for its high permeability and saturation magnetization. The gaps are modelled as air.

The width of the metal and magnets is defined using the variables and can be found using equation 3 and 4 respectively. The definition of the symbols used can be seen in table 1.

$$W_{mag} = \left(Width - W_{gap} \left(N_{mag} - 1 \right) \right) \frac{1 - R_{\frac{Met}{Mag}}}{N_{mag}} \quad (3)$$

$$W_{met} = \frac{1}{2} R_{\frac{Met}{Mag}} W_{mag} \quad (4)$$

Table 3
Optimized magnet configuration for stiffness subjected to constraints: load capacity > 100N, cost < €50, weight < 150 grams. Using the constants in table 2. Fly height for all configurations is 0.1 mm.

Variable	Values	Unit	Up-Down	Up-Up	Up-Left	Left-Right
Magnetization direction of magnets	↑↓, ↑↑, ↑←, ←→	-	Up-Down	Up-Up	Up-Left	Left-Right
Number of magnets	5, 15, 30, 40, 50	-	50	30	30	50
Remanent flux density of the magnet	1, 1.15, 1.3, 1.5	T	1.5	1.5	1.5	1.5
Height of magnet	1, 2, 3	mm	1	1	2	3
Ratio metal/magnet	0, 0.2, 0.4	-	0	0.4	0.2	0.4
Thickness metal bottom plate	0, 1	mm	1	1	0	0
Width of gap	0, 0.1, 0.2	mm	0	0	0.2	0
Material cost		€	24.19	17.28	35.64	51.83
Weight		g	77.5	78.2	67.0	114.6
Load capacity		N	149.63	117.09	128.22	216.46
Stiffness		N/μm	0.52	0.52	0.68	0.76

2.1. Initial optimization

To gain an initial understanding, a parameter sweep performed using several evaluation points in the range of each variable. From the parameter sweep could be concluded that the magnetization direction of the magnets has a great influence on the design of the bearing pad. The results of the parameter sweep were used in an optimization for stiffness. Constraints were added using a penalty method. The imposed constraints were a minimum load of 100N, a maximum weight of 150 grams and a maximum material cost of €50. These constraints are based on a linear stage design where the pressure bearing pads are placed on the mover. Equation 5 relates the cost of the magnetic material per gram (Υ) as a function of the remanent flux density of the magnet (M_{str}).

$$\Upsilon = \left(2.4 \cdot 10^{-3}\right) e^{3.7293 \cdot M_{str}} \tag{5}$$

This function was determined based on data from the online design tool of HKCM[17]. The material cost of metal was assumed to be negligible. Table 3 shows the results of the parameter sweep for different magnet magnetization directions. Some interesting things can be seen:

- All magnetization directions use the highest remanent flux density of the magnet available.

- A gap in between magnets is unwanted in all magnetization directions except up-left, this is a result of a slight increase in stiffness as the gap increases.

- The up-down magnetization array is relatively simple compared to the others, no additional ferromagnetic material or gaps are used.

- The left-right magnetization direction shows the best performance. This however comes at the cost of complexity as small features are required. Much material is required relative to the other magnetization directions, resulting in a higher weight.
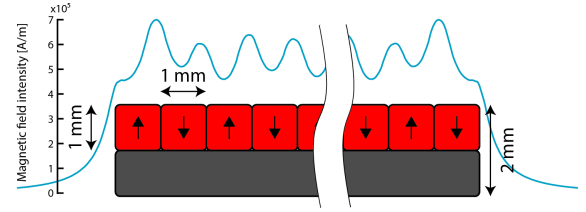

Figure 3: Magnet configuration for up-down magnetization direction with magnetic field intensity at 0.1 mm above magnet surface.

From the initial parameter sweep thus can be concluded that each magnetization direction produces a different optimal configuration of magnets, metal and gaps. The choice of magnetization direction is based on the trade-off between weight, material cost, load capacity, stiffness and complexity. The up-down magnetization configuration for the relatively low material cost and complexity while still having a moderate load capacity. The combination of low material cost and low complexity can result in a very cheap to produce bearing design. The absence of gaps and metal makes for a potentially monolithic producible bearing. The magnetization can then be 'written' on a single block of Ne-Fe-B[18–20]. A single magnet block can significantly reduce assemblage as well as improve tolerances. The up-down and left-right magnetization configurations are both suited for bearing applications and they will be discussed next.

2.2. Up-down magnetization configuration

Figure 3 shows the magnet configuration using the variables in table 3 with the magnetic field intensity at 0.1 mm. The neighbouring magnets provide a low reluctance path which results in a spike in the magnetic field intensity. Due to the large number of magnets, many low reluctance paths are created. This moves the overall magnetic field intensity closer to the magnet, increasing load capacity and stiffness.

Table 4
Logarithmic sensitivity of an increase in the individual variables for the stiffness of the up-down magnetization configuration.

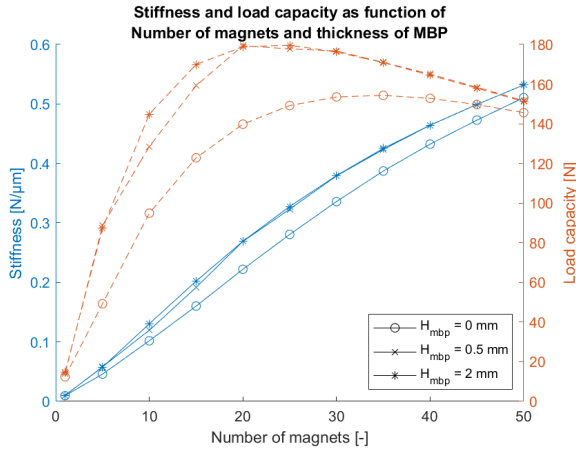|	N_{mag}	W_{gap}	H_{mag}	$R_{\frac{Met}{Mag}}$	Mag_{str}	H_{mbp}	Fly height
Stiffness	0.843	-0.002	0.113	-0.010	1	0.002	-0.282
Load capacity	-0.138	-0.001	0.105	-0.008	1	0.002	-0.280

Figure 4: Stiffness and load capacity as a function of the number of magnets for different thicknesses of the metal bottom. For up-down magnetization configuration.

Figure 5: Stiffness and load capacity as a function of the remanent flux density of the magnet for different heights of the magnets. For up-down magnetization configuration. The lines for magnet height of 0.75 mm and 1 mm coincide.

Table 4 shows the effect of the different variables on the stiffness normalized using logarithmic sensitivity. The sensitivities are determined around the up-down configuration in table 3. As the gap and the factor metal/magnets are already minimal, only the number of magnets, height of magnets, remanent flux density and fly height can improve the stiffness of the bearing. Use of a metal bottom plate has no significant effect on the bearing performance but does add moving mass if the bearing pads are mounted on the mover. An increase in the number of magnets also decreases the load capacity. Thus, a compromise has to be made.

Figure 4 and figure 5 show the influence of the different variables on the stiffness and load capacity. The metal bottom plate is more efficient for a lower of magnets. A relative thin bottom plate of 0.5mm is enough to prevent effects of saturation. Figure 4 again stresses the stresses the importance of many small magnets. It can be seen that the optimum for load capacity lies around 20-25 magnets. The optimum for stiffness however is located outside of the graph. From figure 5 we see that the stiffness and the load capacity scale linearly with the remanent flux density of the magnet. The height of the magnets shows an optimum around 1mm. Further increase of the height reduces the stiffness slightly.

Figure 6 shows the relation between the height of the magnets and the bearing performance for different thicknesses of the MBP. Up to 25% performance gain can be achieved by only 0.5 mm MBP thickness. It can be seen that in most cases it is more economical efficient to use less magnetic material and a thin MBP. Figure 5 and figure 6 contain all
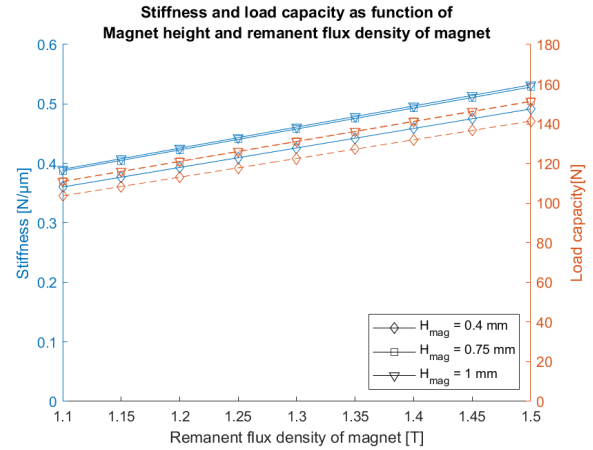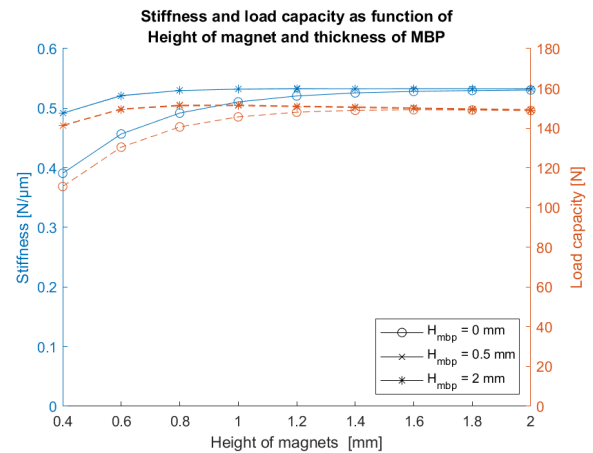

Figure 6: Stiffness and load capacity as a function of height of magnet for different thicknesses of the metal bottom plate. For up-down magnetization configuration. The lines for 0.5 mm and 2 mm bottom plate thickness coincide.

significant variables concerning the respective material cost and weight. It can be seen that a cost-effective bearing is to favour remanent flux density of the magnet over magnet height, while using a metal bottom plate. The same goes for optimizing towards weight, thin magnets combined with a thin MBP.

Table 5
Logarithmic sensitivity of an increase in the individual variables for the left-right magnetization configuration.

	N_{mag}	W_{gap}	H_{mag}	$R_{\frac{Met}{Mag}}$	Mag_{str}	H_{mbp}	Fly height
Stiffness	0.548	-0.012	0.343	-0.063	1	-0.006	-0.550
Load capacity	-0.590	-0.089	0.551	-0.146	1	-0.006	-0.284
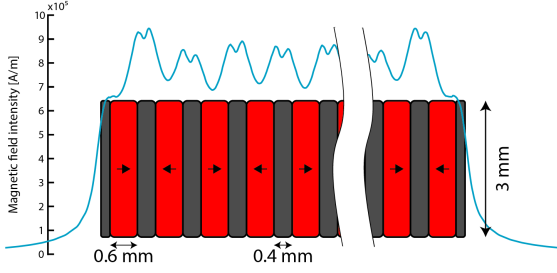
Figure 7: Magnet configuration for left-right magnetization with magnetic field intensity at 0.1 mm above magnet surface.

Figure 9: Stiffness and load capacity as a function of the remanent flux density of the magnet for different heights of the magnets. For left-right magnetization configuration.

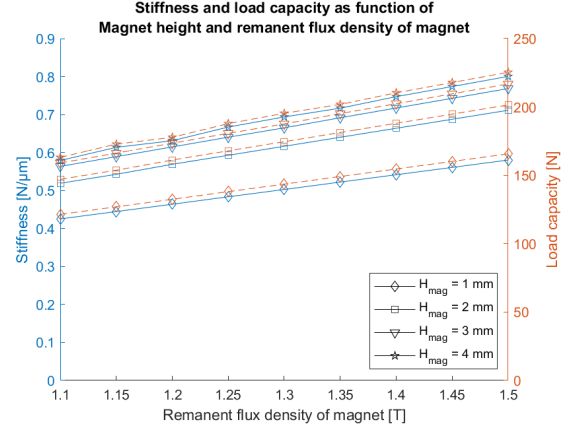**Figure 8:** Stiffness and load capacity as a function of the number of magnets for different ratios of metal/magnet. For left-right magnetization configuration.

2.3. Left-right magnetization configuration

Figure 7 shows the left-right magnetization configuration for the values of the variables in Table 3. The study from the previous section is repeated here for the left-right magnetization configuration.

Table 5 shows the logarithmic sensitivity of the stiffness for the different variables with the configuration in table 3 as initial value. The width of the gap and thickness of the MBP are already zero, thus the ideal configuration doesn't include gaps or an MBP. The response of the load capacity and stiffness on change in the height of the magnet, number of magnets, factor metal/magnet and remanent flux density of the magnet are shown in Figure 9 and Figure 10.

The same dependence of the number of magnets can be observed in figure 8 as with the up-down configuration. There is a distinct difference in the optimum of the load capac-

ity and the stiffness. The addition of metal in between the magnets shows an increase in bearing performance. Some metal is needed to guide the magnetic field. Increasing of the width of this metal reduces the amount of magnetic material in the bearing configuration eventually leading to a reduction of performance. Figure 9 also shows similar behaviour for the remanent flux density of the magnet compared to the up-down configuration.

As the specific weight of neodymium magnets and metal are very similar, the weight of the configuration is determined by the height of the magnets. The material cost is determined by the remanent flux density of the magnet, height of magnets and the factor metal/magnet.

From the influence of the specific variables can be concluded that the configuration using a left-right magnetization depends largely on the cost and weight constraints. As the MBP reduces the bearing performance, remanent flux will be larger using this type of bearing. The stability will also be an issue when choosing a configuration with a small metal/magnet factor.

3. Method for validation

A materials test frame is used to validate the model of the pressure bearing pad. This is done by a fly height sweep of a pad made up of 23 magnets with the dimensions 50x2x2mm (LxWxH) and a remanent flux density of 1.17 T[21]. The magnets are arranged in the up-down magnetization configuration. The pad is placed on a ferritic stainless-steel (AISI 410s) bottom plate and is filled with 5 grams of either the
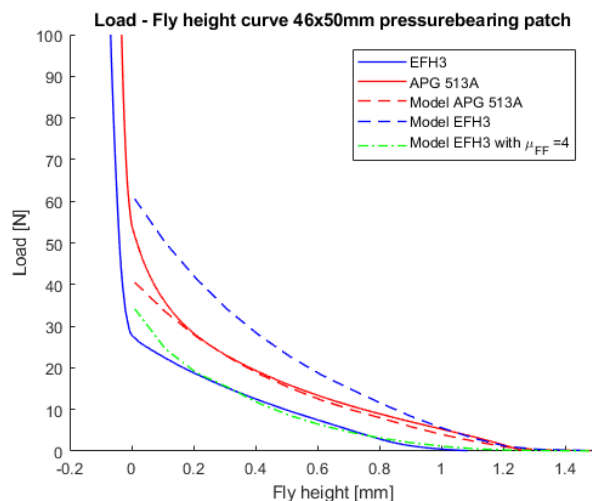
Load - Fly height curve 46x50mm pressurebearing patch

Figure 10: Load-fly height curve of pressure bearing pad with EFH3 and APG 513A ferrofluid and modelled performance of the ferrofluid. pad consists of 23 50x2x2mm magnets from HKCM[21] arranged in up-down configuration. The remanent flux in the magnets is 1.17T, the location of fluid edge is modelled 0.9 mm outside magnet.

EFH3 or the APG 513A ferrofluid.

Both the APG 513A and EFH3 fluid are manufactured by Ferrotec. The APG 513A fluid is chosen as its common in literature and its properties are well known.[22] The EFH3 fluid is chosen for its high magnetic saturation and low viscosity, making it a more suitable ferrofluid for use in bearings in comparison to the APG 513A.

The load of the bearing at the same fly height sweep is modelled. The magnet dimensions, pad dimensions and remanent flux density are modelled as described above. As the location of the ferrofluid edge is found at the point where the magnetic body force acting on the fluid is overcome by the gravity force, it can be determined using a COMSOL simulation of the magnetic field surrounding the bearing pad. This location was found at 0.8 mm outside the bearing pad for the APG 513A fluid and 0.9 mm for the EFH3 fluid. The magnetic saturation of the ferrofluids are set to 32 kA/m for the APG 513A fluid[22] and 52.5 kA/m for the EFH3 fluid[23].

4. Results and discussion

Figure 10 shows the results of the of the fly heights sweep and the calculated load capacity according to the model. Zero fly height was taken to be the point at which the pressure plate touches the magnets in the measurement.

The modelling of the bearing pad using the APG 513A fluid is in close agreement with the measurement. There is a slight divergence of the model and measurement as the fly height approaches zero that can be explained by the squeeze film damping from the relatively viscous (150 mPa·s) ferrofluid.

As can be seen in formula 1, the load capacity of a bear-

ing pad should be proportional to the saturation magnetization. This can be observed when looking at the modelled load vs fly height curve for the APG 513A and EFH3 ferrofluid. When looking at the measurements it can be seen that while the APG 513A measurement and model are in good agreement, the same is not true for EFH3 measurement and model.

The probable cause of this difference is the accumulation of magnetic particles in areas of high magnetic field gradients. The largest gradients in the bearing pad are located at the corners in between two magnets. Accumulation of the magnetite particles there causes effectively a short circuit of the magnetic field, reducing the magnetic field elsewhere. A relatively good approximation of the accumulation can be done by increasing the relative permeability of the ferrofluid, this can be seen in the dash-dot line in figure 10.

The APG 513A fluid achieves a load capacity of 1.75 N/cm^2. This bearing configuration exceeds previous implementations of pressure bearings[9,24,25] and performs comparable or better than implementations of single seal pocket bearings[26–28]. Still, pocket bearings can be made with an even higher load capacity by stacking seals. The downside of this bearing design is the creation of more pockets of air that all need to be managed in order to have a repeatable stage behaviour.

5. Conclusion

The orientation of the different magnets in relation to each other is an important variable in the design op pressure bearing pads. Two distinct magnetization configurations both prove promising. The up-down magnetization configuration for its simplicity, and the left-right configuration for performance.

The up-down magnetization configuration consists out of an array of magnets combined with a metal bottom plate. The number of magnets is the most important variable in this configuration, combined with the remanent flux density of the magnet. Higher amounts of magnets slightly reduce load capacity, but offer more stiffness in return. Current state of the art allows for the 'writing' of the magnetization in the magnets, this technology can allow for monolithic pressure bearings[19,20].

In the left-right magnetization configuration instead of providing low reluctance paths like in the up-down magnetization configuration, the magnets counteract each other. This can prove problematic as the configuration can become instable when designing with a small metal/magnet ratio. This configuration though potentially has more stiffness and load capacity compared to the up-down magnetization configuration.

In the bearing design, cost and weight are important factors. Due to the low height of the magnets required and the ability to be produced monolithically, the up-down configuration performs the best in cost effectiveness and weight effectiveness. If the cost and weight are of less importance the left-right magnetization configuration is the better choice.

The model is validated for use with the APG 513A ferrofluid. The EFH3 fluid shows effects that can be linked to accumulation of particles at the magnet surface. Using the APG 513A ferrofluid a load capacity of 1.75 N/cm^2 was achieved. Potentially this can be higher when the bearing pad is combined with a ferrofluid with a high magnetization saturation and a high colloidal stability in order to prevent accumulation.

The bearing pad that is created using the design guidelines developed in this paper can be used instead of single seal pressure bearing pads without a loss in load capacity, but with an improvement in the repeatability in fly height. Although some precision systems require more load capacity and stiffness, the achieved performance will satisfy the demands in many applications.

This paper has given insight into the variables that go into the design of a pressure bearing pad. This ferrofluid bearing pad is a passive alternative bearing to motion systems that otherwise would have been forced to use an active bearing to eliminate the effects of stick-slip.

References

[1] Frank Wardle. *Ultra Precision Bearings*. Elsevier Ltd, 2 2015.

[2] B Armstrong. Stick Slip and Control in Low-Speed Motion. *IEEE Transactions on Automatic Control*, 38(10):1483–1495, 1993.

[3] Solomon S Papell. Papell - 1965 - Low viscosity magnetic fluids obtained by the colloidal suspension of magnetic particles. *US patent*, 1965.

[4] R. Rosensweig. Buoyancy and stable levitation of a magnetic body immersed in a magnetizable fluid, 1966.

[5] S. G.E. Lampaert, J. W. Spronck, and R. A.J. van Ostayen. Load and stiffness of a planar ferrofluid pocket bearing. *Proceedings of the Institution of Mechanical Engineers, Part J: Journal of Engineering Tribology*, 232(1):14–25, 2018.

[6] Ronald E. Rosensweig. *Ferrohydrodynamics*. Dover Publications, 2013.

[7] S Odenbach. *Colloidal Magnetic Fluids*. Number 763 in Lecture Notes in Physics. Springer Berlin Heidelberg, Berlin, Heidelberg, 2009.

[8] Zhuang Wang, Zhengdong Hu, Wei Huang, and Xiaolei Wang. Elastic support of magnetic fluids bearing. *Journal of Physics D: Applied Physics*, 50(43), 2017.

[9] S van Veen. Planar Ferrofluid Bearings (MSc Thesis), 2013.

[10] Joe S. Hunter and Little J. Little. Magnetic fluid bearing accelerometer, 2010.

[11] B. Assadsangabi, M. H. Tee, and K. Takahata. Ferrofluid-assisted levitation mechanism for micromotor applications. *2013 Transducers and Eurosensors XXVII: The 17th International Conference on Solid-State Sensors, Actuators and Microsystems, TRANSDUCERS and EUROSENSORS 2013*, 17(June):2720–2723, 2013.

[12] G Millet and Arnaud Hubert. Design of a 3 DOF displacement stage based on ferrofluids. *Actuators'06*, pages 656–659, 2006.

[13] A. S.T. Boots, L. E. Krijgsman, B. J.M. de Ruiter, S. G.E. Lampaert, and J. W. Spronck. Increasing the load capacity of planar ferrofluid bearings by the addition of ferromagnetic material. *Tribology International*, 129(May 2018):46–54, 2019.

[14] COMSOL Multiphysics 5.4, 2019.

[15] Matlab R2018b, 2018.

[16] Z. Q. Zhu and D. Howe. Halbach permanent magnet machines and applications: A review. In *IEE Proceedings: Electric Power Applications*, volume 148, pages 299–308, 7 2001.

[17] HKCM.de. HKCM Engineering e.K. Online magnet design.

[18] Larry W. Fullerton and Mark D. Roberts. Magnetizing printer and method for re-magnetizing a least a portion of a previous magnetized magnet., 2016.

[19] Larry W. Fullerton, Mark D. Roberts, and Jason N. Morgan. System and method for producing magnetic structures, 2019.

[20] H Meng, J N Morgan, Q F Wei, and C H Chen. Design of Smart Magnetic Devices. In *Proceedings of 25th International Workshop on Rare-Earth and Future Permanent Magnets and Their Applications*, number Repm, 2018.

[21] HKCM Engineering e.K. Magnet-Cuboid Q50x02x02Ni-N35, 2019.

[22] S. Odenbach. Recent progress in magnetic fluid research. *Journal of Physics Condensed Matter*, 16(32), 2004.

[23] Ferrotec. Data Sheet APG 2100 series, 2013.

[24] J. M. Guldbakke and J. Hesselbach. Development of bearings and a damper based on magnetically controllable fluids. *Journal of Physics Condensed Matter*, 18(38), 2006.

[25] E. Uhlmann and N. Bayat. High precision positioning with ferrofluids as an active medium. *CIRP Annals - Manufacturing Technology*, 55(1):415–418, 2006.

[26] L van Moorsel. A planar precision stage using a single image sensor (MSc Thesis), 2017.

[27] R. Deng, S. Van Veen, M. Café, J. W. Spronck, and R. H. Munnig Schmidt. Linear nano-positioning stage using ferrofluid bearings. *Conference Proceedings - 14th International Conference of the European Society for Precision Engineering and Nanotechnology, EUSPEN 2014*, 1(June):372–375, 2014.

[28] Max Café and Jo Spronck. Nanometer precision Six Degree s of Freedom Planar Motion Stage with Ferrofluid Bearings. *DSPE Conference on Precision Mechatronics*, pages 43–46, 2014.

4

Paper: Long-stroke aerostatic stage replacement based on ferrofluid bearings

Design of a passive alternative for long stroke linear aerostatic stages based on ferrofluid bearings

Stefan W.M. van den Toorn[a], Jo W. Spronck[a], Ron A.J. van Ostayen[a] and Stefan G.E. Lampaert[a]

[a]*Department of Precision and Microsystems Engineering, Delft University of Technology, Delft, The Netherlands*

ARTICLE INFO

ABSTRACT

The objective of this research is to demonstrate the capability of a long stroke linear ferrofluid (FF) stage. This stage can be a passive alternative to existing linear aerostatic stages and can be used in low loaded CNC devices, pick and place machines, microscopy or scanner applications. To compete with aerostatic stages the bearing must be repeatable and achieve sufficient stiffness for the application. The effects of FF trail formation were countered with the use of a FF reservoir located on the mover. To increase stiffness a specially designed magnet configuration is used. A stage was built with outer dimensions of 180x600x80 mm (WxLxH), a mover of 1.8 kg without actuator and payload having 430 mm stroke. The load capacity of the stage was measured to be 120 N, with a stiffness of 0.4 N/μm. The maximum height delta after a stroke with 1 kg payload and a mover velocity of 0.25 m/s was measured to be less ±3 μm, with 1.75 kg payload and a velocity of 0.5 m/s the delta was within ±7 μm. Using a rheometer, it was shown that the effects of evaporation in FF can be reversed by adding carrier fluid, within certain limits of mass loss. The damping is shown to be a function of payload and velocity and was measured to be between 2 and 4 N·s/m for velocities between 0.2 and 0.5 m/s. In comparison to a linear aerostatic stage it can be concluded that while the linear FF stage is outperformed in stiffness and out-of-plane repeatability, the FF stage doesn't require a continuous supply of air and has lower fabrication tolerances due to the higher fly height. Thus, the linear FF stage is a cost-effective alternative to a linear aerostatic stage when the stiffness and straightness are of less importance.

1. Introduction

The aerostatic bearing can't be overlooked in current precision positioning systems. The relatively simple concept of floating on top of a cushion of air has obtained a major market share in the past decades [1]. The use of pressurized air however also has its downside, as the bearing seizes when the air pressure is stopped, the manufacturing tolerances are very tight, the system is difficult to implement in vacuum environments and the low damping gives problems in controlling the movement [2]. In the search for alternatives we find that conventional bearings such as ball or journal bearings suffer from stick-slip, magnetic bearing suffer from complexity and flexures suffer from energy storage and a limited range of motion. A bearing type free from all of these issues is the ferrofluid (FF) bearing.

The ferrofluid bearing consists out of a ferrofluid in between bearing surfaces in a magnetic field. FF is a stable colloidal suspension of magnetic particles (∼10 nm) in a carrier fluid [3]. The bearing itself relies on pressure build-up in the fluid as it is attracted by a magnetic field. This pressure build-up is caused by the displacement of the fluid from a position with a high magnetic field to a position with a lower magnetic field. This generates a normal force onto the bearing surface. Alternatively, the FF can be used to seal a pressurized pocket of air which provides the normal force. The first concept is known as the FF pressure bearing [4], the second is known as the FF pocket bearing [5]. The working principle of these bearings is illustrated in figure 1.

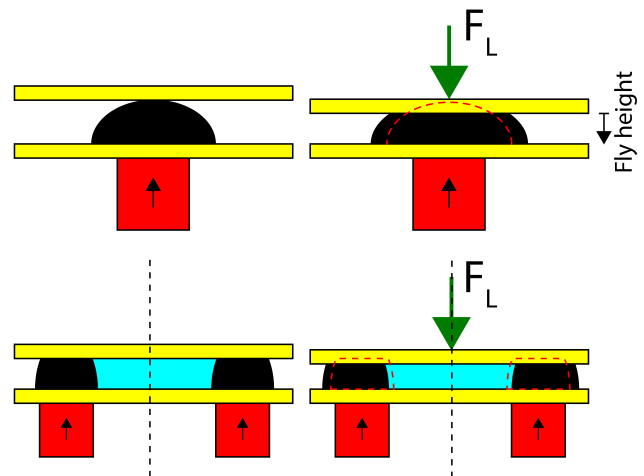✉ stefanvandent@gmail.com (S.W.M. van den Toorn)
ORCID(s):

Figure 1: Working principle pressure bearing (up) and pocket bearing (down).

The relation between the ferrofluid bearing and other bearing solutions can be seen in table 1. The table shows that the aerostatic bearing outperforms the ferrofluid bearing in load capacity and stiffness. However, the ferrofluid bearing can fill a niche that has been left open by the other bearing types i.e. low-cost passive applications requiring a smooth motion without demand for high stiffness. These applications can range from low loaded CNC devices such as 3D printers or laser cutters to optical devices such as microscopy or scanners. An entirely different field of application would be the

Table 1
Ferrofluid bearings in comparison to other bearing solutions for precision positioning [6–10]. The ferrofluid bearing is taken as benchmark, a better performance in precision positioning applications is denoted with +.

	Ferrofluid	Active magnetic	Hydrostatic	Aerostatic	Roller bearing
Load	0	+	+ +	0	+
Stiffness	0	+ +	+ +	+	+ +
Static friction	0	0	0	0	- -
Dynamic friction	0	- -	0	- -	-
Surface finish requirement	0	+ +	-	- -	- -
Complexity	0	- -	-	-	0
Advantage	No stick slip	UH vacuum compatible	Large loads	Contactless	Standardized
Disadvantage	Low stiffness	Inherently unstable	Lubrication oil	Supply Pressure	Stick-slip

use in zero gravity environments, as the fluid is contained in the magnetic field.

The FF bearing has some other advantages. The magnetic field necessary for a Lorentz actuator is already available. The system has a relatively low required tolerances in relation to similar high precision bearings due to the relatively large (∼0.5 mm) distance between bearing surfaces. The FF itself acts as a lubricant. The large surface area in contact with the fluid allows for heat transfer between the bearing surfaces. The broad choice in carrier fluid makes it possible to tune the bearing for different environments, for example a fluid with a low vapour pressure for use in a vacuum, or a fluid with a low viscosity for fast motion. The amount of physical damping makes controlling the system easier. It decreases the sensitivity to high frequency disturbances, thus reducing the need for complicated filtering [11–14] or external damping [15,16].

In the last decade FF bearings were implemented into various planar positioning systems [17–22] and into linear stages [23–25], the behaviour in load capacity and damping were studied [26–32], and finally basic design rules for FF bearings were formulated by Lampaert [33]. Still all existing demonstrators suffer from a low repeatability in the constrained directions and a limited range of motion. These issues are the result of the loss of air from the pocket bearings and loss of FF due to trail formation.

In this study a passive long stroke linear stage based on ferrofluids is proposed. The challenges in the long stroke bearing primarily are achieving a sufficient stiffness, repeatability and stroke length. Problems and implementations of the solutions are discussed, designed and build in a demonstrator stage for the purpose of verification. The specifications for this demonstrator stage are based on those of a commercially available aerostatic linear stage.

2. Stage design

The proposed demonstrator is based on an existing linear bearing stage from Physical Instrumente, the A-110. This air bearing stage is marketed as a high performance affordable nanopositioning stage. The aim of the demonstrator stage is made to be interchangeable with this aerostatic stage, thus

conforming to the same or better specifications. These specifications can be seen in table 2.

2.1. Challenges

In the design of the stage some specific challenges were considered. The most pressing matters were air loss, trail formation and evaporation. Air loss is distinctive for FF pocket bearings, where the fly height is permanently reduced once the bearing is loaded beyond the load capacity of the ferrofluid seal. The fly height is defined as the distance between bearing surfaces and can be seen in figure 1. Trail formation is the occurrence where fluid is left behind as the bearing is translated. Evaporation changes the composition of the ferrofluid suspension and alters the fluid properties such as viscosity and saturation magnetization. If left unaddressed, each problem can severely compromise the performance and repeatability of the stage. Solutions for each of these problems have been implemented in this bearing stage.

The problem of air loss is distinctive to FF pocket bearings only, the FF pressure bearing does not suffer from this problem. In terms of load capacity and stiffness, the pocket bearing outperforms the pressure bearing. As the repeatability of the bearing is considered more desirable than load capacity or stiffness the pressure bearing is the preferred bearing type for this application.

The trail formation problem is solved by the creation of a reservoir on the mover itself. By assuming a Couette flow between the bearings and base the total amount of fluid loss is estimated at 20 ml. As the amount of fluid required is low, this reservoir can be incorporated into the pressure bearings themselves. The ferrofluid can move freely between the individual pressure bearings. This ensure a repeatable behaviour and redistributes the collected trail.

A ferrofluid with a low viscosity is used to decrease trail formation and to limit damping. As this fluid has a higher vapor pressure than is desired the evaporation problem needs to be addressed. In order to do this, the effect of resupplying the evaporated carrier fluid is researched.

The design of the stage is a double u shape as shown in figure 2. The preload increases stiffness and the symmetric design reduces tilt under movement. The in-plane length of the mover is 100 mm, to save weight and to reduce damping.

Table 2
Specifications of A-110.300 linear air bearing stage [34]

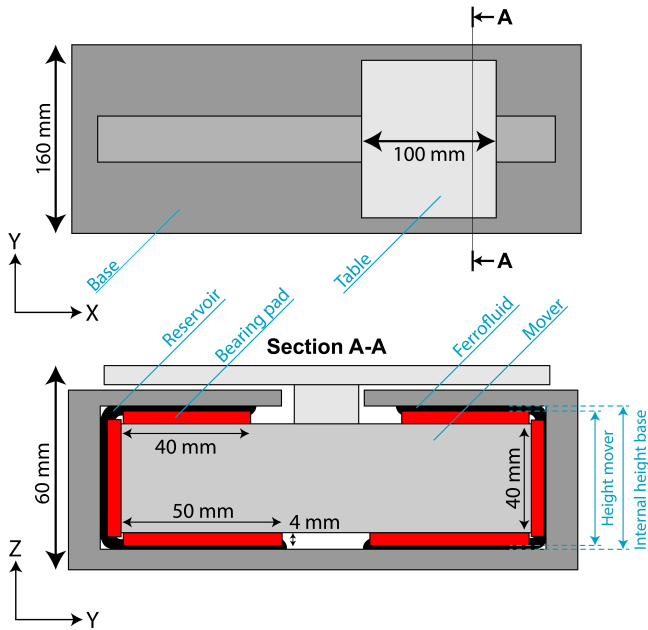| Model	A-110.300
Travel	300 mm
Maximum payload	10 kg normal
Flatness	$< \pm 2 \ \mu m$
Moving mass	2.6 kg
Maximum velocity	1 m/s
Outer dimensions	160 × 575× 60 mm (W × L × H)
Mover dimensions	160 × 200 × 60 mm (W × L × H)

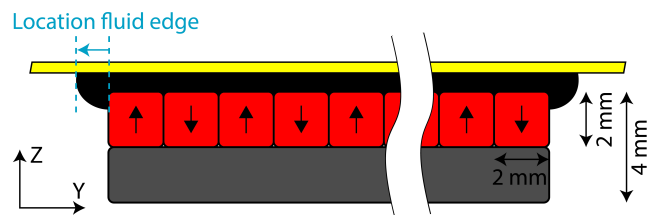**Figure 2:** Schematic bearing design with areas reserved for bearing in red.

Figure 3: Bearing pad cross-section showing the layout. The in-plane length of the bearing pad is 100mm.

The areas marked in red are reserved for 6 bearing pads, two of 50x100x4 mm (W x L x H) for the bottom bearings and four 40x100x4 mm (W x L x H) for the side and top bearings. For this research the kerosene based EFH3 fluid from Ferrotec is chosen. This FF has a relative high saturation magnetization of 66 mT and a viscosity of 12 mPa·s [35].

2.2. Bearing pad

Each bearing pad consists out of 50x2x2 mm magnets from HKCM [36]. These magnets are arranged in an 'up-down' magnetization configuration with the long side in the movement direction as can be seen in figure 3. The bottom bearing pads are arranged in a 2x25 grid (x*y), the top and side bearing pads are slightly smaller and are arranged in a 2x20 grid (x*y). The use of many small magnets results in a concentrated magnetic field close to the magnets with a large gradient in the direction of the fly height. This results in a high load capacity and stiffness for a ferrofluid pressure bearing. Instead of an up-down magnetization configuration, the magnets can also be magnetized facing each other, all in the same way or by means of a Halbach array. Alternatively, also iron can be used in between the magnets to shape the magnetic field. It was found that from these possible configurations the up-down configuration with an iron bottom plate is the most cost-effective way to achieve a high stiffness and load capacity while also having little moving mass [37]. A second benefit of this arrangement is the low stray field, as the individual magnets cancel each other at larger distances. Magnets with a smaller cross-section can increase stiffness of the bearing, but the brittleness and increased number of magnets would make assembly complex. Ferritic stainless steel is used instead of iron due to rust. Although 0.5 mm thickness of the bottom plate would already have yielded the same performance, for assembly purposes a relative thick bottom plate of 2 mm is used. As the pressure bearings are located close together, the magnetic field intensity is relatively high at the adjoining corners of the bearing pad as can be seen in figure 2. The ferrofluid that accumulates there has a negligible effect on the load capacity of the stage, this is used as a reservoir of ferrofluid to counter the effects of trail formation. As this reservoir bridges the different bearing pads it also can transport fluid between the bearing pads, ensuring a repeatable performance.

2.3. Modelling stage load capacity and stiffness

Using a mathematical model of the magnetic field in COMSOL [38] and Matlab [39], the load capacity and stiffness of the bearing pads were determined. The geometry of the pad was built in Matlab using the COMSOL Livelink interface, the magnetic field was then calculated in COMSOL and afterwards post-processed in Matlab. In the model several assumptions are made for the remanent flux density of the magnets (1.17 T), saturation magnetization of the ferrofluid (66 mT) and the location of the fluid edge (5mm). The definition of the fluid edge location is shown in figure 3. The FF itself is modelled as air, having a relative permeability of 1. For the ferritic stainless steel, a relative permeability of 4000 is used with a saturation magnetization of 1.4 T.

The chosen bearing stage design gains added stiffness through a preload. This preload can be varied by varying the difference in height of the mover and the internal height of the base as can be seen in figure 2. The design of the demonstrator is made such that this height difference can be varied easily. Decreasing the height difference decreases the

fly height of the top and bottom bearing pads and thus increases the applied preload. As the ferrofluid bearing can be seen as a spring this increases the stiffness of the bearing. The increased stiffness however comes at the cost of less load capacity and more viscous damping. Decreasing the fly height also reduced the amount of fluid necessary as the physical volume between the bearing surfaces decreases. An additional effect of the preload is a more stable fly height as the trail formation will also occur on the top side and thus, the fluid loss is symmetrical. As the bearing pads on top and bottom differ in size and gravity acts on the mover, the equilibrium position of the top and bottom pad will not be exactly the same.

Table 3 shows the bearing characteristics as function of the fly height according to the model. In order to achieve the same specifications as the A-110 aerostatic stage the fly height in vertical direction will need to be somewhere between 0.5 mm and 0.25 mm. As no horizontal payload is known for this stage a fly height of 1 mm in the horizontal pads is assumed to be sufficient.

Table 3
Bearing characteristics in horizontal and vertical plane for different fly heights. Stiffness is evaluated around equilibrium position. Load capacity is evaluated at the minimum fly height of 0.1 mm.

Horizontal			
Fly height left pad [mm]	Fly height right pad [mm]	Load [N]	Stiffness [N/μm]
0.1	1.9	120	0.23
0.1	0.9	92	0.27
0.1	0.4	49	0.34
0.1	0.15	11	0.43

Vertical			
Fly height bottom pad [mm]	Fly height top pad [mm]	Load [N]	Stiffness [N/μm]
0.1	0.9	231	0.68
0.1	0.4	146	0.81
0.1	0.15	69	0.97

2.4. Eddy current damping in stage

Aluminium is the preferred material for the demonstrator stage due to its availability and machinability. The relative velocity between the good conducting aluminium and the magnetic fields induced by the bearing pads can create eddy currents. The damping induced by these eddy currents is investigated using a COMSOL model. Figure 4 illustrates this model and the direction of the relative velocity between the bearing pad and conductor. In the model the used bearing pad is translated past a long aluminium block. The bearing pad consists out of 2x25 magnets (x*y) of 50x2x2 mm with a remanent flux density of 1.17 T. The results of the modelling can be seen in table 4.

In table 4 can be seen that the simulated eddy current damping is low. The low damping is caused by two factors. Firstly, as the eddy currents are induced by a change in mag-

Table 4
Simulation of eddy current damping in full size pressure bearing pad. Magnet dimensions 50x2x2 mm, arranged in a 2*25 (x*y) grid with long edge in x-direction, magnetized alternating between positive and negative z-direction.

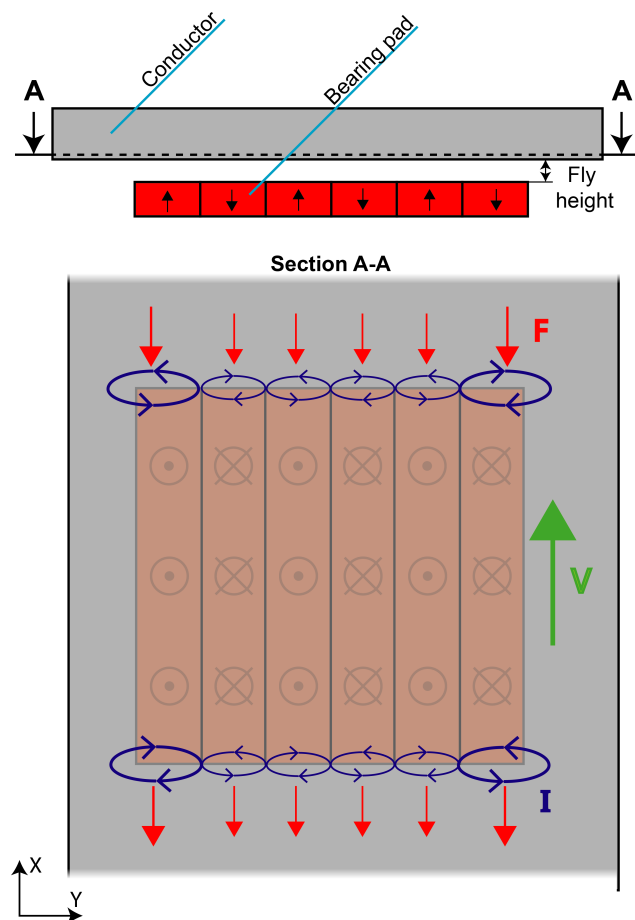| Fly height [mm]	Eddy current damping coefficient [N·s/m]
0.10	0.22
0.25	0.13
0.50	0.07
1.00	0.03

Figure 4: Illustration of the location and magnitude of the eddy currents (I) on the surface of the conductor. With the direction of the relative velocity between conductor and bearing pad (V) in green and damping force (F) direction in red.

netic field the current loops can only occur at the start and end of the bearing pad. Secondly, as the magnetization direction of the magnets alternate the direction of the current alternates as well. This prevents large current loops from forming. Both factors can be seen in figure 4.

3. Methods for design validation

To verify that the functioning of the stage is as intended, first the load capacity and stiffness model of an individual pressure bearing pad are validated. This same model then is used in the verification of the load and stiffness of the full stage. To gain insight in the performance of the stage when in use, the effects of trail formation and evaporation will be measured. Finally, the damping and flow profile between bearing surfaces will be experimentally determined. This can benefit the future actuation of the stage.

3.1. Single pressure bearing pad

The individual tested pressure bearing pad is assembled of 23 50x2x2 magnets[36] with a remanent flux density of 1.17 T structured as seen in figure 3. The pad is tested with 5 ml of EFH3 fluid and with the same amount of APG 513A ferrofluid. The load-fly height curve of the bearing is measured using a materials test frame and compared to the model.

For the modelling of the pressure bearing path the location of the outer fluid edge is needed. This variable is defined in figure 3, and represents the starting point of the pressure build-up in the fluid. The location is primarily dictated by the equilibrium between the gravitational pull and the magnetic body force on the fluid. The effect of surface tension and surface roughness on this location is negated. Using COMSOL the magnetic field surrounding the bearing pad is simulated, resulting in a location of the outer fluid edge of 0.9 mm outside the magnet. The magnetization saturation of the ferrofluid is modelled as 32 kA/m[40] for the APG 513A and 52.5 kA/m for the EFH3[41].

3.2. Demonstrator stage

The demonstrator as seen in figure 5 was constructed from aluminium with ferritic stainless-steel bottom plates for mounting the magnets. The top plate could be raised using shims to increase the fly height of the top and bottom bearing pads. The total material cost for the ferrofluid demonstrator stage are slightly over €1000, the magnets attribute €150.

Table 5
Physical properties of realized demonstrator stage

Travel	460 mm
Moving mass	1.84 kg
Outer dimensions	180 × 640 × 80 mm (W × L × H)
Mover dimensions	139 × 124 × 60 mm (W × L × H)

In table 5 the physical properties of the realized stage can be seen. The base and mover have both been overdesigned. Thicker metal is used in in order to increase production efficiency and to allow for more freedom in the fine-tuning of the height difference between mover and base. Because of this, the width and height of the outer dimensions could both be reduced with 20 mm without any performance loss.

Figure 5 shows the demonstrator and the three Micro-Epsilon optoNCDT 1420 laser distance sensors[42] used. 2 sensors with a range of 10mm were fitted above the table on

Figure 5: Measurement setup of demonstrator with 3 laser distance sensors for position and roll of the mover.

either side. These sensors measure the position of the table relative to a fixed frame. From this the fly height and roll of the stage could be found. One sensor with a range of 200 mm was mounted in front of the mover and was used to measure displacement and velocity of mover. The demonstrator stage was connected to an actuator using a thin wire. By setting the demonstrator at a slight incline, it could thus be actuated in both directions with negligible disturbance to the measurements.

Unless mentioned otherwise, all experiments are conducted using the EFH3 ferrofluid from Ferrotec.

3.2.1. Load and stiffness

The load and stiffness of the stage is determined using three different methods. The first method is by using a materials test frame. In the second method weight is added to the table manually while measuring the height using the later distance sensors. The third method is to set the stage at very small inclination and to add weight until the mover stops moving freely.

3.2.2. Trail formation

Figure 6 shows the trail formation in the bearing. The trail thickness can be deduced from the colour of the trail. The light brown on the right and almost black on the left indicate a strong correlation between the amount of fluid loss and the movement velocity. The influence of this trail formation is experimentally determined by measuring the height of the stage at the end of a stroke. This is done for different amounts of fluid in the system and for different translation speeds.
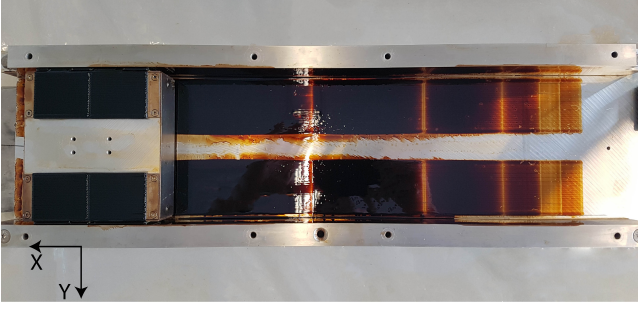
Figure 6: Trail formation in stage. The mover has been displaced in steps increasing in velocity from right to left. The table and top plate were removed before the displacement.

3.2.3. Evaporation

The evaporation rate of the ferrofluid was determined by placing five grams of fluid was in a Petri dish. The fluid-air interface was 58 cm2 and the temperature was kept between 18 and 22 degrees Celsius. The Petri dish with fluid is weighed at several moments in time. The effects of evaporation on the fluid viscosity and magnetic properties are investigated using a rheometer. This rheometer is capable of generating a magnetic field comparable to the field at the surface of the pressure bearing pads. The evaporation rate is established by the mass loss in a controlled volume over time. Fluid with different percentage of mass loss is then evaluated in the rheometer. This same experiment is redone for fluid with the same percentage of mass loss, this time resupplied to original mass by addition of paraffin oil.

3.2.4. Damping

The damping of the stage is evaluated by setting the stage under a defined incline. The external stage is used to pull the mover onto the slope and to release it at the highest point. Gravity will accelerate the stage until it reaches terminal velocity, which is measured using the 200 mm laser distance sensor. This is done for several times for a combination of three different inclinations and three different amounts of payload. As the weight of the stage is known, the driving force can be calculated. The damping coefficient then follows from the terminal velocity and the driving force.

The flow profile in between the bearing plates is derived by combining the data from the damping in the stage with the damping model from Lampaert[31]. The damping model used assumes a Couette flow with negative pressure gradient and derives the pressure gradient by assuming zero trail formation. As can be seen in figure 6, this assumption is invalid for this bearing. Thus, data from the damping in the stage is used to derive the pressure gradient.

In equation 1 shows the velocity profile of the fluid, u_x according to the damping model from Lampaert. With η the shear rate dependent viscosity of the ferrofluid, h the height
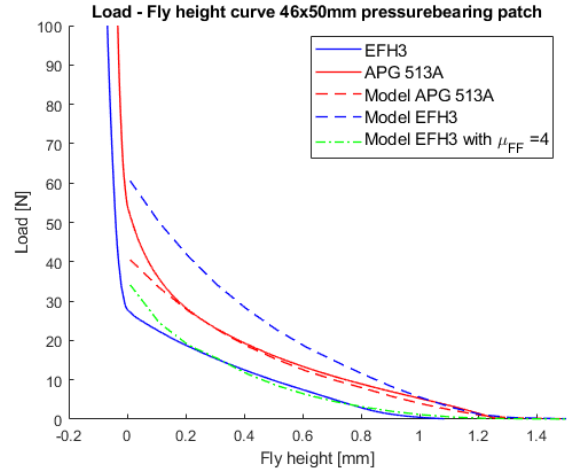

Figure 7: Load-fly height curve of 23x1 pressure bearing pad with EFH3 and APG 513A ferrofluid.

of the FF film and U the velocity of the mover.

$$u_x = \frac{1}{2\eta}\frac{\partial p}{\partial x}(z^2 - hz) + \frac{U}{h}z \tag{1}$$

The $\frac{\partial p}{\partial x}$ describes the pressure drop in the flow direction. This term can be determined based on data from the experiment. Based on initial testing and observations in the trail formation it is assumed that the relation between the damping coefficient and velocity is linear. This results in a quadratic relation between the velocity and the damping force. The damping force can be derived using formula 2 and taking $z=h$, giving following formula 3.

$$\tau_{zx} = \eta\frac{\partial u_x}{\partial z} \tag{2}$$

$$\tau_{zx} = \frac{1}{2}\frac{\partial p}{\partial x}h + \eta\frac{U}{h} \tag{3}$$

The friction force on the mover will be measured by measurement of the terminal velocity. The contribution of a single bearing pads to the friction force can be determined by assuming it is proportional to the contribution when assuming a Couette flow over the bearing pads. The pressure drop term can then be determined using equation 3 and the friction force on a single bearing pad.

4. Bearing design validation

4.1. Single pressure bearing pad

Figure 7 shows the results of the testing of the individual pressure bearing pad. Zero displacement was taken to be the point at which the pressure plate touches the magnets in the measurement.
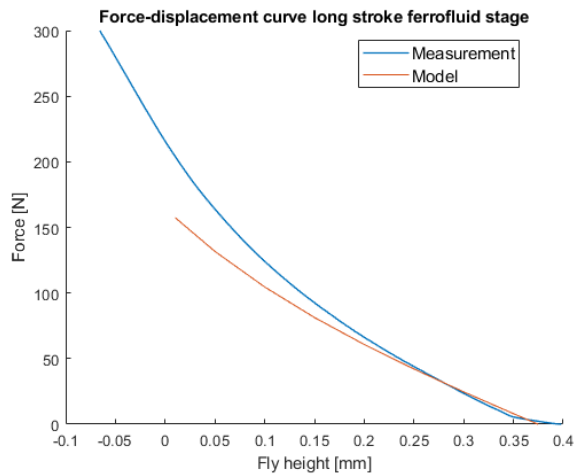
Figure 8: Load-fly height curve of stage. The crosshead velocity of the materials test frame was set to 0.5 mm/min. The initial fly height without payload is 0.39 mm for the bottom bearing pad and 0.36 mm for the top bearing pad. The bearing pads are modelled with a relative permeability of 4 for the ferrofluid.

4.2. Demonstrator stage

4.2.1. Load capacity and stiffness

The experiment from section 4.1 was repeated for the full stage. The results of this is shown in figure 8. The individual fly heights of the top and bottom pad are taken to be such that the modelled load generated by the bottom pad is equal to the modelled load of the top pad combined with the gravity forces. This result in 0.39 mm for the bottom pad and 0.36 mm for the top pad. The fly height of the bottom pad is larger than the top pad as the size of these bearing pads differ.

The maximum sustained load capacity was determined by adding mass to the stage whilst being under a small incline and was found to be 140 N for a stroke of under 100 mm and 120 N for the full stroke.

The stiffness was also determined at different initial fly heights by using the laser displacement sensors and a weight of 3 kg. The model parameters were chosen to be the same as in figure 8. Table 6 shows the results of these measurements. It can be seen that the model corresponds well with the measurements at larger fly heights. When the fly height decreases, the model and measurement diverge.

Table 6
Measured and modelled stiffness of stage for different fly heights for the bottom and top bearing pad.

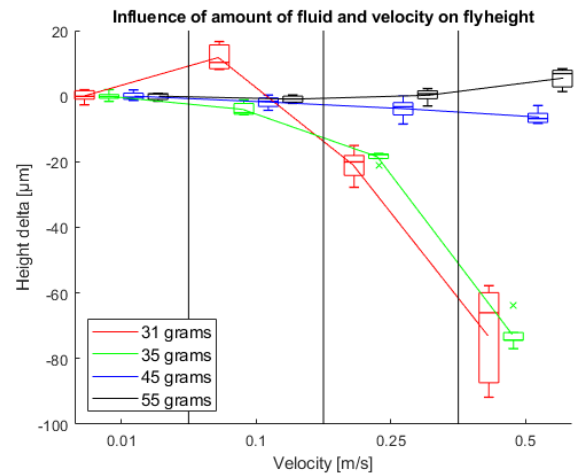| Fly height	[mm]	0.3/0.25	0.4/0.35	0.55/0.50
Measured Stiffness	[N/μm]	0.73	0.44	0.31
Modelled Stiffness	[N/μm]	0.57	0.42	0.36

Figure 9: Height delta of the mover height under translation at different speeds for different amounts of fluid. No payload was added to mover.
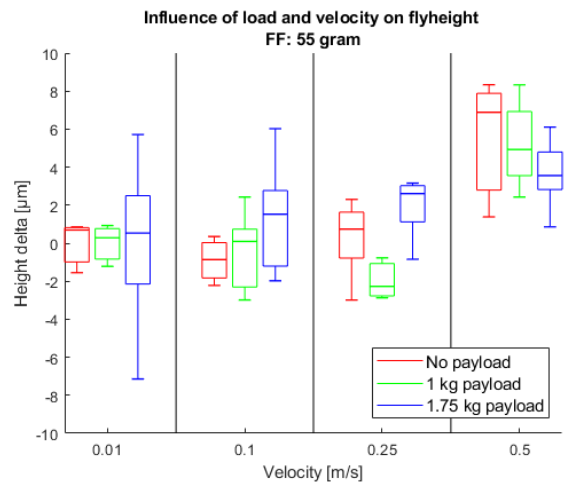

Figure 10: Height delta of the mover height under translation at different speeds when filled with 55 grams of FF.

4.2.2. Trail formation

Figure 9 shows a significant height drop at higher translation velocities using a limited amount of FF. Figure 10 shows the relative height of the stage for 55 grams of fluid and different payload amounts. It can be seen that the payload has no noticeable influence on the repeatability of the height. The zero in these figures is taken as the mean at 0.01 m/s. The initial fly height was set to 0.55 mm for the bottom pad and 0.50 mm for the top pad.

4.2.3. Evaporation

The evaporation measurement resulted in an evaporation rate in the initial 74 hours of $9.0 \cdot 10^{-5}$ g/(cm^2·h) for the EFH3 fluid. The evaporation rate in the next 43 hours was $5.6 \cdot 10^{-5}$ g/(cm^2·h). Using a rheometer, the properties of the ferrofluid were evaluated when subjected to evaporation.
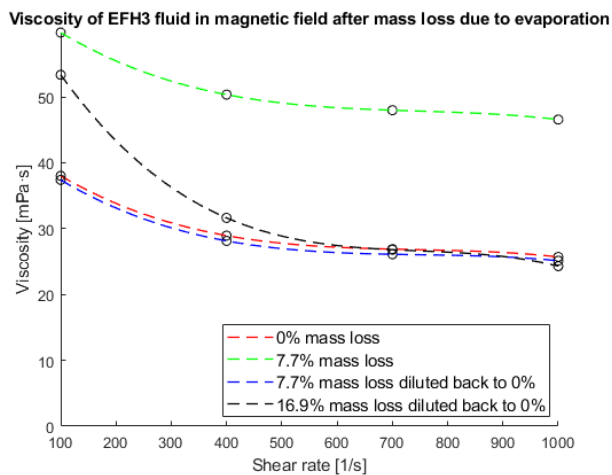
Figure 11: Viscosity of EFH3 fluid for different levels of evaporation and dilution.
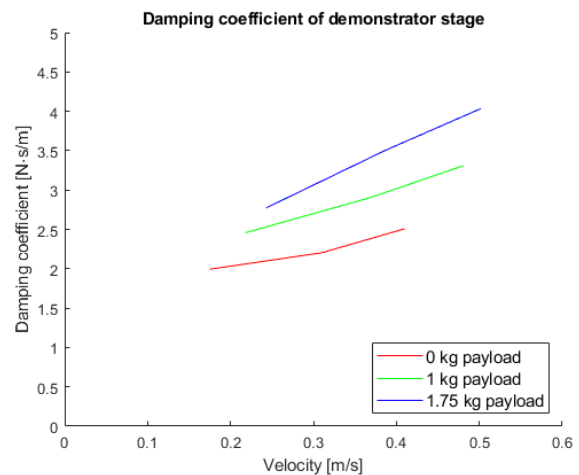

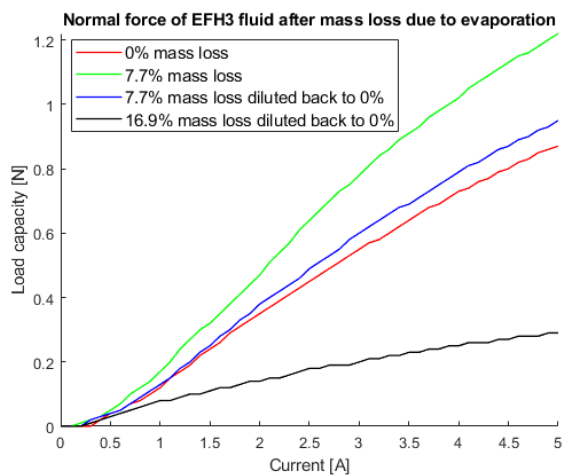Figure 13: Damping coefficient of demonstrator stage for different loads.

Figure 12: Normal force exerted by EFH3 fluid on the rheometer for different levels of evaporation and dilution.
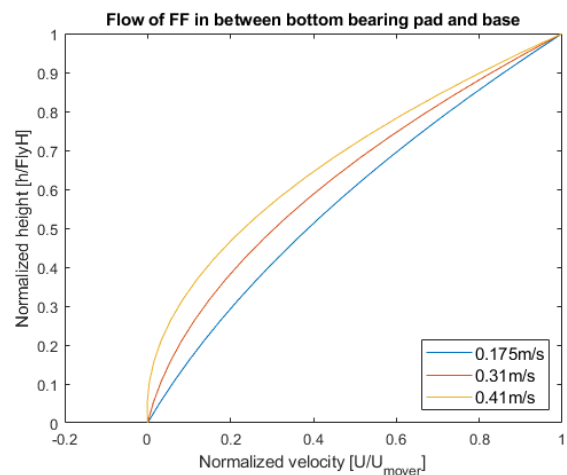

Figure 14: Flow in ferrofluid in between the bottom bearing pad and base based on equation 1 and the data presented in figure 13 for the damping coefficient without payload to fit the pressure drop term.

This was done for the EFH3 fluid subjected to 7.7 % mass evaporation and 16.9 % mass evaporation and can be seen in figures 11 and 12.Figure 11 shows the viscosity in the ferrofluid as a function of the shear rate. Figure 12 shows the normal force exerted on the rheometer by the ferrofluid.

4.2.4. Damping

The results of the damping experiment can be seen in figure 13, the stage was filled with 45 grams of FF and has an unloaded fly height of 0.55 mm for the bottom pad and 0.50 mm for the top pad. There is a strong correlation between the damping coefficient and the load and velocity of the stage.

The pressure drop term is fitted to the data, the found values for the bottom bearing in the measurement without payload are $1.9 \cdot 10^4$, $5.2 \cdot 10^4$ and $9.4 \cdot 10^4$ Pa/m for respective 0.175, 0.31 and 0.41 m/s mover velocity.

5. Discussion

5.1. Single pressure bearing pad

The data from the pressure bearing test using the APG 513A ferrofluid results in a load capacity of 40 N, resulting in 1.8 N/cm^2. The load capacity and stiffness of the bearing could have potentially been higher by opting for pocket bearings instead of pressure bearings. Though, the values for load and stiffness are comparable to a previous implementation of a single pocket bearing stage[21] where a load capacity of 100 N was achieved using a surface area of 84 cm^2, resulting in 1.2 N/cm^2. Thus, to improve over the current design more complex pocket bearings with multiple seals would be required. This would result in more pockets of air which all need to be managed to maintain repeatability.

The load capacity using the EFH3 fluid is lower than with the APG 513A. This is unexpected as the EFH3 has a higher saturation magnetization. This behaviour might be explained by the loss of colloidal stability due to the high gradient in the magnetic field[43]. Magnetic particles will then accumulate at the corners of the magnets. This accumulation can be problematic in this specific magnet geometry as a large build-up of particles in between the two oppositely magnetized magnets will cause a short circuit in the magnetic field.

This behaviour is simulated in the model using an increase of relative permeability. A relative permeability of 4 is in close agreement with the measurement of the EFH3 fluid. This can be seen in figure 7

5.2. Demonstrator stage
5.2.1. Load capacity & Stiffness
The force-fly height curve shows the behaviour of the stage is behaves similar to the model at larger fly heights, the model and measurement diverge when the fly height of the stage approaches zero. This behaviour can be explained by squeeze film damping.

It can be seen that in the sense of load capacity, an FF stage can achieve similar load capacity to a comparable aerostatic stage. The stiffness of the aerostatic stage however is several times higher. The high stiffness is required in the aerostatic stage to move resonance spikes from the underdamped eigenmodes to a frequency well above the desired bandwidth. As the ferrofluid stage uses relatively viscous fluid, the eigenmodes are overdamped and much less of a problem. Thus, from a control point of view the stiffness doesn't necessarily need to be high. As the stiffness of the stage is known and stable under translation, it can easily be compensated for.

The stiffness of the stage can be increased by decreasing the fly height of the top and bottom bearing pads. This can be done by decreasing the difference in height between mover and base. This way a stiffness of up to 0.73 N/μm can be achieved. The increase in stiffness comes at the cost of a reduce in load capacity. The fly height can be chosen based on the application, a larger fly height for applications requiring higher load capacity and a smaller fly height for applications requiring stiffness.

The load capacity in lateral direction isn't directly measured, but can be determined by using the bearing pad model. At a fly height of 1 mm this load capacity would be 80 N. When taking account fluid loss in translation, the effective lateral load capacity would be slightly lower. As the lateral pad is smaller and the reservoir in the mover remains equal in size, the drop in lateral load capacity is estimated to be less than 20 N. Resulting in an estimated 60 N load capacity in lateral direction.

5.2.2. Trail formation
Figure 9 shows that for a limited amount of FF, there is a significant drop in the height of the mover at higher translation velocities. The higher velocity induces more shear

and as a result less fluid is present to support the load of the stage. Using a larger volume of ferrofluid eliminates this height drop, a height increase can even be observed in the height for an increase in pull back velocity. This height gain can partly be explained by the weight reduction associated by the loss in fluid. The loss of 30 grams of fluid would give an increase in fly height of 1 μm at a stiffness of 0.3 N/μm. A further explanation would be a difference in fluid loss and fluid supply in the top and bottom bearing pads. When the top pad has less fluid relatively to the bottom pad, the height of the mover will increase.

The increased stability in fly height can be explained by the reservoirs at the corners of the bearing pads as seen in figure 2. A larger volume of ferrofluid ensures there is an excess amount of fluid available on the mover to replace lost ferrofluid due to trail formation.

Figure 10 shows the relative height of the mover for 55 grams of fluid and different payload amounts. It can be seen that the payload has limited influence on the repeatability of the height of the mover. This figure shows the stage can accommodate a payload of 1 kg at a maximum velocity of 0.25 m/s with an out-of-plane height stability of ± 3 μm, and ± 7 μm for a payload of 1.75 kg at a maximum velocity of 0.5 m/s.

In past implementations of ferrofluid bearings into precision movement stages, the performance has been severely limited by trail formation. Typical values are a stroke of several centimetres and the loss of mover height is in the order of 1 μm/mm translation[21,23]. In comparison, both the attained stroke and stability of the mover height in the realized demonstrator stage are of exceptional performance.

5.2.3. Evaporation
Figure 11 shows a severe increase in viscosity, both with and without magnetic field under evaporation of the fluid. When the fluid is diluted back to the original mass the viscosity of the fluid also reverts back to original, but this was observed only for the 7.7 % evaporated fluid. A very probable explanation is the loss of colloidal stability of the fluid when evaporation exceed a certain value. Individual particles then agglomerate and no longer disperse when diluted back to original mass.

Figure 12 shows the normal force exerted on the rheometer by the ferrofluid. This endorses the theorized refilling of the carrier fluid for small levels of evaporation. Again, here can be seen that there is less normal force for the further evaporated fluid, which can also be caused by agglomerations in the fluid.

Due to the relatively large wetted surface in the bearing, the overall mass loss due to evaporation using the EFH3 fluid will be in the order of a percent per day. This means that after a week the viscosity in the fluid has doubled. After a few more days the fluid will lose colloidal stability and the individual particles will agglomerate. This process can be reversed by 'lubricating' the bearing occasionally through the addition of carrier fluid. The properties of the fluid will then return to their original specification. This has yet to be tested

Table 7
Comparison of specifications of aerostatic bearing stage and ferrofluid demonstrator stage. * No actuation is added to the demonstrator stage at this stage. ** Outer dimensions of demonstrator can be reduced without loss of performance.

	Unit	PI aerostatic bearing A-110.300	Ferrofluid demonstrator stage	Goal achieved
Travel	mm	300	460	✓
Maximum payload	N	100 normal	120 normal, 60 lateral	✓
Stiffness	N/μm	30-60 (estimated)	0.4	X
Moving mass	kg	2.6	1.8*	✓
Outer dimensions (W x L x H)	mm	160 x 575 x 60	180 x 600 x 80	✓**
Mover dimensions (W x L x H)	mm	160 x 200 x 60	139 x 124 x 60	✓
Straightness & Flatness	μm	< ± 2	< ± 7 (Fluid loss only)	X
Maximum velocity	m/s	1	-	?

inside a working bearing system, however experiments using a rheometer look very promising.

Alternatively, a different solution to the evaporation problem would have been the use of a ferrofluid with a very low vapor pressure. Where kerosene based EFH3 ferrofluid has a vapour pressure of 0.1 kPa[35], the vapour pressure of the H9-LT ferrofluid from Liquid-Research has a vapour pressure of $\sim 1 \cdot 10^{-7}$ kPa[44]. Based on the difference in vapour pressure the evaporation rate of the H9-LT ferrofluid will be several orders higher than the evaporation rate of the EFH3 ferrofluid[45]. This would make a system for resupplying unnecessary as the effects of evaporation will only be noticeable after several years. Low vapour pressure ferrofluids however are expensive and have a high viscosity. The H9-LT ferrofluid has a viscosity of 300 mPa·s, which is 25 times higher than the used EFH3 ferrofluid. Primarily the high viscosity is problematic as it will increase damping and trail formation, thus reducing the possible stroke length and mover velocity.

5.2.4. Damping

The damping in the system is relatively constant and predictable, a function of movement velocity and payload. This makes open loop controlling a possibility in systems with lower positioning requirements. For high precision requirements, the damping attenuates high frequency noise and makes implementing a PID controller less difficult[11]. The strong correlation of the damping coefficient with the velocity however is puzzling, no explanation could be found for this occurrence.

Figure 14 shows the flow profile in the ferrofluid as modelled using a Couette flow with back pressure. Due to the limited back pressure at a low velocity the flow profile approximates that of a Couette flow. As the velocity increases the back pressure increases and the flow profile becomes similar to the flow profile theorized by Lampaert[31]. These flow profiles would indicate less fluid loss at higher velocities, which is in contrast with observations in the demonstrator (figure 6) where the fluid loss was seen to increase with velocity.

The modelled flow profile in the fluid between mover and base suggests the presence of a recirculation of the fluid on the sides of the bearing pad. Figure 15 shows an explanation
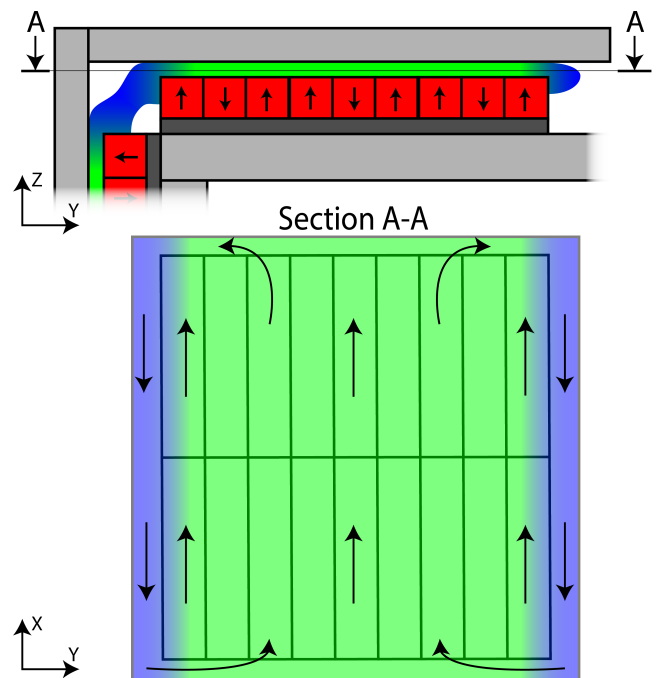

Figure 15: Top and front view of a pressure bearing pad with a reverse flow channel (blue). The arrows show the direction of net fluid flow for a mover translation in positive x-direction. Fluid coloured green flows in the positive x-direction, blue flows in the opposite direction.

of this recirculation path using reverse flow channels.

The existence of a reverse flow channel on the magnet pads would allow the fluid the circulate almost freely at low speeds. While at higher speeds, the volume flow in the reverse flow channels increases and a significant back pressure is created. This increase in pressure increases the loss of fluid as well. The circulation of the fluid is observed when the top of the bearing is removed. The fluid then uses the free top surface to circulate fluid from the side and bottom bearing pads

5.3. Comparison with aerostatic stage

The goal of this research was to demonstrate the possibility of a passive linear guide using ferrofluid pressure bearings capable of competing with an existing aerostatic stage. Table 7 shows the comparison between the realized demonstrator model and the PI linear stage with air bearings. It can be seen that the stage is only outperformed by the aerostatic bearing stage at 2 points, stiffness and straightness. The maximum velocity of the stage has yet to be determined.

6. Conclusion

In comparison to previous implementations of ferrofluid bearings, the realized stage greatly improves the stroke length and out-of-plane stability in mover height. Though, the attained stability and stiffness is less than an aerostatic bearing stage can achieve. Thus, the use of this stage is not recommended in applications where this is very critical, such as in sub-micrometre lithography stages. However, in comparison to aerostatic stages, the ferrofluid bearing can provide the same stick-slip-free motion without the need for a constant supply of air and tight manufacturing tolerances. Moreover, the ferrofluid bearing approaches the same out-of-plane stability for a lower payload and velocity. There can be concluded that the ferrofluid bearing is a feasible alternative to aerostatic bearings, depending on the demands of the application.

From the findings in this research the following conclusions can be drawn:

- Optimized ferrofluid pressure bearings can compete with single seal pocket bearings

- Magnets can be used in close proximity to conductors without significant eddy current damping by choosing the geometry and orientation of the magnets properly.

- The use of a reservoir on the mover results in a stable fly height under translation.

- The magnetic and viscous properties of ferrofluids subjected to moderate evaporation can be restored by re-supplying with carrier fluid.

- The damping in the stage is purely viscous in nature and primarily affected by velocity and size of payload.

- It is possible to design and manufacture a linear ferrofluid stage to specification.

References

[1] Luigi Lentini, M. Moradi, and F. Colombo. A historical review of gas lubrication: From reynolds to active compensations, 6 2018.
[2] Kok Kiong Tan, Sunan Huang, Wenyu Liang, and Shuang Yu. Development for precise positioning of air bearing stages. In *2012 IEEE International Conference on Mechatronics and Automation, ICMA 2012*, pages 1943–1948, 2012.
[3] Solomon S Papell. Papell - 1965 - Low viscosity magnetic fluids obtained by the colloidal suspension of magnetic particles. *US patent*, 1965.
[4] R. Rosensweig. Buoyancy and stable levitation of a magnetic body immersed in a magnetizable fluid, 1966.
[5] R. Rosensweig. Bearing arrangement with magnetic fluid defining bearing pads, 1971.
[6] Anton Van Beek. *Engineering Design Lifetime Performance and Reliability*. TU Delft, Delft, 2012.
[7] A. T.A. Peijnenburg, J. P.M. Vermeulen, and J. van Eijk. Magnetic levitation systems compared to conventional bearing systems. *Microelectronic Engineering*, 83(4-9 SPEC. ISS.):1372–1375, 2006.
[8] Matt Reck. Air Bearings : When to Use and Air Bearings: When to Use and When to Avoid in Your Motion Application.
[9] A.S.T. Boots. Operational range of a ferrofluid pocket bearing (MSc Thesis), 2018.
[10] W. Brian Rowe. *Hydrostatic, Aerostatic and Hybrid Bearing Design*. Elsevier Inc., 2012.
[11] Christian Schmidt, Joachim Heinzl, and Günther Brandenburg. Control approaches for high-precision machine tools with air bearings. *IEEE Transactions on Industrial Electronics*, 46(5):979–989, 1999.
[12] Zeguang Dong, Pinkuan Liu, and Han Ding. Kalman estimator-based state-feedback high-precision positioning control for a micro-scale air-bearing stage. In *Lecture Notes in Computer Science (including subseries Lecture Notes in Artificial Intelligence and Lecture Notes in Bioinformatics)*, volume 5928 LNAI, pages 765–775, 2009.
[13] Khalid L. Sorensen, William Singhose, and Stephen Dickerson. A controller enabling precise positioning and sway reduction in bridge and gantry cranes. *Control Engineering Practice*, 15(7):825–837, 7 2007.
[14] Andrew J. Fleming, Sumeet S. Aphale, and S. O.Reza Moheimani. A new robust damping and tracking controller for SPM positioning stages. In *Proceedings of the American Control Conference*, pages 289–294, 2009.
[15] Eunho Sung, Chang-hoon Seo, Hyunmin Song, Byungjoo Choi, Yongho Jeon, Young-Man Choi, Kihyun Kim, and Moon G Lee. Design and experiment of noncontact eddy current damping module in air bearing–guided linear motion system. *Advances in Mechanical Engineering*, 11(8):168781401987142, 8 2019.
[16] Takumi Tsumura, Hayato Yoshioka, Hidenori Shinno, and Hiroshi Sawano. Magnetically preloaded aerostatic guideway for high speed nanometer positioning. *Journal of Advanced Mechanical Design, Systems and Manufacturing*, 8(4):JAMDSM0054–JAMDSM0054, 2014.
[17] Max Café and Jo Spronck. Nanometer precision Six Degree s of Freedom Planar Motion Stage with Ferrofluid Bearings. *DSPE Conference on Precision Mechatronics*, pages 43–46, 2014.
[18] Max Café. Nanometer precision Six Degrees of Freedom Planar Motion Stage with Ferrofluid Bearings. Technical report, TU Delft, 2014.
[19] Gihin Mok. The design of a planar precision stage using cost effective optical mouse sensors (MSc Thesis), 2015.
[20] Alejandro Alvarez-Aguirre, Gihin Mok, S. Hassan HosseinNia, and Jo Spronck. Performance improvement of optical mouse sensors: Application in a precision planar stage. *2016 International Conference on Manipulation, Automation and Robotics at Small Scales, MARSS 2016*, 2016.
[21] L van Moorsel. A planar precision stage using a single image sensor (MSc Thesis), 2017.
[22] E. Uhlmann and N. Bayat. High precision positioning with ferrofluids as an active medium. *CIRP Annals - Manufacturing Technology*, 55(1):415–418, 2006.
[23] S van Veen. Planar Ferrofluid Bearings (MSc Thesis), 2013.
[24] R. Deng, S. Van Veen, M. Café, J. W. Spronck, and R. H. Munnig Schmidt. Linear nano-positioning stage using ferrofluid bearings. *Conference Proceedings - 14th International Conference of the European Society for Precision Engineering and Nanotechnology, EUSPEN 2014*, 1(June):372–375, 2014.
[25] B. Assadsangabi, M. H. Tee, and K. Takahata. Ferrofluid-assisted levitation mechanism for micromotor applications. *2013 Transducers and Eurosensors XXVII: The 17th International Conference on Solid-State Sensors, Actuators and Microsystems, TRANSDUCERS and EUROSENSORS 2013*, 17(June):2720–2723, 2013.

[26] T. A. Osman, G. S. Nada, and Z. S. Safar. Static and dynamic characteristics of magnetized journal bearings lubricated with ferrofluid. *Tribology International*, 34(6):369–380, 2001.

[27] R. Ravaud, G. Lemarquand, and V. Lemarquand. Mechanical properties of ferrofluid applications: Centering effect and capacity of a seal. *Tribology International*, 43(1-2):76–82, 2010.

[28] S Odenbach. *Colloidal Magnetic Fluids*. Number 763 in Lecture Notes in Physics. Springer Berlin Heidelberg, Berlin, Heidelberg, 2009.

[29] Zhuang Wang, Zhengdong Hu, Wei Huang, and Xiaolei Wang. Elastic support of magnetic fluids bearing. *Journal of Physics D: Applied Physics*, 50(43), 2017.

[30] A. S.T. Boots, L. E. Krijgsman, B. J.M. de Ruiter, S. G.E. Lampaert, and J. W. Spronck. Increasing the load capacity of planar ferrofluid bearings by the addition of ferromagnetic material. *Tribology International*, 129(May 2018):46–54, 2019.

[31] S. G.E. Lampaert, B. J. Fellinger, J. W. Spronck, and R. A.J. van Ostayen. In-plane friction behaviour of a ferrofluid bearing. *Precision Engineering*, 54(May):163–170, 2018.

[32] S. G.E. Lampaert, J. W. Spronck, and R. A.J. van Ostayen. Load and stiffness of a planar ferrofluid pocket bearing. *Proceedings of the Institution of Mechanical Engineers, Part J: Journal of Engineering Tribology*, 232(1):14–25, 2018.

[33] S.G.E. Lampaert. Planar Ferrofluid Bearings Modelling and Design Principles (MSc Thesis), 2015.

[34] Physik Instrumente. PIglide Air Bearing Technology datasheet, 2019.

[35] Ferrotec. Ferrofluid data sheet EFH series. 2011.

[36] HKCM Engineering e.K. Magnet-Cuboid Q50x02x02Ni-N35, 2019.

[37] S W M van den Toorn, S G E Lampaert, J W Spronck, and R A J van Ostayen. Design considerations of ferrofluid pressure bearing pads for use in engineering applications. *Unpublished*, pages 1–6, 2020.

[38] COMSOL Multiphysics 5.4, 2019.

[39] Matlab R2018b, 2018.

[40] S. Odenbach. Recent progress in magnetic fluid research. *Journal of Physics Condensed Matter*, 16(32), 2004.

[41] Ferrotec. Data Sheet APG 2100 series, 2013.

[42] Micro-Epsilon. Datasheet optoNCDT 1420.

[43] Geoffrey D. Moeser, Kaitlin A. Roach, William H. Green, T. Alan Hatton, and Paul E. Laibinis. High-gradient magnetic separation of coated magnetic nanoparticles. *AIChE Journal*, 50(11):2835–2848, 11 2004.

[44] Liquids Research Ltd.

[45] Donald Mackay and Ian Van Wesenbeeck. Correlation of Chemical Evaporation Rate with Vapor Pressure. *Environ. Sci. Technol*, 48:10259–10263, 2014.

5

Discussion

The objective of this study is to improve the performance of the ferrofluid bearing by removing or improving the limitations in stroke length and repeatability. This chapter will discuss the main results of this study. First the design of pressure bearing pads is discussed, followed by a discussion of the design of long stroke ferrofluid stages. A comparison between different bearing types will conclude this chapter.

5.1. Design considerations of ferrofluid pressure bearing pads

The paper in chapter 3 presents the findings about the design considerations for ferrofluid pressure bearing pads. Although the pressure bearing was used in several instances in literature [8, 29, 47], the influences of different variables in the magnet configuration was unknown or incomplete.

5.1.1. Magnet configuration

Figure 5.1 shows the varied design variables in the geometry of the pressure bearing pad. Using an initial parameter sweep, the influence of the different design variables on load capacity and stiffness is determined, as well as weight and cost of the magnet configuration. Extended plots on the interaction between variables can be found in appendix D. The most influential variable in the magnet configuration was found to be the magnetization direction of the magnets in relation to each other. Four magnetization directions were simulated: up-down, up-up, up-left and left-right. Missing here is the Halbach array, where magnets are rotated 90 degrees from the neighbouring magnets. This configuration directs a high magnetic field intensity to one side of the magnet array and has been used in a number of actuator designs [32]. For this application aside from magnetic field intensity, the gradient in the magnetic field is also of importance for the stiffness of the bearing. Halbach bearings are primarily used for their constant magnetic field, thus little gradient [49]. A ferrofluid pressure bearing using a Halbach bearing would thus have a high load capacity with little stiffness, which is unwanted in this application. The use of the Halbach array will also lead to significant stray fields. Therefore, the Halbach configuration was left out of the simulation.
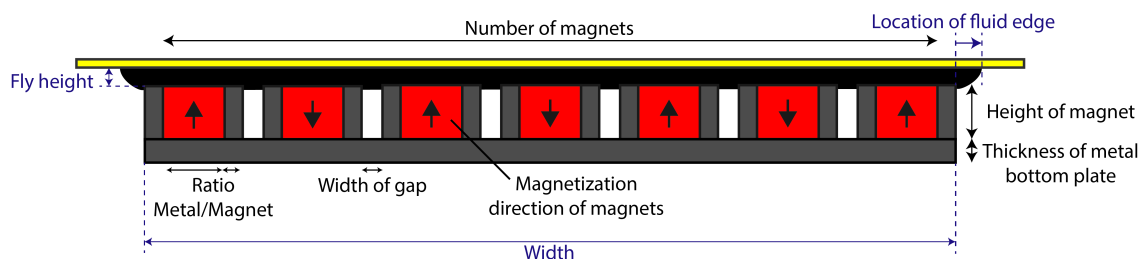

Figure 5.1: Design variables (black) and model constants (blue) in a cross-section of the bearing pad. The length of the pad is defined into the plane. Figure from chapter 3.

Beyond the magnetization direction, the remanent flux density in the magnets and the number of magnets are of importance for the load capacity and stiffness of the bearing. The remanent flux density is limited due to the material properties, but this limit is shifting continuously. Today by using Nd-Fe-B, a remanent flux density of around 1.6 T is possible, while 40 years ago the maximum was around 1 T. [9]. The number of magnets is limited by manufacturing and assemblage. This is due to the brittleness of neodymium-based magnets and the magnet interaction during assembly. A possible solution to these problems would be to 'write' the magnetic field on a monolithic piece of Ne-Fe-B. The technology to magnetize individual circles with a diameter of ~1 mm has been patented by Fullerton, et al. [15, 28]. The creation of high gradients in the remanent flux inside the material is done by an initial magnetization of the whole magnet material in the one direction, individual areas can then be 'overwritten' with a magnetization in the opposite direction. [14].

It must be noted that little information is available about this exact process and the magnetic performance of the final magnet. This manufacturing method is not available for the production of left-right magnetization configuration, both because of the in-plane direction of magnetization and the need for metal with high magnetic permeability in between the magnets.

The model assumes a 2D geometry continuing infinitely in and out of the plane as seen in figure 5.1. While the 2D geometry does give advantages in assembly and eddy current damping, a 3D arrangement of the magnets could produce a higher bearing performance in terms of load capacity and stiffness. In a checkerboard array for example, the oppositely magnetized magnets have more contact and therefore decreasing the amount of distance the field has to travel through air. This effect is comparable to increasing the number of magnets in the 2D geometry with the associated trade-off between load capacity and stiffness. Depending on the application, it can be beneficial to look into the 3D geometry. For the demonstrator stage a 3D geometry is unnecessary as the trade-off between load capacity and stiffness can be varied by altering the preload and thus, a 2D geometry having less assembly effort and eddy current damping is chosen.

5.1.2. Load and stiffness
Measurements were taken of a 46x50mm bearing pad consisting of 23 50x2x2mm magnets [19], arranged in an up-down magnetization configuration. The pad was filled with 5 grams of either the EFH3 ferrofluid or the APG 513A. The load-fly height characteristic for each of these ferrofluids was determined using a Zwick materials test frame. This can be seen in figure 5.2.

The same load-fly height was also modelled. The modelling of the bearing pad using the APG fluid shows a good correspondence to the measurement. There is a slight divergence of the model and measurement as the fly height approaches zero that can be explained by the squeeze film damping from the relatively viscous (150 mPa·s) ferrofluid.

The measured load capacity of the bearing pad using the EFH3 fluid differs significantly from modelled value. The most probable explanation of this discrepancy is the (partial) loss of colloidal stability of the ferrofluid. An accumulation of the particles in between the magnet fillets can effectively short the magnetic field, which reduces the intensity of the magnetic field around the bearing pad significantly. Usually the ferrofluid is modelled as air due to the low magnetization saturation. As the magnetization saturation locally increases when particles accumulate this assumption is no longer valid. As can be seen in figure 5.2 the EFH3 measurement can be well approximated by increasing the relative permeability to 4.

The reason the APG 513A fluid doesn't suffer from accumulation would be a higher colloidal stability. This higher stability compared to the EFH3 fluid can be the result of the lower amount of magnetic particle in the fluid, a thicker layer of surfactant or a smaller fraction of larger particles [30].
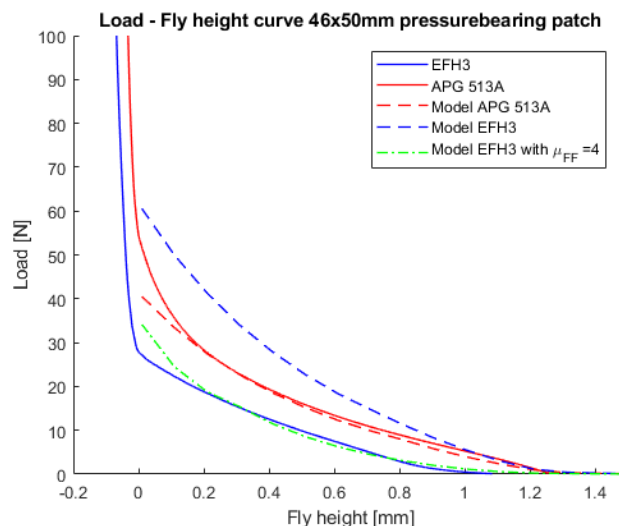
Figure 5.2: Load-fly height curve of pressure bearing pad with EFH3 [12] or APG 513A [13] ferrofluid. The pad consists out of 23 50x2x2mm [19] magnets with a remanent flux of 1.17 T, arranged in up-down configuration. Model constants used: Location of fluid edge: 0.8 mm APG 513A and 0.9 mm EFH3, Magnetic saturation: 32 kA/m for APG 513A, 52.5 kA/m for EFH3. Figure from chapter 3.

5.1.3. Design rules for ferrofluid pressure bearings using up-down magnetization direction in a 2D geometry

By summarizing chapter 3, the following design rules are formulated for the design of ferrofluid bearing pads:

- Use long slender magnets to increase stiffness and load capacity.

- Increasing the remanent flux density proportionally increases stiffness and load capacity.

- By varying the number of magnets for the same width a compromise between stiffness and of load capacity can be found.

- Iron bottom plates reduce effort in assemblage and reduces the height of the magnets for the same performance.

- Consider the diffusion of particles in the FF in the modelling.

- Increasing the number of magnets for the same width decreases stray field.

5.2. Discussion of design for long stroke ferrofluid bearings

Chapter 4 discusses the design of a passive ferrofluid stage capable of a stroke of 460 mm without the effects of stick-slip. The previously discussed pressure bearing pads using the up-down magnetization configuration were used in this bearing. The pressure bearing pads were implemented such that they can be overfilled to serve as a reservoir to counter the effects of trail formation. The bearing pads were placed in close proximity to allow the fluid to move between the individual bearing pads.

5.2.1. Load capacity and stiffness

The load capacity and stiffness of the stage was evaluated using a Zwick materials test frame. In comparison to the model the stiffness of the stage is slightly higher at higher loads. The exact cause for this is unclear, although it can be caused by a misalignment between the test frame and the mover. This results in premature contact between mover and base, increasing the stiffness. The actual load capacity is validated by placing a weight of 120 N on top of the mover and placing the setup under a very slight angle. Due to the lack of stick-slip, there will be a translation in the mover. The angle was kept small enough to prevent translation when the mover and base make contact.

Due to the pre-loaded nature of the bearing, the load capacity and stiffness can be varied by increasing
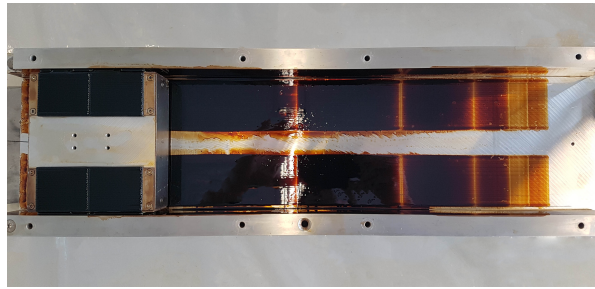
Figure 5.3: Trail formation in stage with top plate removed. The mover has been displaced in steps increasing in velocity from right to left. Figure from chapter 4.

the gap in the base. This was done using 0.1 mm spacers. This setup reduces the overall stiffness of the top plate and compromises the straightness of the top plate. To prevent significant deformations of the top plate, the bolts were all torqued to similar specification. Even though care was taken to construct a rigid setup, the stiffness of the mover and base is not infinite, thus influences the measured stiffness. The stiffness of the mover is evaluated using COMSOL [2] to be > 20 N/µm, thus this influence can be considered negligible.

5.2.2. Trail formation
The repeatable behaviour of the stage is affected by trail formation and evaporation. Trail formation occurs in translation when the shear force on the fluid exceeds the magnetic body force. The flow profile in the ferrofluid and especially the end effects are not fully understood and thus the modelling shear force is difficult. The viscosity of the ferrofluid is the main contributor to the shear force on the fluid, other contributors to the shear in the ferrofluid are adhesion and capillary forces [26]. The trail formation can be reduced by reducing the viscosity or decreasing mover velocity, thus decreasing the viscosity part of the shear force on the fluid. This was noticed in the demonstrator setup. Figure 2.3 shows the effect of mover velocity on trail formation.

The relation between viscosity and trail formation was seen when the EFH3 fluid was substituted for the more viscous APG 513A, the trail formation was increased dramatically, full strokes could only be made at low velocity. Granted, this increase in trail formation is caused by the decrease in saturation magnetization relative to the EFH3 ferrofluid as well. The relation between trail formation and fly height is more intricate. Increasing the fly height will reduce shear force on the fluid, but will also increase the distance between fluid and magnet thus reducing the field gradient.

The worst possible fluid loss can be found by assuming a Couette flow between the bearing surfaces and integration over total stroke. Assuming a fly height of 0.5 mm for all six bearing pads in the system, this evaluates to a fluid loss of ~20 ml. The stage is filled with 55 grams of ferrofluid, which is ~38 ml. The volume between the bearing surfaces is 15 ml, thus theoretically ~15 ml can be lost due to trail formation before the mover height is compromised. This would result in a layer thickness of around 15 µm, which is very similar to the 15 µm trail height described by Lampaert [24].

The height of mover was measured at the end of several repeated strokes with different velocities. As can be seen in figures 5.4 and 5.5 the mover height remains constant for all velocities when filled with higher amounts of fluid, even with added payload. As the height is only measured at one point in the stroke this is no measure for the flatness over the whole stroke. However, it does give an accurate representation of the influence of the trail formation on the mover height. From the increase in mover height as seen in figure 5.5 ~ 1-2 µm can be attributed to the weight loss due to ferrofluid loss. The other 3-4 µm could be explained by a different amount of fluid on the top bearing. As the fly heights differ between top and bottom bearing it is possible the top bearing loses more fluid and thus the clamping force on the stage is reduced slightly.

The maximum difference in mover height is less than ± 7 µm, this is achieved with a mover velocity of 0.5 m/s and a payload of 1.75 kg. When limited to 1 kg at 0.25 m/s the out-of-plane height difference is reduced to less than ± 3 µm. This corresponds with the observations of the increase in trail formation with an increase in velocity.
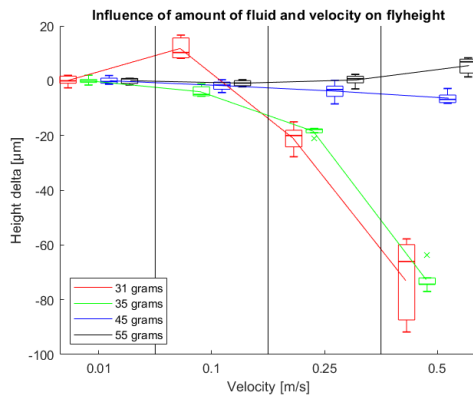
Figure 5.4: Height loss under translation at different speeds for different amounts of fluid. No payload was added to mover. Figure from chapter 4.
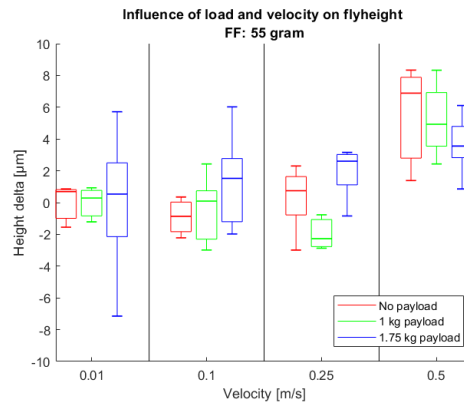
Figure 5.5: Height loss under translation at different speeds when filled with 55 grams of FF. Figure from chapter 4.

5.2.3. Evaporation

With a maximum trail surface of ~900 cm^2 and filled with 55 grams of EFH3 fluid, the stage will have evaporated 7.5% of the carrier fluid after 75 hours. This will increase the viscosity with 50%. This is under the assumption that the fluid is well mixed and the whole stroke is covered in ferrofluid trail. Using a rheometer, the hypothesis of reversing the effects of the evaporation by resupplying with carrier fluid is confirmed. When implemented, this resupplying can be done continuously or at discrete moments. Though the time between resupply intervals must be short enough to prevent larger amounts of evaporation. This resupply can be compared to normal lubrication of bearings. With slight adjustments existing lubrication solutions can be used, such as gas or spring driven automatic lubrication pumps [41]. Though, the resupply has yet to be tested in a functioning stage.

A different solution to the evaporation problem would have been the use of a ferrofluid with a very low vapor pressure. The H9-LT ferrofluid from Liquid-Research has a vapour pressure of $\sim 1 \cdot 10^{-7}$ kPa [1] which will reduce the vapour pressure to the point of negligible evaporation [27], thus making this ferrofluid a potential lubricated-for-life solution. Low vapour pressure ferrofluids however are expensive and have a high viscosity. The H9-LT ferrofluid has a viscosity of 300 mPa·s, which is 25 times higher than the used EFH3 ferrofluid. Thus, the use of this ferrofluid will increase damping and trail formation, thus reducing the possible stroke length and mover velocity.

5.2.4. Damping

The friction of the stage is due to viscous damping only, caused by the viscosity of the ferrofluid. The contribution of the eddy current damping is very low due to the use of long slender magnet and the alternation of the magnetization direction. These long slender magnets are positioned with their length into the movement direction, this provides constant magnetic field in the movement direction with only field gradients at the beginning and end of the magnet. The limited width and alternation of the magnetization direction break up the current loops into smaller loops. The dividing of an eddy current loop into two smaller loops halves the current in each loop, this halves the total damping force as the electric energy loss as is defined as $I^2 R$. As there are 20-25 magnets in the bearing pads only limited currents are created, resulting in a low damping. Appendix A shows the modelling of the eddy current damping for a variety of bearing pads. The damping is shown to be highly anisotropic. This is beneficial for controllability of the stage mover, as the resonance peaks of the other movement modes are damped.
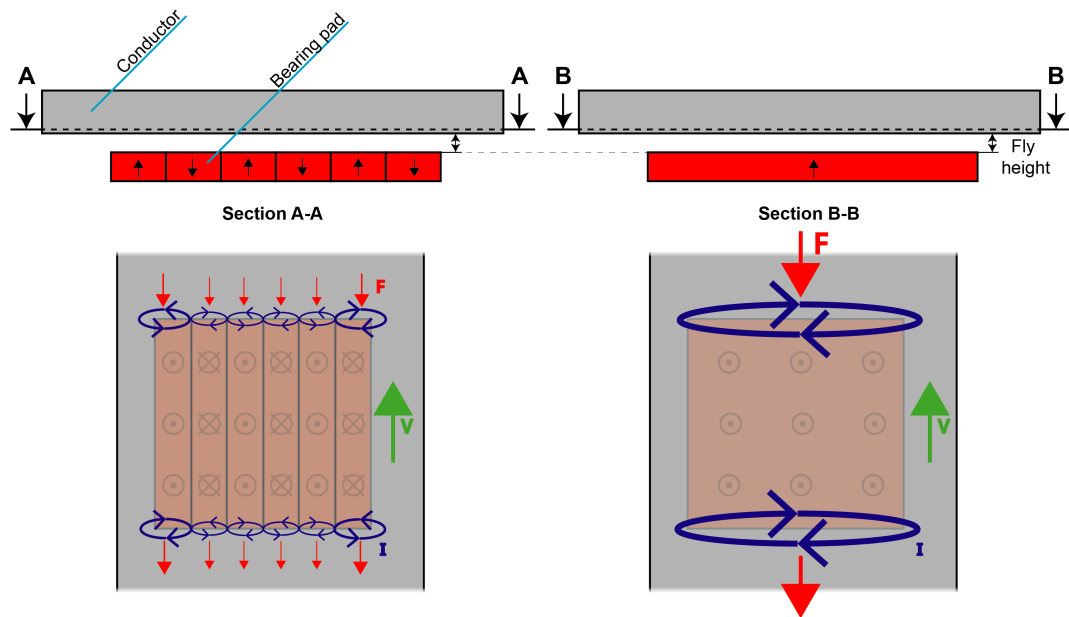
Figure 5.6: Illustration of the location and magnitude of the eddy-current damping using an up-down magnet configuration with slender magnets and a single magnet, with the relative velocity between bearing pad and conductor (V), the damping force (F) and the current in the eddy-current loops (I).

In order to provide more detailed understanding of the flow profile between the bearing surfaces, the measured damping data and the research done by Lampaert [22] are used to create a model. Lampaert assumes a net zero volume flow in between the bearing surfaces, this assumption is not applicable to bearings with strokes $>\sim 1$ mm as there is trail formation and thus also net volume flow. The model fitted is a Couette flow with pressure gradient. The model does show an interesting flow profile, high net volume flow at low velocities and lower net volume flow at higher velocities. This is the exact opposite of what is seen in figure 5.3. This can point at the possibility of a reverse flow channel at the sides of the pressure bearings. From the model no physical significance could be obtained, leading to the conclusion that more variables are influencing the pressure gradient such as the height in the reverse flow channel.

5.2.5. Design rules for linear ferrofluid stages based on pressure bearing pads
By summarizing chapter 4, the following design rules can be formulated for the design of long stroke ferrofluid stages

- Place the different bearing pads as close to each other as possible to allow for fluid transfer between pads

- Choose a ferrofluid with low viscosity and high saturation magnetization to reduce fluid loss.

- Create recirculation channels to decrease damping and reduce fluid loss

- Use reservoirs to eliminate effects of trail formation.

- Place reservoirs close to the bearings to allow for instant replenishing of the lost trail.

- Stiffness can be increased by using a clamped-in design, by increasing the saturation magnetization of the ferrofluid or by changing the design of the bearing pad.

5.3. Ferrofluid bearing types
Several choices were made in the design of the stage, among which the choice of ferrofluid bearing type. While the load and stiffness of the pocket bearing exceeds the pressure bearing, it suffers from air loss. This problem is only enlarged by the addition of multiple seals, as each air pocket will have their own operational range [6]. Additionally, to apply the same strategy as used in the stage for the creation

of the reservoirs, no iron can be used next to the magnets as this would reduce the magnetic field outside of the magnet. This will compromise load and stiffness of the pocket bearing, thus separate systems have to be designed to transport fluid to and from a reservoir. Such systems would both need to be passive, don't affect the magnetic field around the seal and have a relatively high volume flow of several ml/second. The eddy current damping in the pocket bearings is much larger than in the pressure bearings. Using COMSOL models a damping of 10-20 N·s/m was estimated for a mover with similar specifications (Appendix A). Finally, the ring or disc is the most efficient shape for a magnet in a pocket bearing. Due to being axisymmetric the magnetic field is uniform at the edge, ensuring no weak points in the seal. A rectangular magnet shows a non-uniform field at the corners, this creates a weakness in the pocket seal or can even prevent the forming of a sealed pocket entirely. This need for round shapes complicates the design of the stage.

This combination of bad repeatability, complexity and excessive damping shows the correct choice was made in choosing the pressure bearing over the pocket bearing in the design of the linear ferrofluid long stroke stage.

5.4. Comparison to other bearing types

It was summarized in the introduction that the ferrofluid bearing can fill a niche in the market where low cost, passive smooth motion is required without a demand for high out of plane accuracy. As there is no direct competitor for this new bearing type, the stage is compared to the closest competitors and to earlier ferrofluid based demonstrator stages.

5.4.1. Ferrofluid bearing stages

The stage from Van Veen [47] is an earlier demonstrator design. The design was based on pressure bearings and supported a payload of up to 0.6 N with a stiffness of 0.017 N/µm. The footprint of this stage is 107x110 mm, supporting a stroke of up to 20 mm. The stage suffered from increase in damping and reduction of fly height due to trail formation at strokes of 14 mm. The stage designed in this research outperforms the bearing created by van Veen in all aspects.

A 3 DoF stage was built by van Moorsel more recently [46]. Based on pocket bearings, this stage supported a payload of up to 100 N with a stiffness of 0.81 N/µm. The pocket bearing used has a diameter of 150 mm and was build-up using individual segments for an increase in rotational stiffness. The footprint of this stage is similar to the stage designed in this research although, the stage from van Moorsel is less high due to the lack of horizontal constraint. The load capacity and stiffness of the stages are comparable as well, showing the that the optimized pressure bearing pads can compete with single seal pocket bearings. The stroke of this stage was 30 mm and suffered from 60 µm reduction in fly height due to trail formation after the maximum stroke of 30 mm. The demonstrator stage has more than 15 times the stroke of this bearing and does this with a 10 times more stable fly height.

5.4.2. Rolling contact bearings

Though rolling contact bearings suffer from stick-slip it is the current passive alternative to air bearing stages. These bearing types exceed the load capacity and stiffness of the designed stage [31]. Aside from the stick slip behaviour, the roller bearing exhibits other downsides. The rails though require very precise machining to prevent the carriage from seizing and to ensure a constant friction. Static and dynamic overloading, contamination or manufacturing errors of the roller bearing can result in imperfections in the bearing [4]. These imperfections can cause vibrations and will in the long-term lead to premature bearing failure [37]. A ferrofluid bearing suffers from none of these problems.

5.4.3. Air bearing stage

The designed stage performs comparable to the air bearing stage on which it was based in terms of load capacity, moving mass and compactness. However, in terms of out of plane stiffness and height reproducibility the air bearing stage well exceeds the performance of the stage. These problems are fundamental to the ferrofluid bearing, even though they can be improved, the level of the aerostatic bearings will never be reached. However, the unique feature of the ferrofluid based stage is the passive ability. Depending on the application this will result in the choice of a ferrofluid based bearing over an aerostatic stage.

The ferrofluid bearing can also compete in terms of cost. The total material cost for the ferrofluid demonstrator stage are slightly over €1000, the magnets attribute €150 and the FF €50. The material cost of a comparable air bearing stage alone will be similar, but the total material costs of the air bearing system will be higher due to costs of the required air supply components. The production costs of the ferrofluid bearing will be lower than an aerostatic bearing of similar specification. This is due to the lower manufacturing tolerances caused by the higher fly height of the ferrofluid bearing.

5.4.4. Comparison between ferrofluid bearing types
A comparison between the pressure and pocket bearing is done based on the discussion in this chapter. This is done specifically for the use in long stroke bearing applications. The pressure bearing is here taken as a benchmark, a + denotes a better performance.

Aspect	Pressure bearing	Single seal pocket bearing	Multiple seal pocket bearing
Load capacity	0	0	++
Stiffness	0	0	++
Friction	0	-	- -
Complexity	0	-	- -
Repeatability in height	0	-	- -

Table 5.1: Comparison between pressure and pocket bearings using single or multiple seals

6

Conclusions

This chapter presents the conclusions of this thesis divided into four sections. Section 6.1 contains general conclusions that are relevant to this thesis. Section 6.2 contains the conclusions pertaining to ferrofluid pressure bearing pads. Section 6.3 contains the conclusions pertaining to long stroke ferrofluid stages and section 6.4 contains the conclusions of the comparison of ferrofluid bearings to other bearing types.

6.1. General conclusions

This thesis discusses a passive linear long stroke ferrofluid stage. This stage can be considered as a revolution over previous ferrofluid bearing instances. The bad reproducibility in height and restrictions in stroke are no longer a major drawback of the ferrofluid bearing. It is shown that this pressure bearing based stage performs comparable to a single seal pocket bearing based stage in terms of load capacity and stiffness. In terms of stability in fly height, the designed stage well exceeds previously built stages. Thus, the objective of improving the performance of the ferrofluid bearing by removing or improving the limitations in stroke length and repeatability is attained.

In comparison to commercially available passive bearing options such as linear roller bearings, the demonstrator stage has no stick-slip, requires less strict manufacturing tolerances and doesn't suffer from vibrations. In comparison to aerostatic bearing stages the demonstrator stage is only outperformed in terms of out of plane stiffness and height reproducibility, but it can accomplish the same smooth motion without the need for a constant supply of air or tight manufacturing tolerances. Moreover, the demonstrator stage bearing approaches the same out-of-plane stability for limited payload and velocity. Making the ferrofluid bearing a feasible alternative to aerostatic bearings, depending on the demands of the application.

6.2. Ferrofluid pressure bearing pads

The main conclusions for the research into ferrofluid pressure bearing pads can be summarized in the following bullets:

- Load capacity and stiffness is primarily limited by the maximum remanent flux density in the magnet, the saturation magnetization of the ferrofluid and the minimal size of the magnets due to assembly and manufacturing.

- By arranging slender magnets in an up-down magnetization configuration and by adding a thin metal bottom plate it is possible to create a low cost and low weight pressure bearing pad with negligible stray field.

- Pressure bearings in the up-down magnetization configuration can be produced monolithic.

- The pressure bearing can be made to perform comparable to a single seal pocket bearing in terms of load capacity and stiffness.

43

- Care has to be taken in selecting a ferrofluid that is colloidally stable even in high gradients in magnetic field intensity.

6.3. Long stroke ferrofluid stage

The main conclusions for the research into long stroke ferrofluid stages can be summarized in the following bullets:

- A long stroke bearing with a stable out of plane height can be created by using pressure bearing pads, in combination with a ferrofluid reservoir.

- As the amount of trail formation is limited, an adequate reservoir can be created by overfilling the pressure bearing pads.

- Trail formation can be reduced by increasing the gradient in the magnetic field at the ends of the pressure pad, by increasing the saturation magnetization or by lowering the viscosity of the ferrofluid.

- The use of a symmetric bearing design improves the stiffness and out of plane repeatability.

- The eddy current damping can be reduced by the use of long slender magnets and translation in the length direction of the magnets.

- The effects of evaporation of a ferrofluid on the viscosity and normal force in a magnetic field can be restored by resupplying with carrier fluid.

- The implementation of a reverse flow channel can reduce both trail formation and damping.

6.4. Comparison to other bearing types

The main conclusions of the comparison between the ferrofluid bearing and other bearing types can be summarized in the following bullets:

- Ferrofluid bearings can be used instead of rolling contact bearings to eliminate vibrations and premature bearing failure due to contamination.

- Ferrofluid bearings can improve performance over rolling contact bearings in applications where a passive bearing is required and performance is limited by stick slip.

- Ferrofluid bearings can be produced at low cost relative to aerostatic stages.

- The ferrofluid pressure bearing can compete with an aerostatic stage when out of plane stiffness and repeatability are of less importance.

- The ferrofluid pressure bearing is an alternative to bearings when a permanent supply of air is unwanted and the out of plane stiffness and repeatability are not crucial.

7

Recommendations

In this chapter several recommendations are shown for further research. Long stroke ferrofluid bearings show great potential, and thus the overall recommendation is to maintain the research effort in this field of bearings. Several recommendations are done on the following topics in order to further guide this research towards the goal of commercial availability of the ferrofluid bearing.
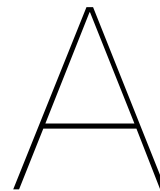
7.1. Pressure bearing pads

- Improve the understanding of the behaviour of the EFH3 ferrofluid in large magnetic field gradients.

- Increase the performance of the bearing pads by use of a high colloidal stable ferrofluid with a high magnetization saturation.

- Evaluate the performance of 'written' magnet configurations to reduce the assembly cost of the bearing pads.

7.2. Long stroke ferrofluid stages

- Partner with a company with affinity in bearing systems, interested in the same goal of commercial availability of the ferrofluid bearing stage.

- Design, manufacture and validate a ferrofluid more suitable for use in bearing applications.

- Redesign the stage for more containment of the ferrofluid trail, to implement solution for the evaporation through resupply of the carrier fluid if necessary and to increase the ferrofluid reservoirs to accommodate the trail formation of a more viscous ferrofluid.

- Design and implement an integrated actuator for the ferrofluid stage.

- Research the performance of the stage under dynamic conditions, including but not limited to the bandwidth, the modal responses, and the pitch, yaw and roll of mover under a constant velocity.

7.3. General recommendations for future research

- Develop a stage and ferrofluid specifically intended to replace aerostatic bearings in vacuum environments.

- Look into the creation of pocket bearings using magnets with rounded corners.

A

Eddy-current damping

A.1. Pressure bearing

When displacing a magnetic field through a conductor, an eddy-current is created. This eddy current is induced by a change in the magnetic field in the conductor. As the conductor has a resistance energy will be dissipated, resulting in a damping force. As the targeted material for the base is aluminium eddy current damping can potentially be a large problem. A similar problem has been solved by [44]. Here the relative velocity between conductor and magnetic field was removed by placing the conductor on an actuator. In order to estimate the severity of the problem, a simulation of was done in COMSOL. A pressure bearing pad was simulated with geometry parameters as seen in figure A.1. This pad was placed parallel to an aluminium conductor at a set distance. The pad was then displaced in either the Y or X direction with 1 m/s.
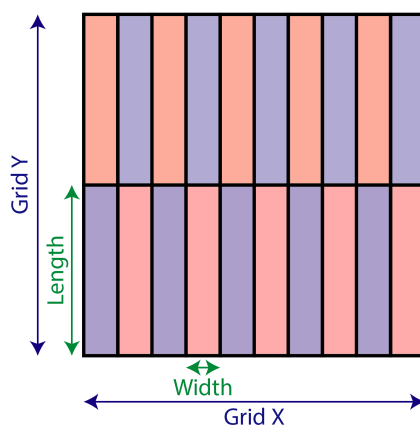

Figure A.1: Eddy current simulation pad parameters. The magnetization direction is into the plane when red and out of the plane when blue

Using this model, the absolute induced damping force of this velocity was determined. The distance between the pad and conductor was set to be the fly height, 0.1 mm. The remanent flux density of the magnet was 1.17 T. Both were kept constant. No metal bottom plate was used. The results of the simulation can be seen in Table A.1.

It can be seen that there a dramatic increase in damping for translations perpendicular to the magnet length as opposed to translation along the magnet length. Figure A.2 shows the eddy current loops generated. The configuration on the left is ideal for the creations of large eddy currents as there are many large gradients in the magnetic flux in the movement direction. Because the magnets are uniform perpendicular to the movement direction the currents are amplified. This in contrast to when we

47

Grid (X*Y)	Magnet dimension (LxWxH) [mm]	Damping coefficient x-direction [N·s/m]	Damping coefficient y-direction [N·s/m]	Increase factor x-direction	Increase factor y-direction
20x1	20x1x1	0.333	0.005	1	1
40x1	20x1x1	0.643	0.009	1.93	1.59
20x1	20x2x1	1.593	0.037	4.79	6.87
20x1	40x1x1	0.675	0.006	2.03	1.12
20x2	20x1x1	0.658	0.016	1.98	2.98
20x3	20x1x1	0.997	0.036	2.99	6.58

Table A.1: Simulation of damping's coefficient for different pressure bearing pad geometries.
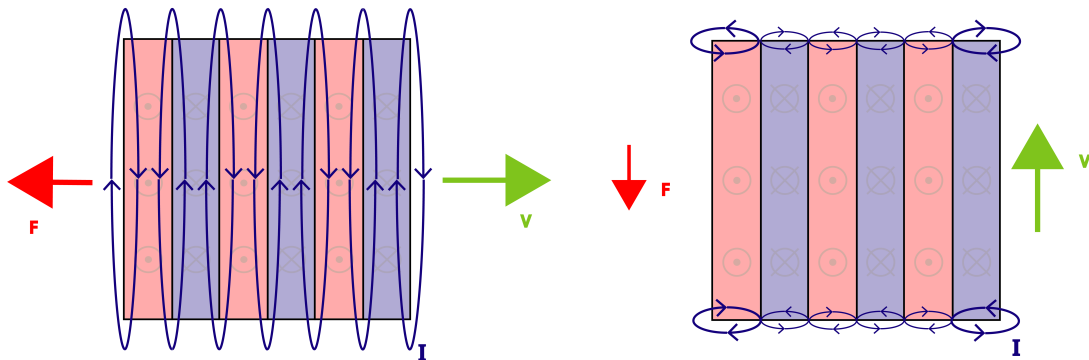

Figure A.2: Eddy currents in for different movement directions in a square bearing pad, with current loops (I), velocity (V) and damping force (F).

move along the magnet length. There are only 2 places at which there is a gradient in the magnetic flux, the begin and end of the pad. The magnetic field is interrupted in the direction perpendicular to the movement direction, thus only small current loops can form. As energy dissipation is a quadratic function of the current this will create an even larger difference in damping between the two movement directions.

The simulation for the full-size bearing pad can be seen in table A.2. As expected from the smaller scale experiment, there is negligible eddy current damping in the movement direction of the system. The damping in the already constraint directions of the linear stage will aid in noise attenuation at higher frequencies.

FlyH [mm]	Damping coefficient x-direction [N·s/m]	Damping coefficient y-direction [N·s/m]
0.10	11.695	0.219
0.25	7.311	0.127
0.50	3.463	0.070
1.00	0.863	0.034

Table A.2: Simulation of eddy current in full size pressure bearing pad. Magnet dimensions 50x2x2 mm, arranged in a 25x2 grid, up-down magnetized.

Experiments measuring the damping in the demonstrator indicate the validity of the simulation. There is a large uncertainty due to the not knowing of the exact flow profile in the fluid film. Despite this the damping is significantly lower than would be using a single magnet of equal dimensions. This solution can also be adapted into other applications. One of them could be in linear aerostatic bearing stages as discussed previously.

A.2. Pocket bearing

The eddy current is also evaluated for a comparable pocket bearing setup. This bearing uses four 42x25x3mm (Dxdxh) ring magnets on the bottom of the mover, two on either side, four 35x25x3mm (Dxdxh) ring magnets on the top and the two of the same ring magnets on each side. As it is a ring magnet, the eddy current damping is similar in translation in x or y direction.
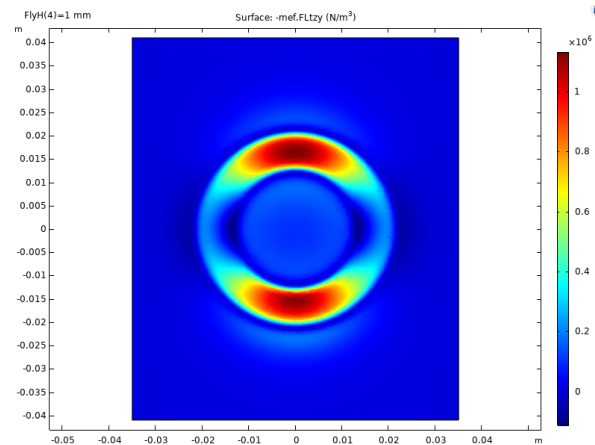

Figure A.3: Location and intensity of eddy current damping in conductor place at surface of conductor placed 0.1 mm from ring magnet with dimensions 42x25x3mm (Dxdxh), magnetized into the plane with a remanent flux density of 1.17 T.

FlyH [mm]	42x25x3mm [N·s/m]	35x25x3mm [N·s/m]
0.10	3.2321	1.7593
0.25	2.9514	1.5647
0.50	2.5581	1.3033
1.00	1.9562	0.93138

Table A.3: Eddy current damping coefficient in 42x25x3mm and 35x25x3mm ring magnet (Dxdxh)

It can be seen that the eddy current damping is both much higher and it is much more constant than in the pressure bearing. This is due to the penetration depth of the field being much higher in the ring magnet than in the pressure bearing pad.

B

Evaporation of APG 513A ferrofluid

The evaporation rate of the ferrofluid was determined in a simple experiment. Five grams of fluid was placed in a Petri dish. The fluid-air interface was 58 cm2 and the temperature was kept between 18 and 22 degrees Celsius. The petri dish with fluid were weight at several moments in time. This resulted in an evaporation rate in the initial 74 hours $2.7 \cdot 10^{-6}$ gram/(cm$^2 \cdot$h) for the APG 513A. The evaporation rate in subsequentially 43 hours was $9.52 \cdot 10^{-6}$ gram/(cm$^2 \cdot$h). This is a factor 60 lower than the EFH3 ferrofluid. Both fluids showed a decline in evaporation rate which can be explained by the initial evaporation of shorter molecules in the carrier fluid. The decline is larger in the APG fluid as it consists mainly of large chained molecules in contrast to the EFH3.

Using a rheometer, the properties of the APG 513A ferrofluid were evaluated when subjected to evaporation. The strength of the used magnetic field is comparable to the field at the surface of the used magnets at 2.5A. The mass evaporation is 0.23% and 0.31% after respectively 74 and 117 hours.

Figure B.1 shows that the evaporation has a very slight influence on the viscosity. The difference is however insignificant when taking into account that the amount of fluid inside the rheometer is dosed manually. As the APG 513A fluid is relatively viscous, the dosage of an exact amount was difficult. Figure B.2 shows a similar result. Although there is a slight increase in normal load in the evaporated fluid, the difference is insignificant in comparison to the relatively inaccurate dosing.

An attempt was made to use the APG 513A fluid in the bearing system. However, as this fluid has a larger viscosity and lower saturation magnetization relative to the EFH3 fluid, the trail formation is increased. This increase caused problems in the containment of the fluid and loss in fly height. Small modifications to the mover and base would have solved these problems. However, lack of time and resources prevented this.
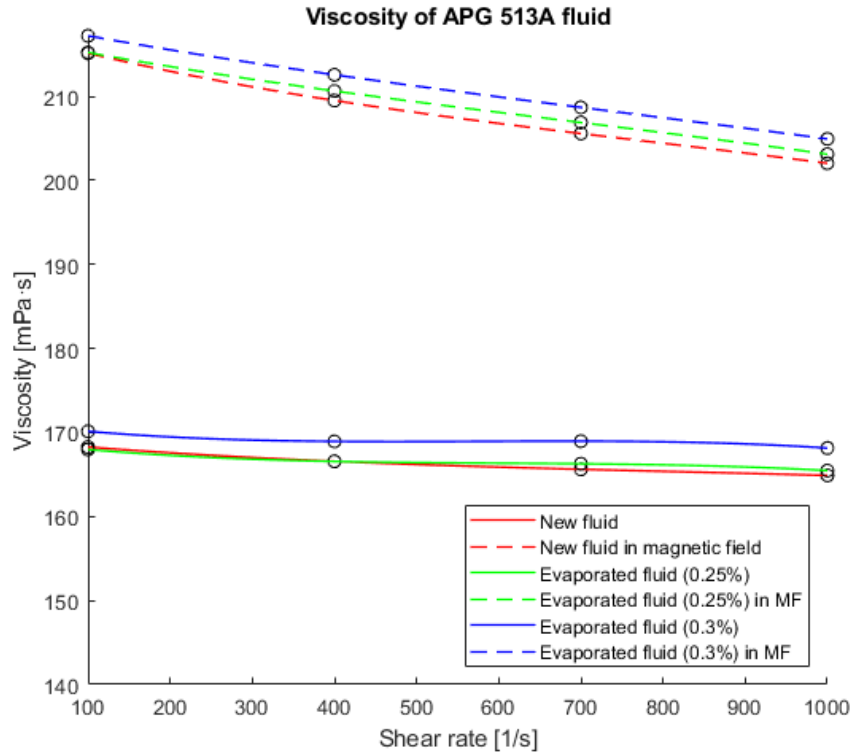
Figure B.1: Viscosity of APG 513A fluid for different levels of evaporation and dilution. The magnetic field was induced with a current of 2.5A.
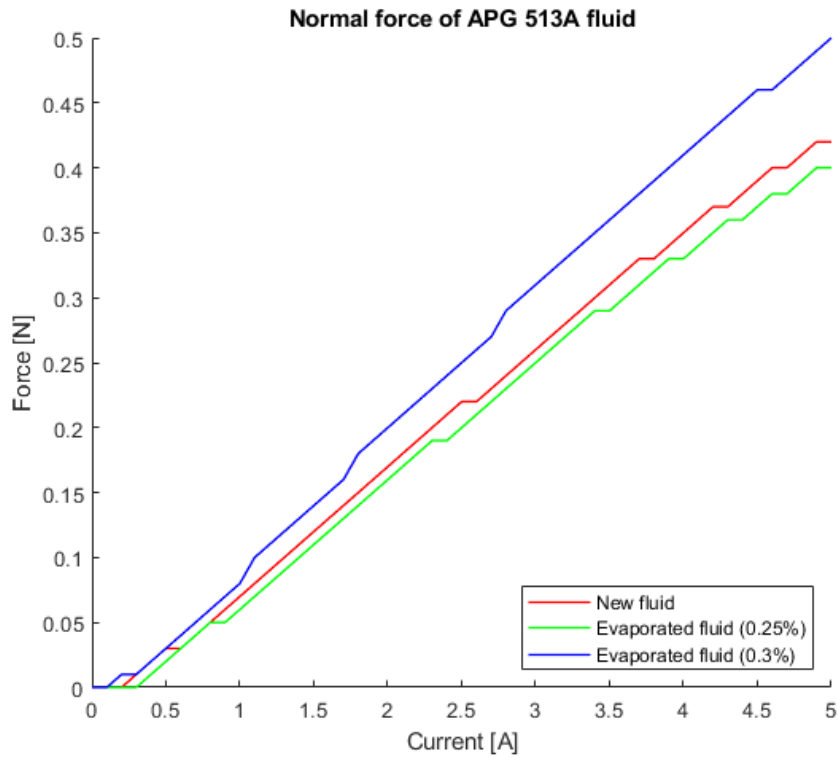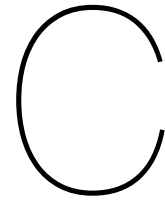

Figure B.2: Normal force exerted by the APG 513A fluid on the rheometer for different levels of evaporation and dilution.

C

Influence of trail thickness on free fall velocity

The thickness of the trail also is of influence on the damping coefficient. This influence is small but noticeable as can be seen in figure C.1 and figure C.2. In these measurements the mover has been pulled back to the position for where it is dropped at different velocities. As discussed before, the trail formation increases with velocity. The measurements are done with 50 grams of FF in the system and a gap of 1.05 mm. The fly height was constant as verified using the 2 laser distance sensors.

The terminal velocity of the mover increases when the thickness of the trail is increased. The influence is larger at higher terminal velocities. As the fly height is constant, this indicates that the thicker trail slightly alters the flow profile in the bearing.
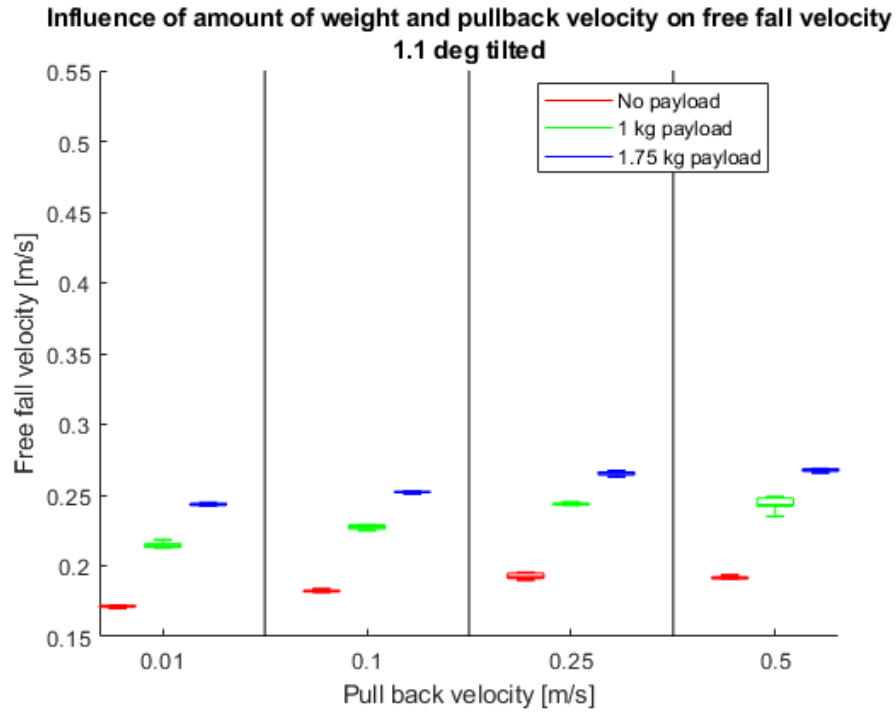
Figure C.1: Influence of thickness of trail on terminal velocity at 1.1 deg incline. Note that the Y-axis doesn't start at zero to improve visibility. Each boxplot represents a series of 5 back to back measurements.
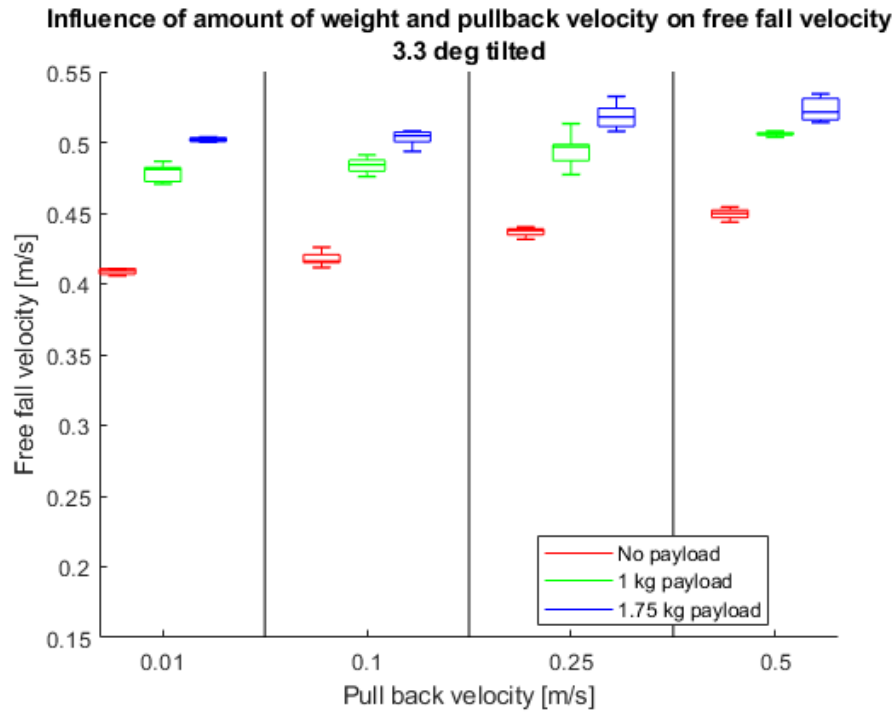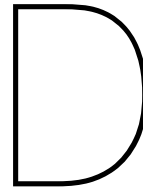

Figure C.2: Influence of thickness of trail on terminal velocity at 3.3 deg incline. Note that the Y-axis doesn't start at zero to improve visibility. Each boxplot represents a series of 5 back to back measurements.

D

Ferrofluid pressure bearing parameter sweep

Figures D.1 and D.2 show the results of the parameter sweep done in chapter 3 for all combinations of all varied variables. Table D.1 shows the values of the individual variables when not varied. Table D.2 shows the constants used in the modelling.

Table D.1: Value of the individual variables when not varied.

Variable	Symbol	Unit	Up-Down Mag. dir.	Left-Right Mag. dir.
Number of magnets	N_{mag}	-	50	50
Remanent flux density of the magnet	Mag_{str}	T	1.5	1.5
Height of magnet	H_{mag}	mm	1	3
Ratio metal/magnet	$R_{\frac{Met}{Mag}}$	-	0	0.4
Metal bottom plate thickness	H_{mbp}	mm	1	0
Width of gap	W_{gap}	mm	0	0

Table D.2: Model constants.

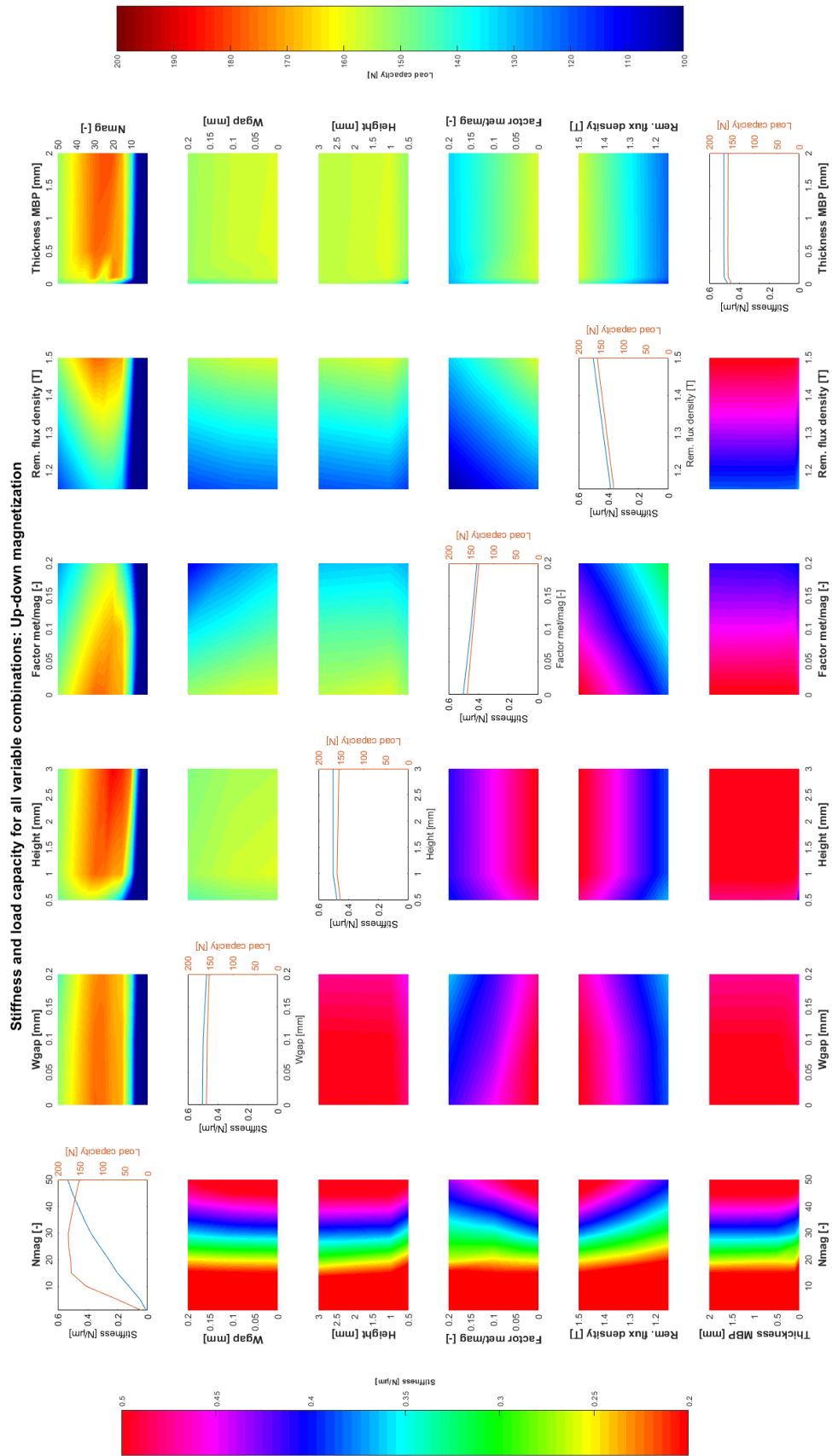| Constant	Value	Unit
Width	50	mm
Length	100	mm
Fly height	0.1	mm
Relative permeability ferrofluid	1	-
Saturation magnetization ferrofluid	$66 \cdot 10^{-3}$	T
Relative permeability metal	4000	-
Saturation magnetization metal	1.4	T
Relative permeability magnets	1	-
Location of air-liquid interface	5	mm

Figure D.1: Stiffness and load capacity as a function of all varied parameters in the up-down magnetization bearing configuration
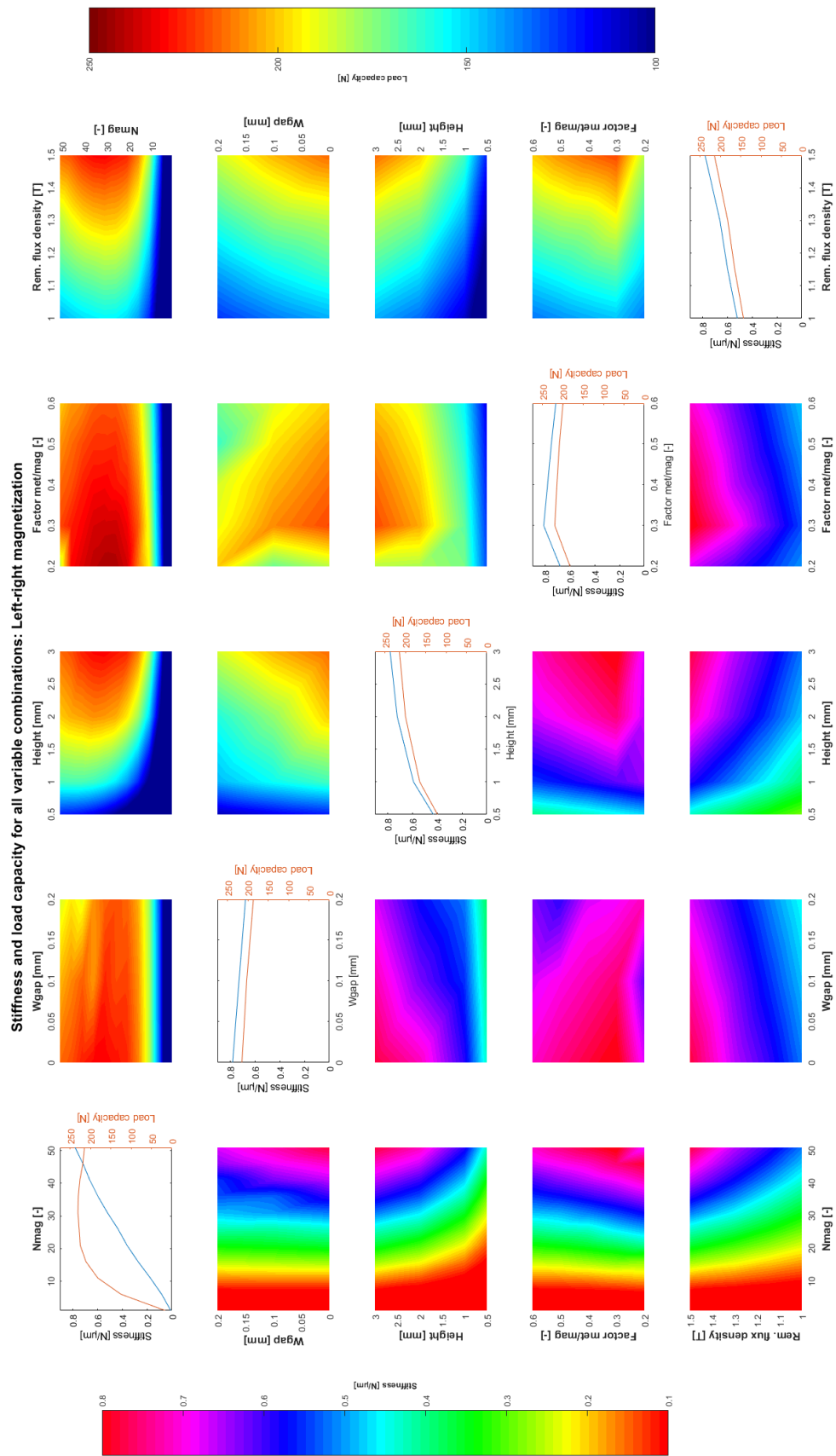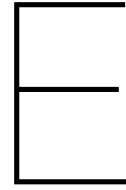
Figure D.2: Stiffness and load capacity as a function of all varied parameters in the left-right magnetization bearing configuration

E

Detailed design

This chapter provides an overview of the necessary parts and their dimensions for the construction of the ferrofluid demonstrator stage.

Item	Material	#
Bolt countersunk M3x5	Stainless steel	24
Bolt countersunk M3x40	Stainless steel	4
Bolt countersunk M4x12	Stainless steel	9
Bolt countersunk M4x25	Stainless steel	4
Bolt countersunk M6x20	Stainless steel	4
Bolt countersunk M6x60	Stainless steel	3
Hex head bolt M6x20	Stainless steel	4
Hex head bolt M6x45	Stainless steel	2
Washer M6 1mm	Stainless steel	6
Washer M6 0.1mm	Stainless steel	100
Base		
Bottom	Aluminium tooling plate 20 mm	1
Top	Aluminium tooling plate 5 mm	1
Side left	Aluminium 6082	1
Side right	Aluminium 6082	1
Mover		
Bottom plate	Aluminium tooling plate 5 mm	1
Top plate	Aluminium tooling plate 5 mm	1
Table plate	Aluminium tooling plate 5 mm	1
Side	Aluminium 6082	2
Spacer	Aluminium 6082	1
Pressure bearing		
Magnet 50x2x2mm 1.17T [19]	Neodymium alloy	240
Bottom back plate	AISI 410S	2
Side back plate	AISI 410S	2
Top back plate	AISI 410S	2
Ferrotec EFH3	Magnetite-Kerosene	55 ml

Table E.1: List of parts with material and required amount.

E.1. Base

Bottom   **Top**

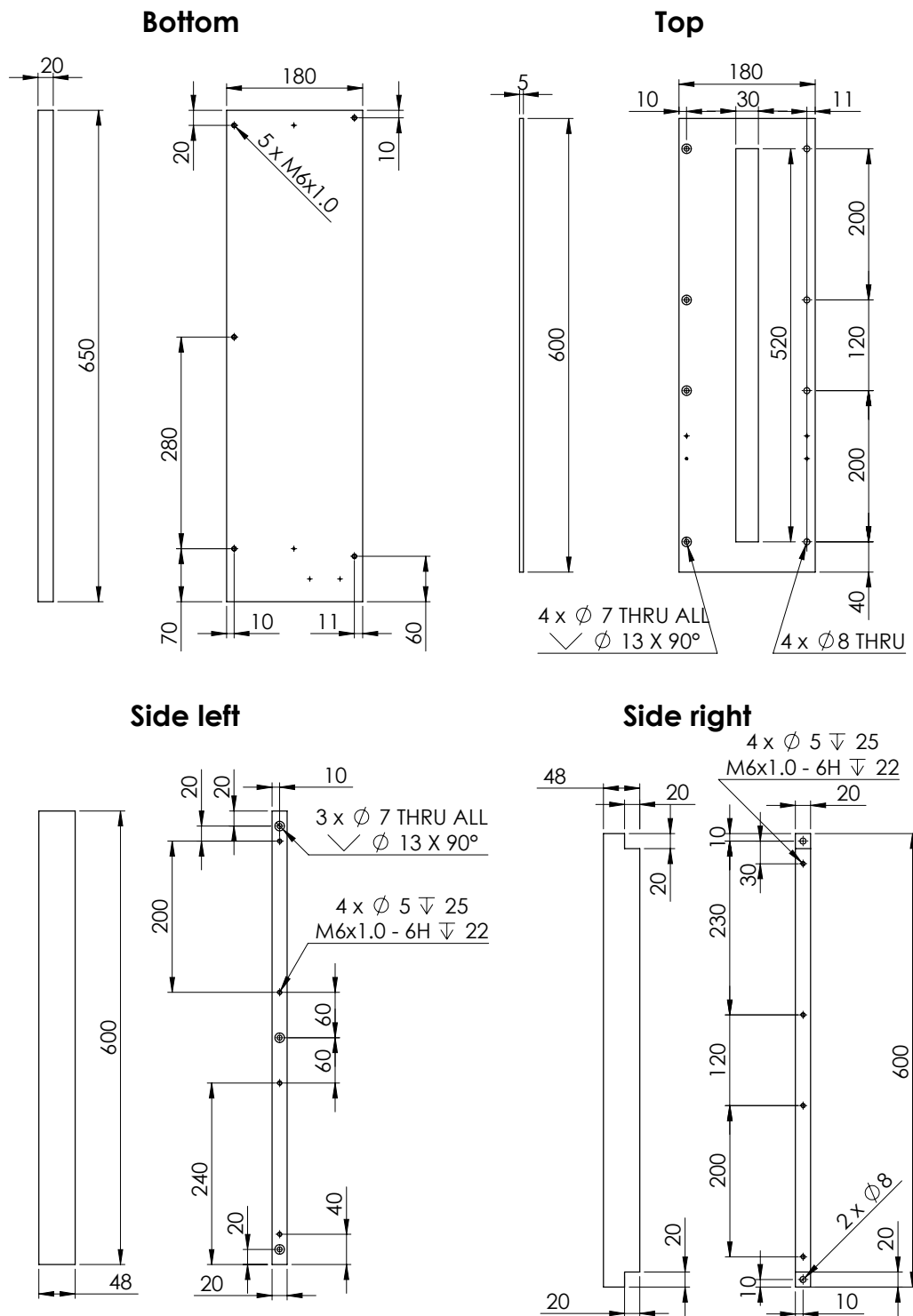**Side left**   **Side right**

Figure E.1: Detailed design of base, all dimensions in mm.
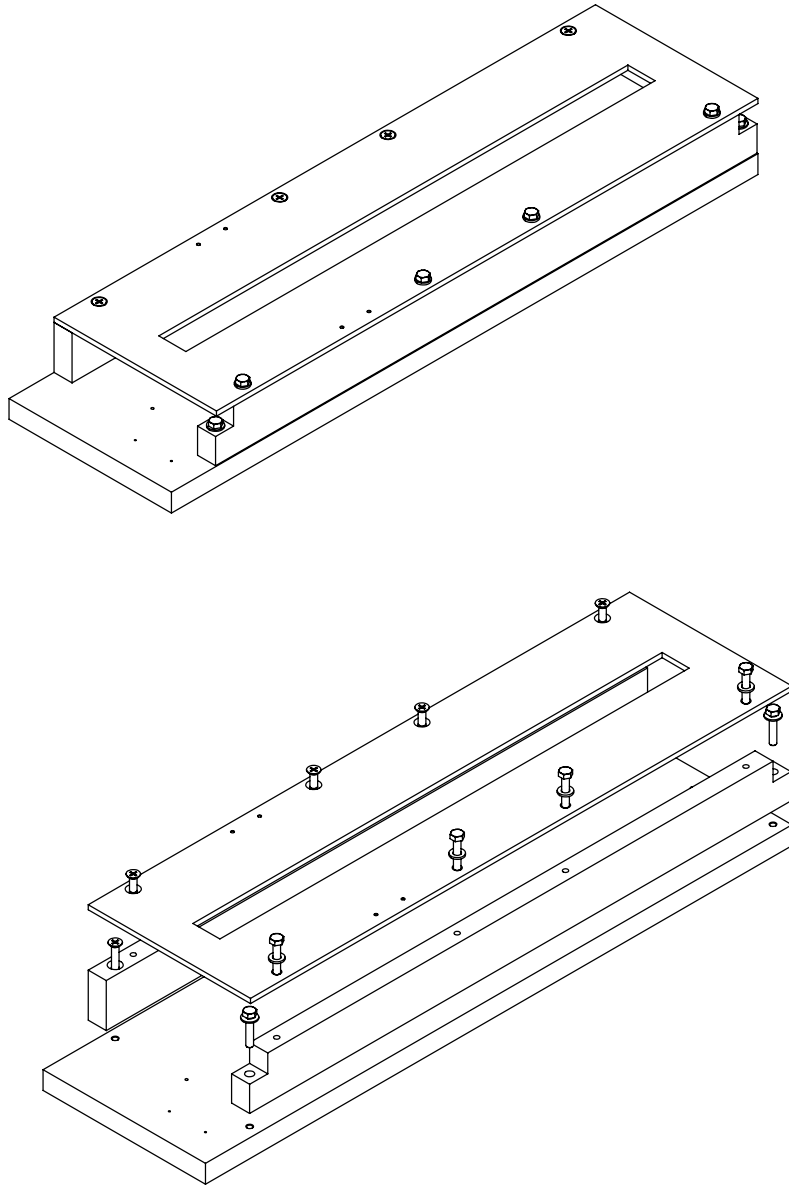
Figure E.2: Exploded view of Base

E.2. Mover

Bottom plate

Top plate

Spacer
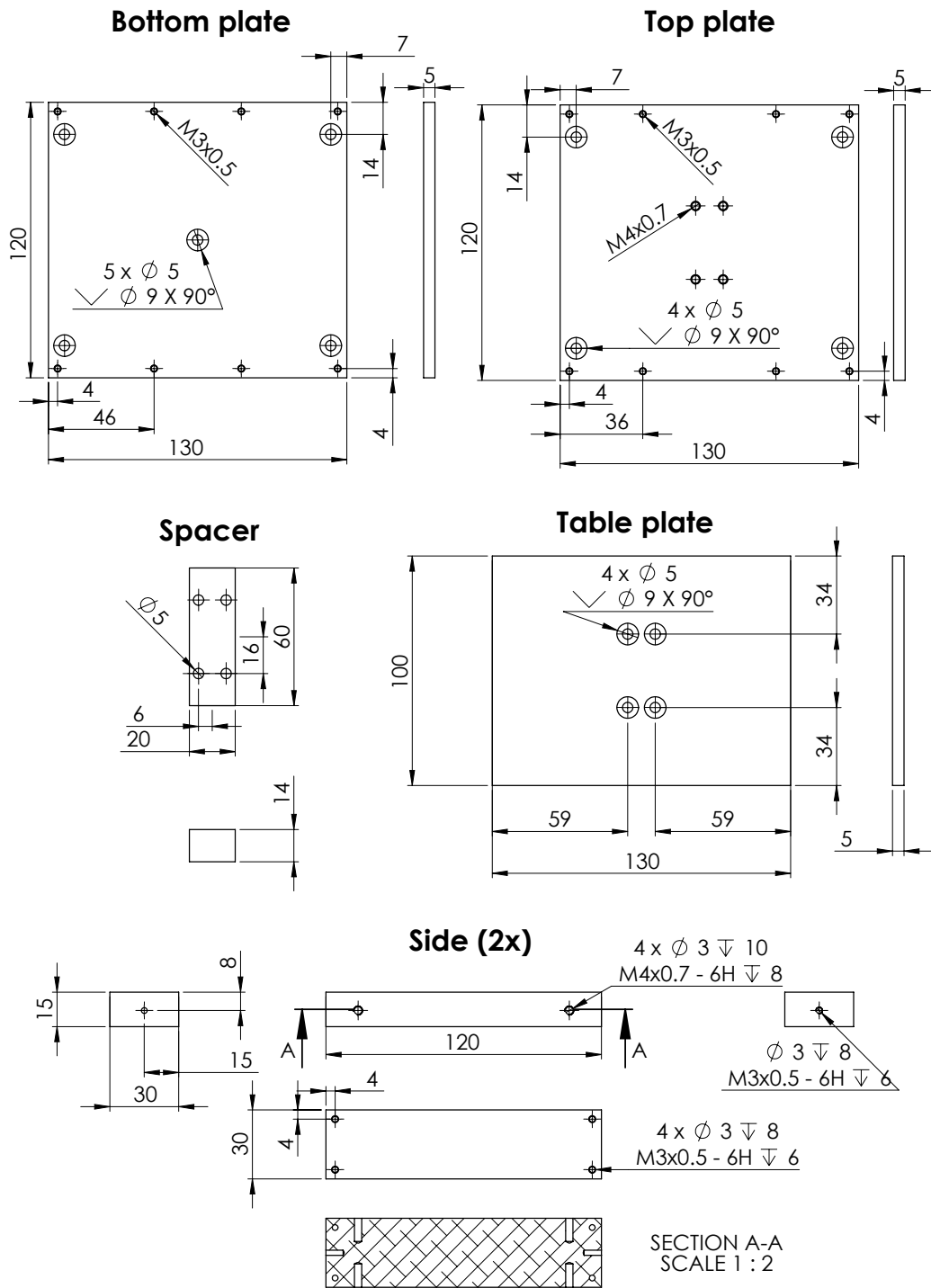
Table plate

Side (2x)

SECTION A-A
SCALE 1 : 2

Figure E.3: Detailed design of mover, all dimensions in mm.
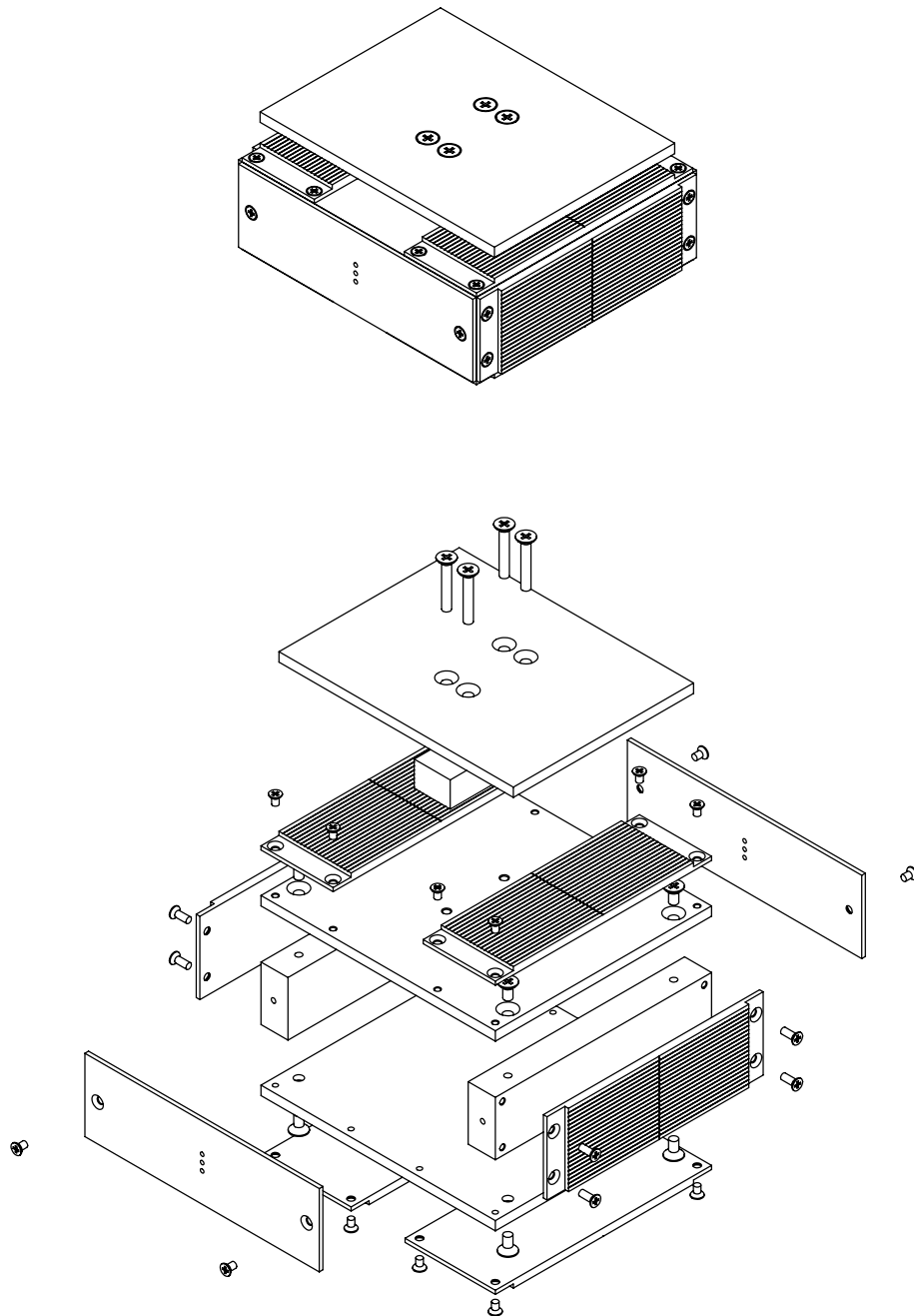
Figure E.4: Exploded view of mover

Bottom bearing patch

Side bearing patch

Top bearing patch
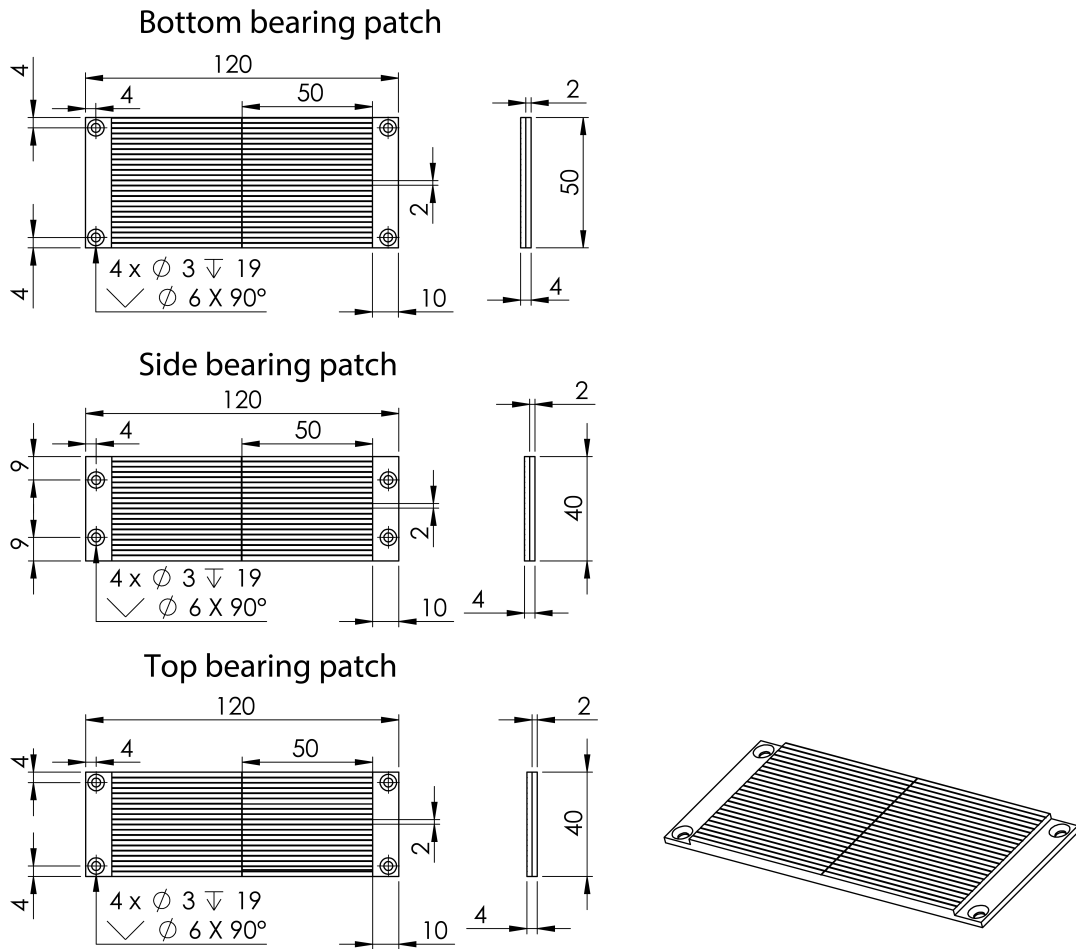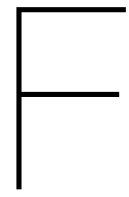

Figure E.5: Detailed design of pressure bearing pads, all dimensions in mm.

F

Magnet

F.1. Specifications

Please refer in correspondence: HKCM-Drawing number 9964-53809

QR-CODE

h = 2 mm

b = 2 mm

a = 50 mm

N
S

Magnet-Cuboid Q50x02x02Ni-N35

Tolerances : DIN ISO 2768-1m (Website Download Center)	
ROHs (2011/65/EU) & REACh (2007/EU)	
Length(a) = 50 mm	
Width(b) = 2 mm	
Height(H) = 2 mm	
Material/grade: NdFeB / N35	
Coating: Nickel	
max.operation temperature = 80°C	
Flux density inside the magnet = 1.17 Tesla	
Temperature coefficient and flux = 0.11% per 1°K	
Dead weight: 1.493 g	
Holding force on iron 10.99 Newton	
Weight, which the magnet can lift: 1.12 kg	

HKCM Engineering e.K.
Ottestr.20
D-24340 Eckernfoerde
p: +49 (0) 4351 726 461
f: +49 (0) 4351 726 463
e: sales@hkcm.de
w: https://www.hkcm.de
VAT-Id No.: DE 814 756 521
HKCM® Registered Trade Mark of HKCM Engineering e.K.

Copyright by HKCM Engineering e.K. Instant Update - Copy 16 December 2019 08:26:42

All calculations, diagrams and drawings are computed automatically and should not be used as the sole source of design data. The factors of your application may change these values considerably. All details are subject to alterations at any time.
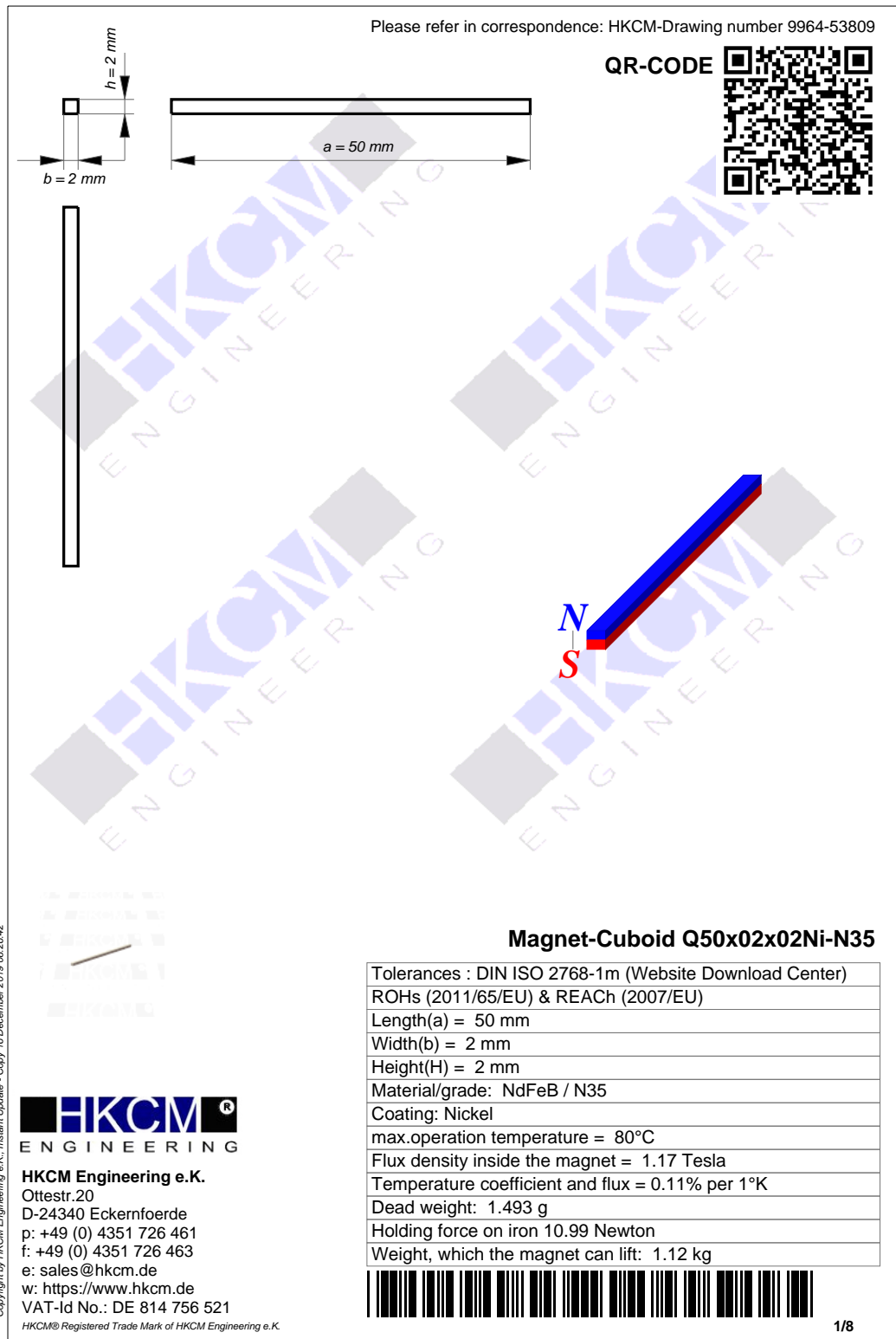
1/8

Figure F.1: HKCM datasheet for 50x2x2mm cuboid magnet

F.2. Influence of coating on the magnetic flux outside the magnet

Magnet is coated in 3 layers: an outer layer of nickel, a middle layer of copper and an inner layer of nickel (Ni-Cu-Ni). The layers are respectively 3, 15, 6.6 µm thick [25]. The total thickness of the layer is 25 µm, consistent with measurements done on the used magnets.
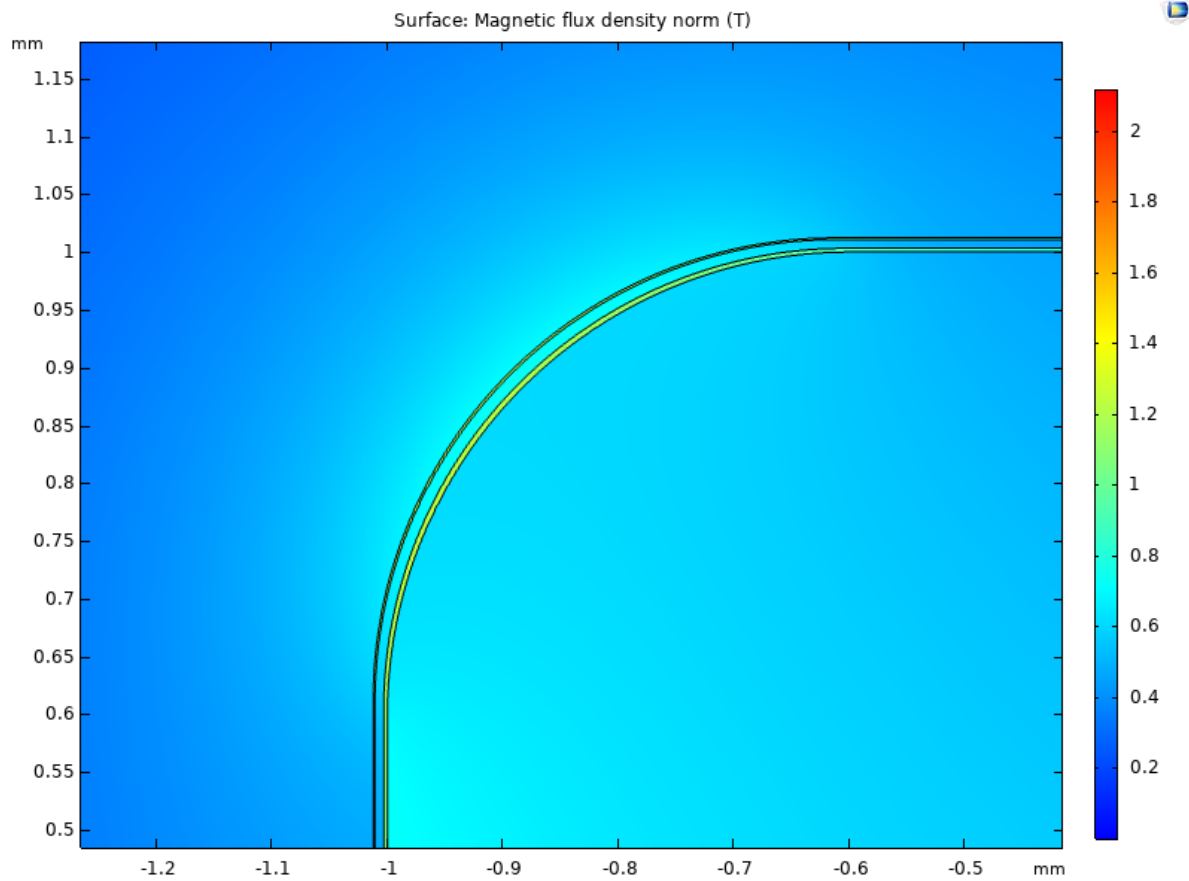

Figure F.2: Magnetic flux on a corner of the used magnets with modelled coating

Using a COMSOL model, the effect of the coating is investigated. Assumed is vacuum deposited nickel with a relative permeability of 50 and a saturation magnetization of 513 kA/m [42].
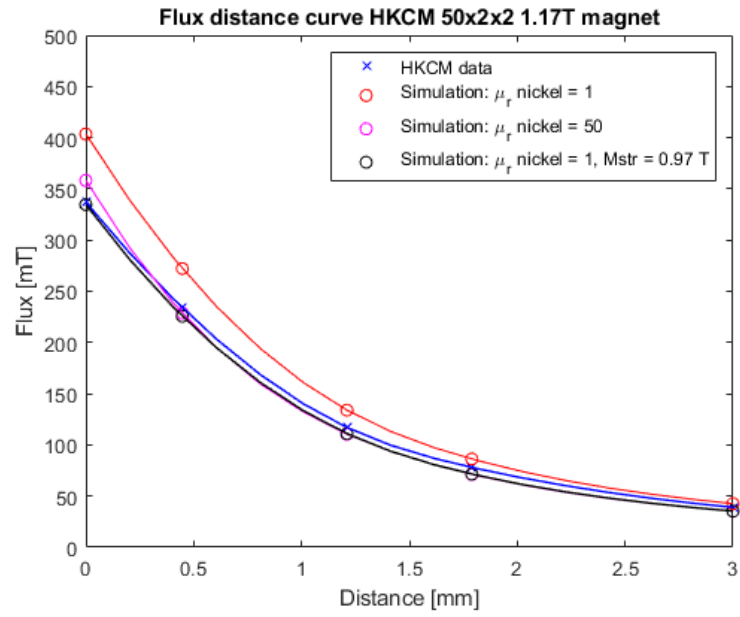
Figure F.3: Magnetic flux against distance for different simulation values

The simulation is compared to the HKCM data. It can be seen that the simulation without the nickel coating is producing a flux density that is higher than the HKCM data suggests. The simulation with the nickel shows that this layer probably is responsible for the missing flux. In order to more efficiently compute the magnetic field, instead of simulating the nickel layer, the magnetization strength is lowered.

Bibliography

[1] Liquids Research Ltd. URL `https://www.liquidsresearch.co.uk/en-GB/for_sealing_applications_si-61.aspx`.

[2] COMSOL Multiphysics 5.4, 2019. URL `www.comsol.com`.

[3] B Armstrong. Stick Slip and Control in Low-Speed Motion. *IEEE Transactions on Automatic Control*, 38(10):1483–1495, 1993.

[4] A Ashtekar, F Sadeghi, and L-E Stacke. Surface defects effects on bearing dynamics. 2010. doi: 10.1243/13506501JET578.

[5] B. Assadsangabi, M. H. Tee, and K. Takahata. Ferrofluid-assisted levitation mechanism for micro-motor applications. *2013 Transducers and Eurosensors XXVII: The 17th International Conference on Solid-State Sensors, Actuators and Microsystems, TRANSDUCERS and EUROSENSORS 2013*, 17(June):2720–2723, 2013. doi: 10.1109/Transducers.2013.6627368.

[6] A S T Boots, J W Spronck, R A J van Ostayen, and S G E Lampaert. Operational range of a ferrofluid pocket bearing. *Smart Materials and Structures*, 28(11):115030, 11 2019. ISSN 0964-1726. doi: 10.1088/1361-665x/ab2b60.

[7] A. S.T. Boots, L. E. Krijgsman, B. J.M. de Ruiter, S. G.E. Lampaert, and J. W. Spronck. Increasing the load capacity of planar ferrofluid bearings by the addition of ferromagnetic material. *Tribology International*, 129(May 2018):46–54, 2019. ISSN 0301679X. doi: 10.1016/j.triboint.2018.07.048. URL `https://doi.org/10.1016/j.triboint.2018.07.048`.

[8] Max Café and Jo Spronck. Nanometer precision Six Degree s of Freedom Planar Motion Stage with Ferrofluid Bearings. *DSPE Conference on Precision Mechatronics*, pages 43–46, 2014.

[9] J.M.D. Coey. Perspective and Prospects for Rare Earth Permanent Magnets. *Engineering*, 6 2019. ISSN 20958099. doi: 10.1016/j.eng.2018.11.034.

[10] Zeguang Dong, Pinkuan Liu, and Han Ding. Kalman estimator-based state-feedback high-precision positioning control for a micro-scale air-bearing stage. In *Lecture Notes in Computer Science (including subseries Lecture Notes in Artificial Intelligence and Lecture Notes in Bioinformatics)*, volume 5928 LNAI, pages 765–775, 2009. ISBN 3642108164. doi: 10.1007/978-3-642-10817-4{_}76.

[11] Ferrotec. Ferrofluid data sheet EFH series. 2011.

[12] Ferrotec. Data Sheet APG 2100 series, 2013.

[13] Ferrotec. Ferrofluid Data Sheet APG 500 series. 2013.

[14] Larry W. Fullerton and Mark D. Roberts. Magnetizing printer and method for re-magnetizing a least a portion of a previous magnetized magnet., 2016.

[15] Larry W. Fullerton, Mark D. Roberts, and Jason N. Morgan. System and method for producing magnetic structures, 2019.

[16] Seval Genc and Bora Derin. Synthesis and rheology of ferrofluids: A review, 2014. ISSN 22113398.

[17] L. A. Girifalco. Temperature dependence of viscosity and its relation to vapor pressure for associated liquids, 1955. ISSN 00219606.

[18] Haris Habib. Design of a three Degrees of Freedom planar precision stage using a single Position Sensitive Detector (MSc Thesis), 2015.

[19] HKCM Engineering e.K. Magnet-Cuboid Q50x02x02Ni-N35, 2019. URL `https://www.hkcm.de/HKCM_allinone.php?l=&id=53809&tolerance=1&force=1&flux=1&coating=1&bh=1&l=en`.

[20] Y. Kligerman and M. Varenberg. Elimination of stick-slip motion in sliding of split or rough surface. *Tribology Letters*, 53(2):395–399, 2014. ISSN 10238883. doi: 10.1007/s11249-013-0278-8.

[21] Irvin M Krieger and Thomas J Dougherty. A Mechanism for Non-Newtonian Flow in Suspensions of Rigid Spheres. 137(3), 1959. doi: 10.1122/1.548848.

[22] S. G.E. Lampaert, B. J. Fellinger, J. W. Spronck, and R. A.J. van Ostayen. In-plane friction behaviour of a ferrofluid bearing. *Precision Engineering*, 54(May):163–170, 2018. ISSN 01416359. doi: 10.1016/j.precisioneng.2018.05.013.

[23] S. G.E. Lampaert, J. W. Spronck, and R. A.J. van Ostayen. Load and stiffness of a planar ferrofluid pocket bearing. *Proceedings of the Institution of Mechanical Engineers, Part J: Journal of Engineering Tribology*, 232(1):14–25, 2018. ISSN 2041305X. doi: 10.1177/1350650117739200.

[24] S.G.E. Lampaert. Planar Ferrofluid Bearings Modelling and Design Principles (MSc Thesis), 2015.

[25] Stanislav Lasek, Nela Dobrovodská, and Katerina Skotnicová. Properties of Ni/Cu/Ni and Ni coatings for corrosion protection of NdFeB base magnets. In *METAL 2013 - 22nd International Conference on Metallurgy and Materials, Conference Proceedings*, pages 1371–1376, 2013. ISBN 9788087294413.

[26] Mika Latikka, Matilda Backholm, Jaakko V.I. Timonen, and Robin H.A. Ras. Wetting of ferrofluids: Phenomena and control. *Current Opinion in Colloid and Interface Science*, 36(January):118–129, 2018. ISSN 18790399. doi: 10.1016/j.cocis.2018.04.003. URL `https://doi.org/10.1016/j.cocis.2018.04.003`.

[27] Donald Mackay and Ian Van Wesenbeeck. Correlation of Chemical Evaporation Rate with Vapor Pressure. *Environ. Sci. Technol*, 48:10259–10263, 2014. doi: 10.1021/es5029074. URL `https://pubs.acs.org/sharingguidelines`.

[28] H Meng, J N Morgan, Q F Wei, and C H Chen. Design of Smart Magnetic Devices. In *Proceedings of 25th International Workshop on Rare-Earth and Future Permanent Magnets and Their Applications*, number Repm, 2018. URL `https://www.researchgate.net/profile/Christina_Chen10/publication/329796911_Design_of_Smart_Magnetic_Devices/links/5c1ae910a6fdccfc705aca6a/Design-of-Smart-Magnetic-Devices.pdf`.

[29] Gihin Mok. The design of a planar precision stage using cost effective optical mouse sensors (MSc Thesis), 2015.

[30] S. Odenbach. Recent progress in magnetic fluid research. *Journal of Physics Condensed Matter*, 16(32), 2004. ISSN 09538984. doi: 10.1088/0953-8984/16/32/R02.

[31] A. T.A. Peijnenburg, J. P.M. Vermeulen, and J. van Eijk. Magnetic levitation systems compared to conventional bearing systems. *Microelectronic Engineering*, 83(4-9 SPEC. ISS.):1372–1375, 2006. ISSN 01679317. doi: 10.1016/j.mee.2006.01.248.

[32] Camelia Petrescu and Radu Olaru. Analysis of a novel type of ferrofluid actuator with permanent magnets in Halbach pattern. In *EPE 2014 - Proceedings of the 2014 International Conference and Exposition on Electrical and Power Engineering*, pages 222–225. Institute of Electrical and Electronics Engineers Inc., 12 2014. ISBN 9781479958498. doi: 10.1109/ICEPE.2014.6969901.

[33] Physik Instrumente. PIglide Air Bearing Technology datasheet, 2019.

[34] R. Rosensweig. Buoyancy and stable levitation of a magnetic body immersed in a magnetizable fluid, 1966. ISSN 00280836.

[35] R. Rosensweig. Bearing arrangement with magnetic fluid defining bearing pads, 1971.

[36] Ronald E. Rosensweig. *Ferrohydrodynamics*. Dover Publications, 2013. ISBN 9780486783000.

[37] R S Sayles. Debris Damage in Boiling Bearings and Its Effects on Fatigue Life. Technical report, 1988. URL `https://asmedigitalcollection.asme.org/tribology/article-pdf/110/1/26/5732375/26_1.pdf`.

[38] Christian Schmidt, Joachim Heinzl, and Günther Brandenburg. Control approaches for high-precision machine tools with air bearings. *IEEE Transactions on Industrial Electronics*, 46(5): 979–989, 1999. ISSN 02780046. doi: 10.1109/41.793347.

[39] P. C. Scholten. Some material problems in magnetic fluids. *Chemical Engineering Communications*, 67(1):331–340, 1988. ISSN 15635201. doi: 10.1080/00986448808940392.

[40] M. I. Shliomis. Effective Viscosity of Magnetic Suspensions. 34(6):3–6, 1972.

[41] SKF. Extending the Bearing Life Cycle SKF Maintenance and Lubrication Products Alignment Lubrication Mounting Buy a bearing Basic condition monitoring Dismounting. pages 161–167. URL `https://www.skf.com/binary/21-163650/0901d196800637eb-03000EN.pdf`.

[42] Connor S. Smith, Shehaab Savliwala, Sara C. Mills, Jennifer S. Andrew, Carlos Rinaldi, and David P. Arnold. Electro-infiltrated nickel/iron-oxide and permalloy/iron-oxide nanocomposites for integrated power inductors. *Journal of Magnetism and Magnetic Materials*, 493(August 2019):165718, 2020. ISSN 03048853. doi: 10.1016/j.jmmm.2019.165718. URL `https://doi.org/10.1016/j.jmmm.2019.165718`.

[43] Eunho Sung, Chang-hoon Seo, Hyunmin Song, Byungjoo Choi, Yongho Jeon, Young-Man Choi, Kihyun Kim, and Moon G Lee. Design and experiment of noncontact eddy current damping module in air bearing–guided linear motion system. *Advances in Mechanical Engineering*, 11 (8):168781401987142, 8 2019. ISSN 1687-8140. doi: 10.1177/1687814019871424. URL `http://journals.sagepub.com/doi/10.1177/1687814019871424`.

[44] Takumi Tsumura, Hayato Yoshioka, Hidenori Shinno, and Hiroshi Sawano. Magnetically preloaded aerostatic guideway for high speed nanometer positioning. *Journal of Advanced Mechanical Design, Systems and Manufacturing*, 8(4):JAMDSM0054–JAMDSM0054, 2014. ISSN 18813054. doi: 10.1299/jamdsm.2014jamdsm0054. URL `http://jlc.jst.go.jp/DN/JST.JSTAGE/jamdsm/2014jamdsm0054?lang=en&from=CrossRef&type=abstract`.

[45] Ian Van, Wesenbeeck Ae, Jeffrey Driver, and John Ross. Relationship Between the Evaporation Rate and Vapor Pressure of Moderately and Highly Volatile Chemicals. doi: 10.1007/s00128-008-9380-2.

[46] L van Moorsel. A planar precision stage using a single image sensor (MSc Thesis), 2017.

[47] S van Veen. Planar Ferrofluid Bearings (MSc Thesis), 2013.

[48] Liming Xiu. Time Moore: Exploiting Moore's Law from the Perspective of Time, 12 2019. ISSN 19430590.

[49] Z. Q. Zhu and D. Howe. Halbach permanent magnet machines and applications: A review. In *IEE Proceedings: Electric Power Applications*, volume 148, pages 299–308, 7 2001. doi: 10.1049/ip-epa:20010479.